NAG 4-1

PURDUE UNIVERSITY
SCHOOL OF AERONAUTICS AND ASTRONAUTICS

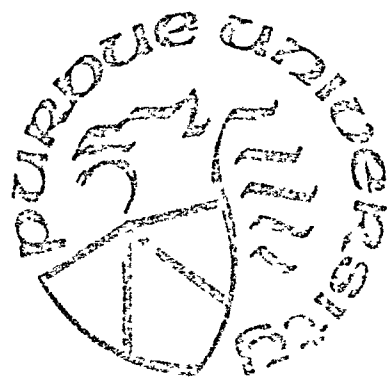

West Lafayette, Indiana 47907

(NASA-CR-176166) THE INTEGRATED MANUAL AND AUTOMATIC CONTROL OF COMPLEX FLIGHT SYSTEMS Semiannual Status Report, Jan. - Aug. 1985 (Purdue Univ.) 112 p HC A06/MF A01 CSCL 01C

N85-35201

Unclas

N85-35201#

THE INTEGRATED
MANUAL AND AUTOMATIC CONTROL
OF COMPLEX FLIGHT SYSTEMS

Semi-Annual Status Report

January 1985 - August 1985

Principal Investigator: Dr. David K. Schmidt
School of Aeronautics & Astronautics
Purdue University
West Lafayette, IN 47907

NASA Technical Officer: Mr. Donald T. Berry
Vehicle Dynamics and Control Division
Ames Research Center
Dryden Flight Research Facility
P.O. Box 273
Edwards, CA 93523

Grant No. NAG4-1

September 17, 1985

TABLE OF CONTENTS

INTRODUCTION

This constitutes a status report on the research being performed by Purdue University's School of Aeronautics and Astronautics for NASA Ames/Dryden under grant number NAG4-1. The topics of research in this program include pilot/vehicle analysis techniques, identification of pilot dynamics, and control synthesis techniques for optimizing aircraft handling qualities. This report presents project activity in the area of pilot/vehicle analysis techniques for the period January 1, 1985 to August 31, 1985.

CURRENT TECHNICAL ACTIVITY

During the current project period, an analysis has been underway of the flight-test results obtained recently (1984) by the CALSPAN Corporation on "Pitch-Rate Flight Control Systems in the Flared Landing Task", (Ref. 1), with the Total In-Flight Simulator (TIFS). The analysis approach considered here is based on the Optimal Control/Frequency Domain (OC/FD) techniques developed under this grant at Purdue. These techniques originally stem from an optimal-control approach to perform a Neal-Smith-like analysis on aircraft attitude dynamics (Ref. 2), but have recently been extended and used successfully to analyze the flared landing task. This extended

analysis method was reported at the 1985 AIAA Guidance and Control Conference (Ref. 3) and is further documented in Ref. 4. (A copy of Ref. 3 is attached as an Appendix.)

A recent status report (Ref. 5) documented some early work performed on the TIFS configurations. Further analysis of the data base is documented in this present status report. Comparisons are made to the results in Ref. 3 and some modifications to the analysis technique are suggested and discussed. Finally, an in-depth analysis of the effect of the experimental variables (i.e. prefilter, ω_{sp}, ...) is conducted to gain some further insight into the flared landing task for this class of vehicle dynamics.

REVIEW OF OC/FD TECHNIQUES FOR THE FLARED LANDING TASK

The OC/FD analysis uses an optimal-control approach to estimate the pilot describing functions. Model-based metrics obtained from the corresponding frequency-domain analysis are then used to explain experimental pilot ratings. The analysis technique in Ref. 3 for the flared landing task includes the assumption that critical to the landing task is the pilot's ability to precisely control flight-path, expressed as the multi-loop control task pictured in Figure 1. (This assumes a conventional "frontside" landing technique where the pilot uses pitch attitude to control flight-path-angle.)

The analysis approach first considers, however, an evaluation of just the attitude dynamics, using a variation of the Neal-Smith-like procedure of Ref 2. This is done to expose undesirable inner-loop attitude dynamics which would be detrimental to any longitudinal task. Attention then turns towards an investigation of the

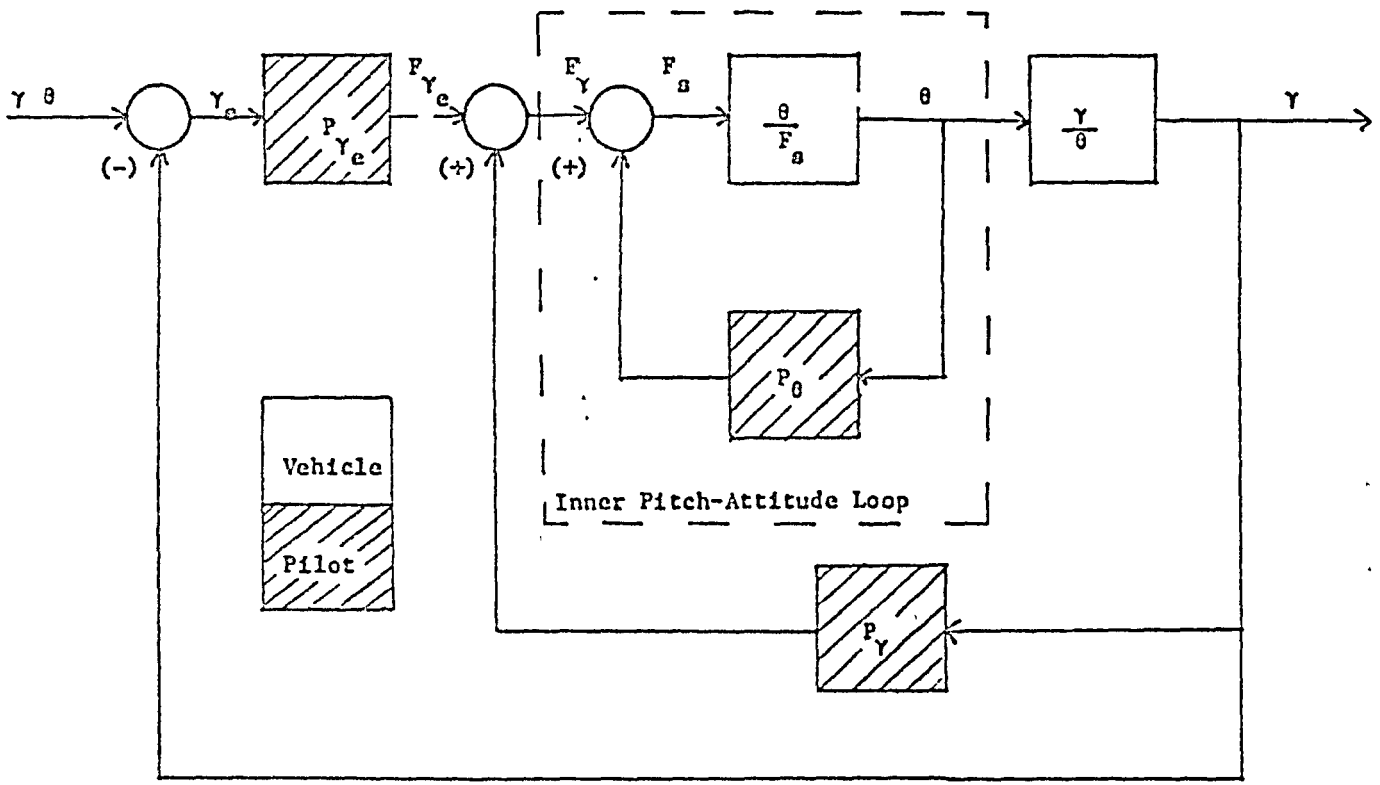

Figure 1
The Multi-Loop Flight-Path Tracking Task

flight-path tracking task, as modeled in Figure 1.

Attitude Analysis

A slight modification to the methods of Ref 2 was presented in the previous status report. This modification uses a sensitivity parameter (SP) defined as

$$SP = \langle \text{ Droop, dB } \rangle \times \left| \Delta\left\langle \frac{\theta}{\theta_c} \right\rangle_{max} / \Delta \text{ DC Gain, dB} \right|$$

as a measure of loop quality. This parameter has the same interpretation as the original "Resonance Peak" of Neal and Smith in terms of oscillatory tendency. However, it also reflects the sensitivity of the closed-loop dynamics to slight variations in pilot aggressiveness, expressed in terms of forward path gain. As before, this sensitivity parameter is plotted versus the pilot's phase compensation. The results shown in Figures 2 and 3, for example, include the Neal-Smith data and the LAHOS data respectively Both data sets group nicely in terms of Level 1, 2, and 3 pilot opinion ratings.

Note from the figures that it appears that the pilot accepts generating a larger amount of phase lead in the landing task (LAHOS) as opposed to up-and-away flight (Neal-Smith). That is, configurations rated Level 1 in the landing task would have received a Level 2 rating in the precision attitude-control task evaluated by Neal and Smith. Therefore, it would appear that the Neal-Smith criteria cannot be used to directly predict handling qualities in the flared landing task

Performing this attitude analysis on the TIFS configurations leads to the results in Figure 4 and Table 1. It is clear that these configurations do not group

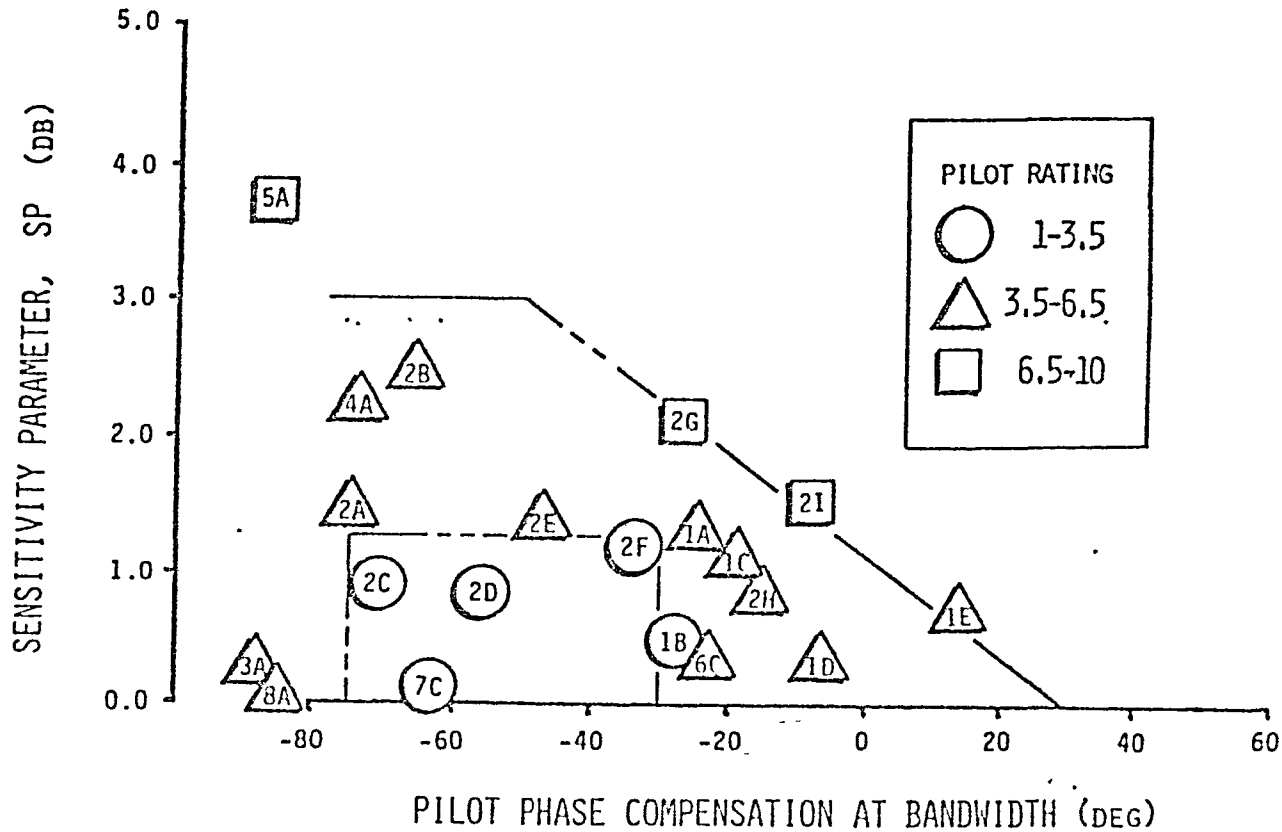

Figure 2
Neal-Smith Results
Pitch-Attitude Tracking Task

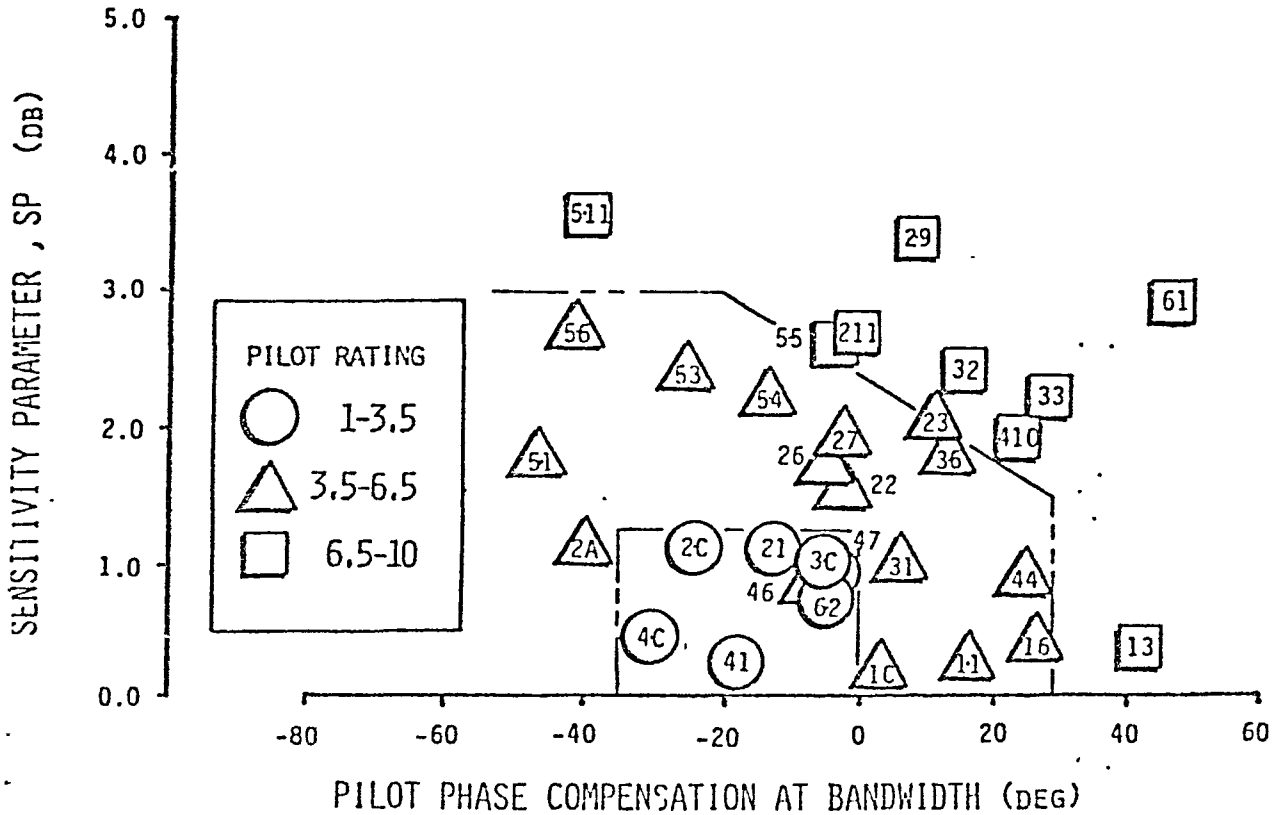

Figure 3
LAHOS Data
Pitch-Attitude Tracking Task

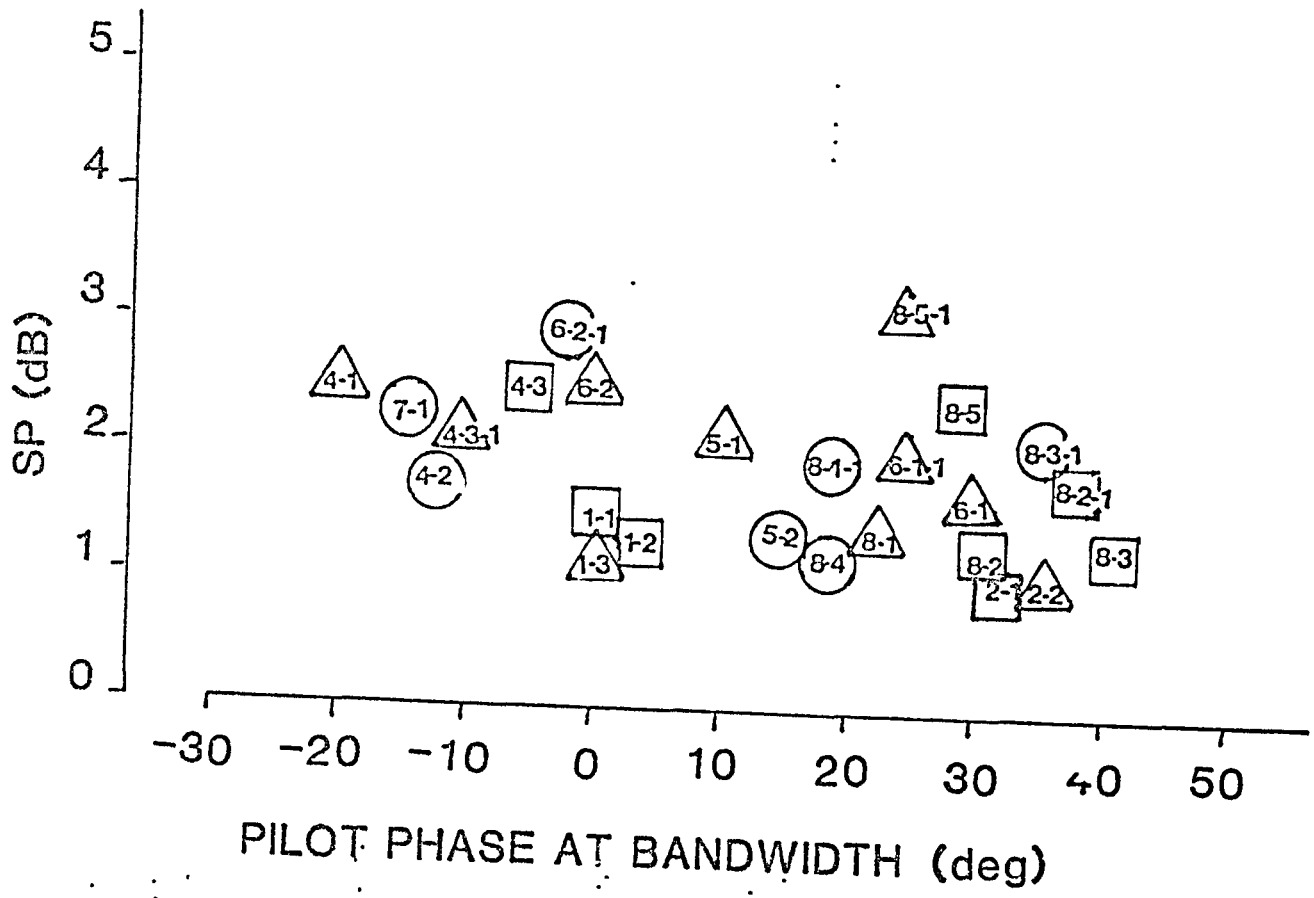

Figure 4
TIFS Results; Pitch-Attitude Tracking Task

Table 1

Attitude Analysis

Conf.	Pilot Ratings	Closed-Loop Bandwidth (rad/sec)	SP	Pilot Phase Compensation at BW (deg)
1-1	7,5	2.66	1.32	0.4
1-2	8,7,5.5	2.66	1.32	0.3
1-3	5,4,7	2.66	1.31	0.2
4-1	2.5,5	2.87	2.55	-19.7
4-2	2,3	2.79	1.93	-15.0
4-3	7	2.71	2.59	-6.1
4-3-1	4	2.73	2.10	-9.7
7-1	2.5,3	2.79	2.29	-16.8
2-1	6,7	2.51	1.12	31.0
2-2	4.5,3	2.51	1.12	31.1
5-1	4.5,4.5	2.67	2.00	9.3
5-2	2,3	2.62	1.55	16.3
6-1	3,5,6	2.57	1.45	27.1
6-2	5,4,2	2.85	2.50	0.1
6-1-1	4	2.60	2.03	23.5
6-2-1	3	2.88	2.89	-3.5
8-1	5.5,6	2.62	1.60	21.4
8-1-1	2	2.66	2.10	17.2
8-2	9,8,7	2.52	1.40	29.8
8-2-1	7	2.43	1.72	37.9
8-3	8,7	2.35	1.36	40.5
8-3-1	3	2.38	2.14	36.1
8-4	1	2.64	1.57	18.6
8-5	7	2.33	2.57	28.7
8-5-1	4	2.37	3.21	24.5

together as nicely as the LAHOS configurations in Figure 3. Some TIFS configurations (e.g. 5-2) were rated Level 1, yet require relatively high pilot phase compensation for precision attitude control.

Flight-Path Analysis

For the flight-path-tracking task, identifying the pilot's phase compensation is not easily accomplished with the multi-loop block diagram arrangement in Figure 1. However, once the individual blocks in Figure 1 have been obtained via the optimal-control modeling, the block diagram can be manipulated to give an equivalent, single-loop representation of the flight-path-tracking task. This equivalent form is shown in Figure 5. As reported in References 4 and 5, equivalent pilot phase compensation, as obtained from the pilot block (P_{eq}) of the equivalent, single-loop representation, correlated strongly with pilot ratings. This parameter is defined in Figure 6. In addition, the deviation from the desired -20 dB/decade characteristic of the pilot/vehicle open-loop Bode magnitude, expressed in terms of a "High-Frequency Open-Loop Peak" (see Figure 7), was used as an indicator of loop robustness. These two closed-loop parameters were used to evaluate the LAHOS configurations. Those results are shown in Figure 8.

An additional measure of loop quality is presented in Ref. 3. This measure is related to the pilot's objective of precisely controlling flight-path error. Neglecting noise sources, the steady-state, mean-squared flight-path error can be expressed as

$$\sigma^2_{\gamma_e} = \frac{1}{\pi}\int_0^{\infty} \left|\frac{\gamma_e}{\gamma_c}(j\omega)\right|^2 S_{\gamma_c}(\omega)d\omega \qquad 1$$

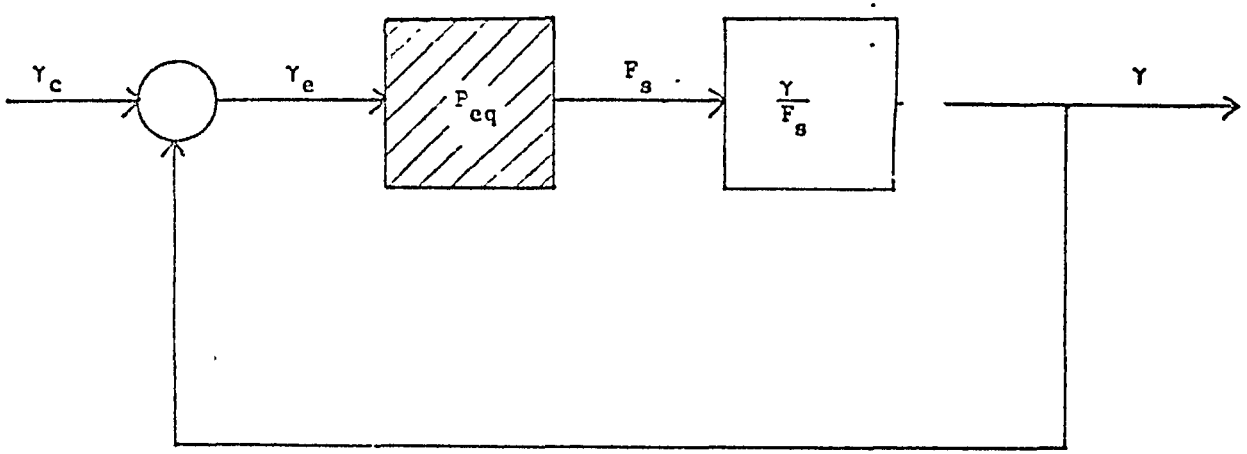

Figure 5
Equivalent Single Loop Flight Path Tracking Task

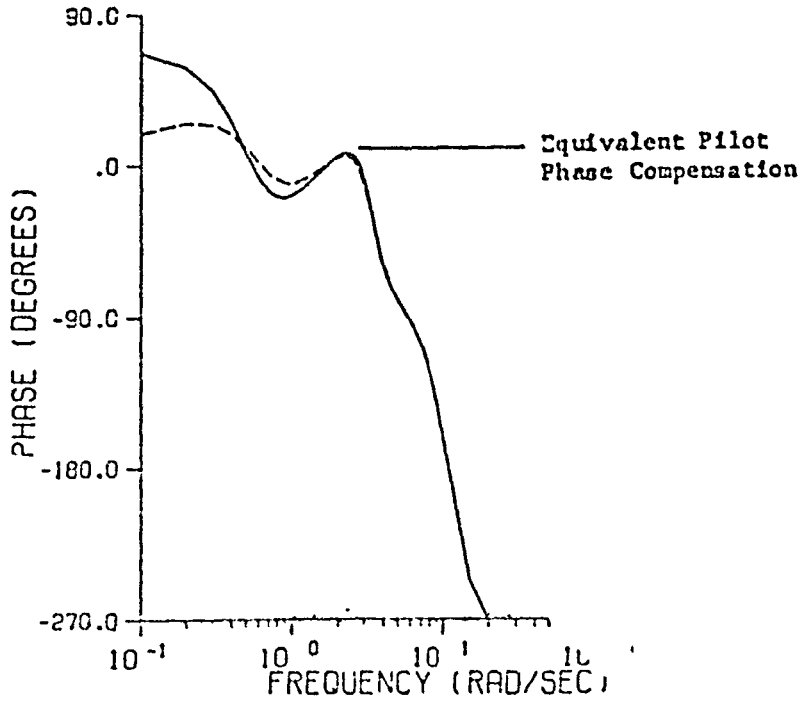

Figure 6
Equivalent, Single Loop Pilot Fenchian Phase

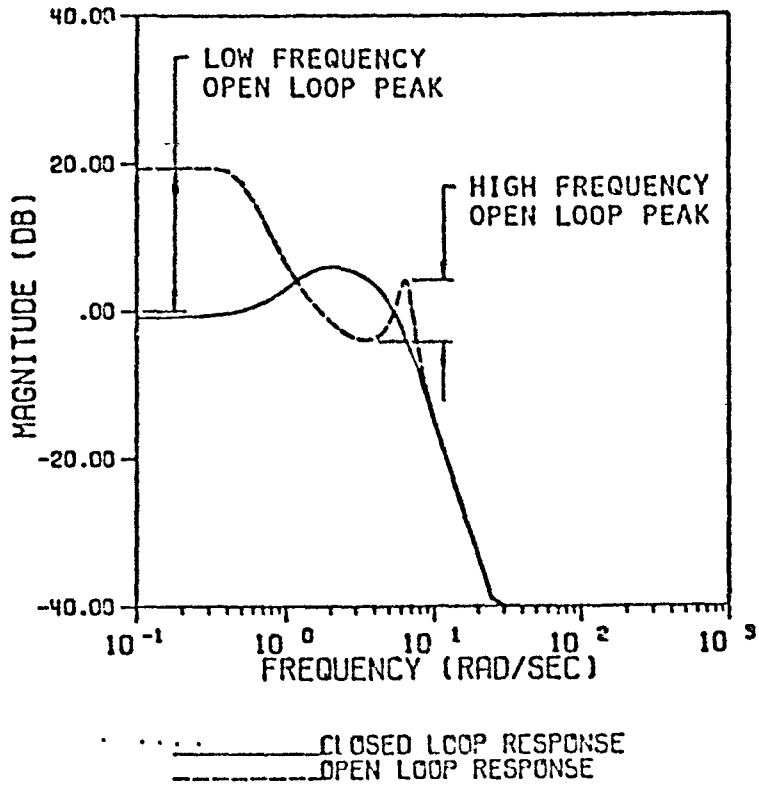
40.00
20.00
.00
-20.00
-40.00
MAGNITUDE (DB)
LOW FREQUENCY
OPEN LOOP PEAK
HIGH FREQUENCY
OPEN LOOP PEAK
10^{-1}
10^{0}
10^{1}
10^{2}
10^{3}
FREQUENCY (RAD/SEC)
CLOSED LOOP RESPONSE
OPEN LOOP RESPONSE

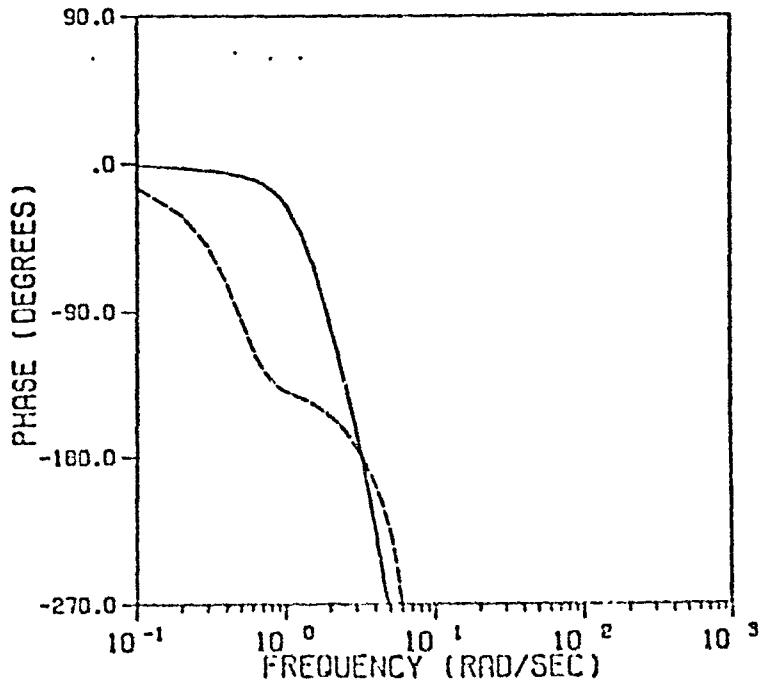
90.0
.0
-90.0
-180.0
-270.0
PHASE (DEGREES)
10^{-1}
10^{0}
10^{1}
10^{2}
10^{3}
FREQUENCY (RAD/SEC)

Figure 7

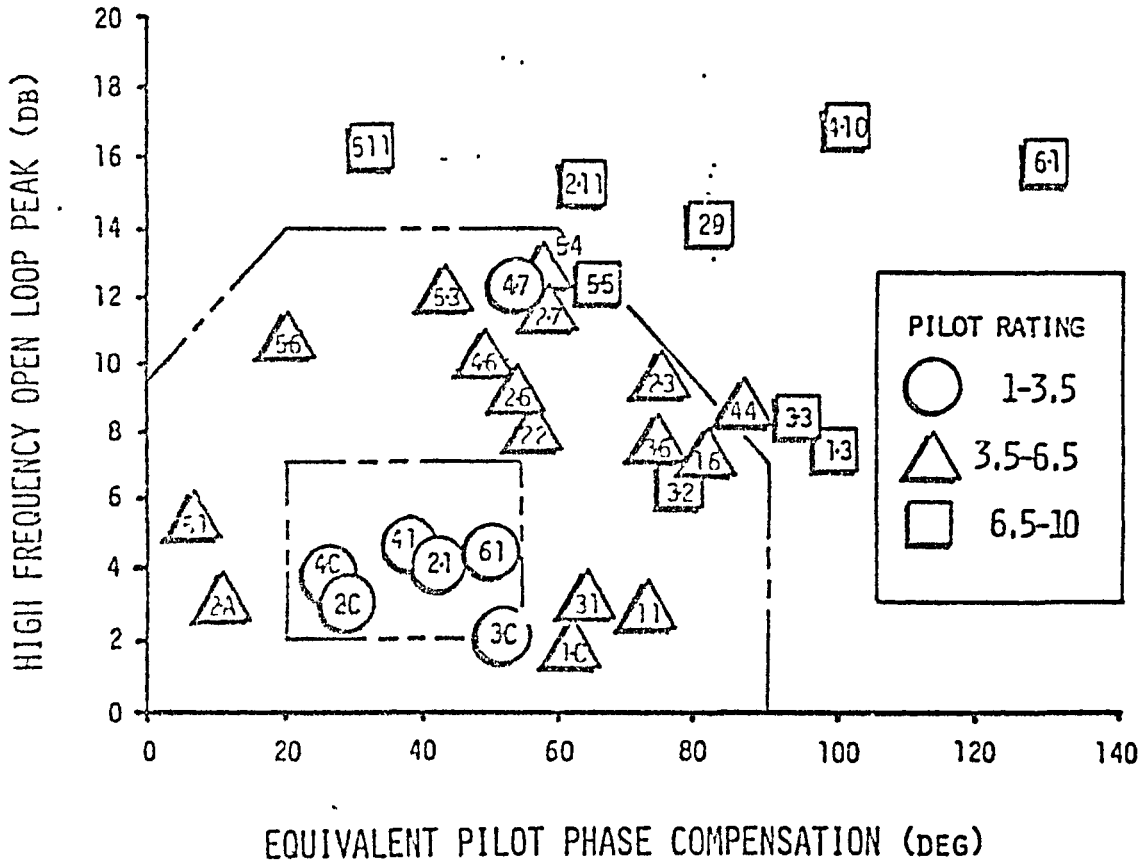

Figure 8

LAHOS Results; High-Frequency Open Loop Peak versus Equivalent Pilot Phase Compensation

where $S_{\gamma_c}(\omega)$ is the power spectral density of the commanded input. From Eq. 1 it is clear that to minimize $\sigma^2_{\gamma_e}$, $\left|\frac{\gamma_e}{\gamma_c}(j\omega)\right|^2$ must be small when $S_{\gamma_c}(\omega)$ is large. This objective forces $\left|\frac{\gamma}{\gamma_e}(j\omega)\right|^2$ to be large at low frequencies since $\left|\frac{\gamma_c}{\gamma}(j\omega)\right|^2 \approx 1$ for a tracking system. For this reason, the maximum magnitude of the pilot/vehicle open-loop Bode (loop gain) at low frequencies will provide an indication of the tracking performance. This is labeled the "Low-Frequency Open-Loop Peak" in Figure 7. The resulting values of this parameter, obtained from the OC/FD analysis, have been plotted versus the equivalent pilot phase compensation (workload metric) in Figure 9. Once again, the configurations group very well in terms of pilot opinion ratings.

In the LAHOS experiment, the cockpit, aircraft c.g., and center of rotation (c.r.) locations were very close on the longitudinal axis. In the TIFS experiment, this is not true. The question therefore arises as to what are the appropriate vehicle responses to be evaluated. The responses at the vehicle c.r. were chosen initially for a number of reasons. This selection eliminates the kinematic effect of the rotational motion and focuses attention on the "point-mass" performance of the flight vehicle. It is noted that, in this case, the open- and closed-loop frequency responses were similar to those for the LAHOS data set. This is shown in the resulting pilot/vehicle open-loop Bode plots in Figure 10. This data is very similar to that shown in Figure 7, obtained in the analysis of the LAHOS configurations.

Performing the above flight-path analysis on the TIFS configurations (dynamics of the c.r.) leads to the results

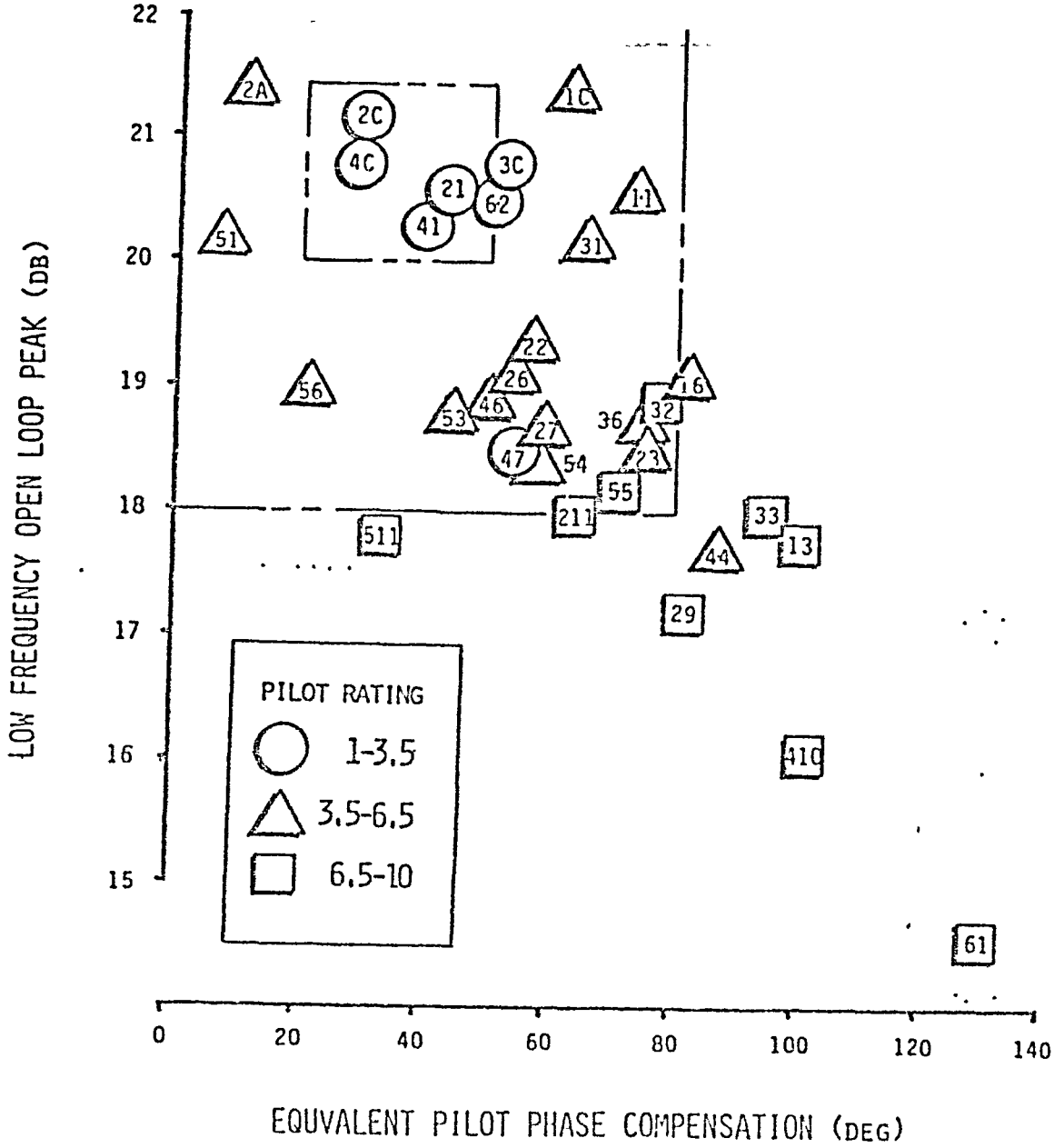

Figure 9

LAHOS Results: Low-Frequency Open-Loop Peak versus Equivalent Pilot Phase Compensation

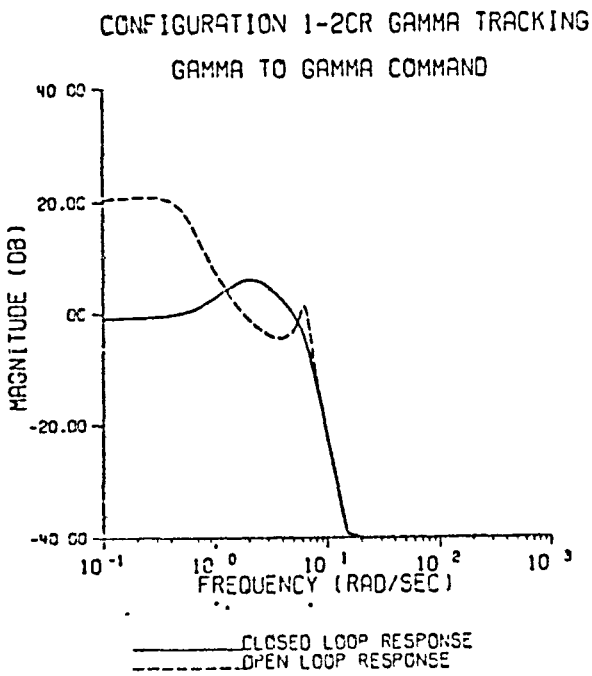

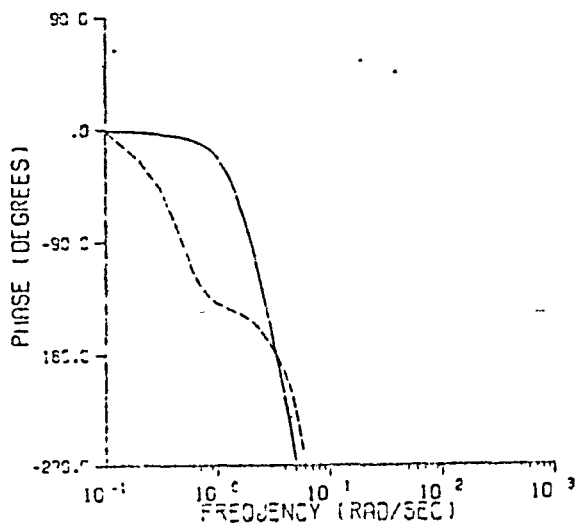

Figure 10
Typical Pilot/Vehicle Bode for TIFS dynamics at the c.r.

in Figures 11 and 12. Quite clearly, the configurations do not group nicely in terms of pilot ratings. In fact, Configuration 8-3-1, rated Level 1, lies in the Level 3 region of Figure 8. Likewise, Configurations 8-1-1 and 8-3-1, as shown in Figure 12, lie in the Level 3 region of Figure 9. Obviously some additional analysis is required.

CLOSER ANALYSIS

Care is required in applying the analysis technique used for the LAHOS data to the TIFS configurations. There are several differences between the two experiments that may be significant. The differences and/or key issues are;

1. Cockpit location
2. Variable T_{θ_2}
3. $T_{\theta_2} - T_q$ prefilter
4. Washout filter

In the LAHOS experiment, the cockpit, aircraft c.g., and center of rotation (c.r.) locations were very close on the longitudinal axis. The aircraft had conventional aircraft dynamics, plus leads and lags. T_{θ_2} was constant, and there was essentially no additional time delay. Finally, the two real (airframe) zeros (one >0 and one <0) in the n_z / F_s transfer functions were large in magnitude (10-20 rad/sec.). In the TIFS Pitch-Rate experiment, none of the above is true.

Table 2 presents the form of the θ / F_s and $n_{z_{c.r.}}$ / F_s transfer functions and indicates how they vary with the addition of the prefilter and the washout filter. The prefilter essentially cancels the dynamics introduced by the pitch-rate feedback control system. The washout

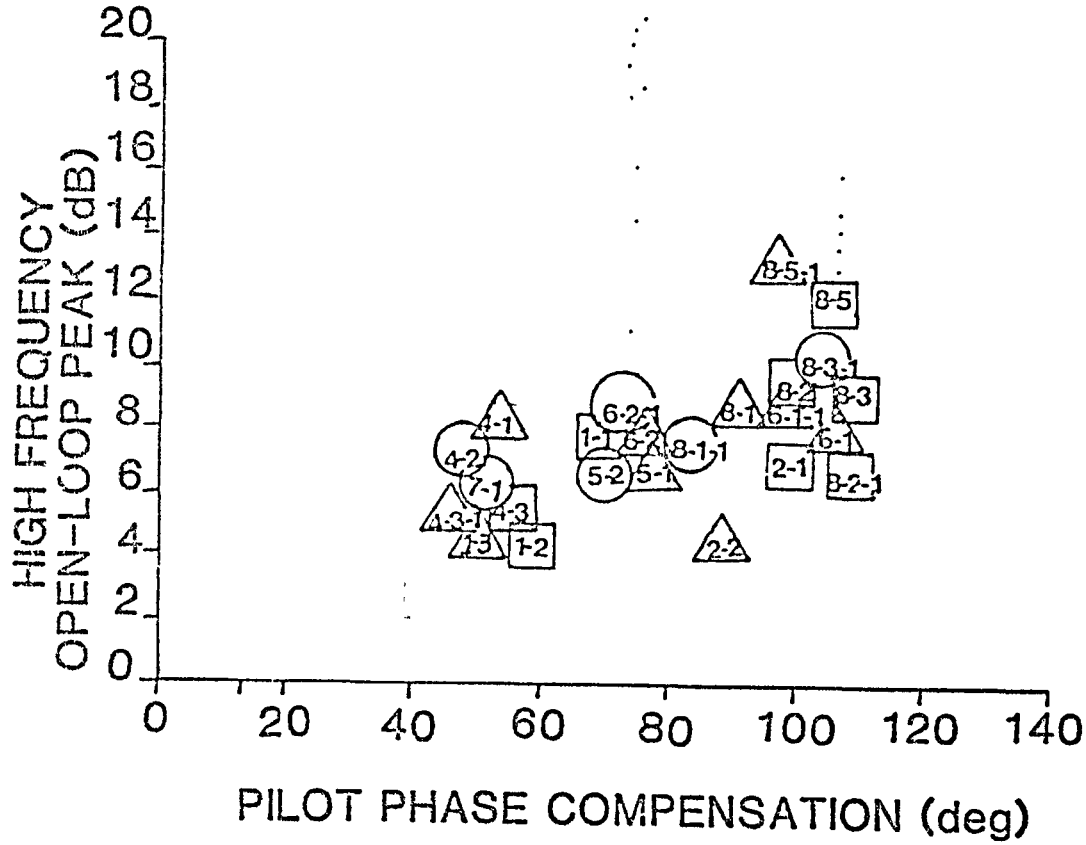

Figure 11

TIFS Results at c.r.; High-Frequency Open-Loop Peak versus Equivalent Pilot Phase Compensation

ORIGINAL PAGE IS
OF POOR QUALITY

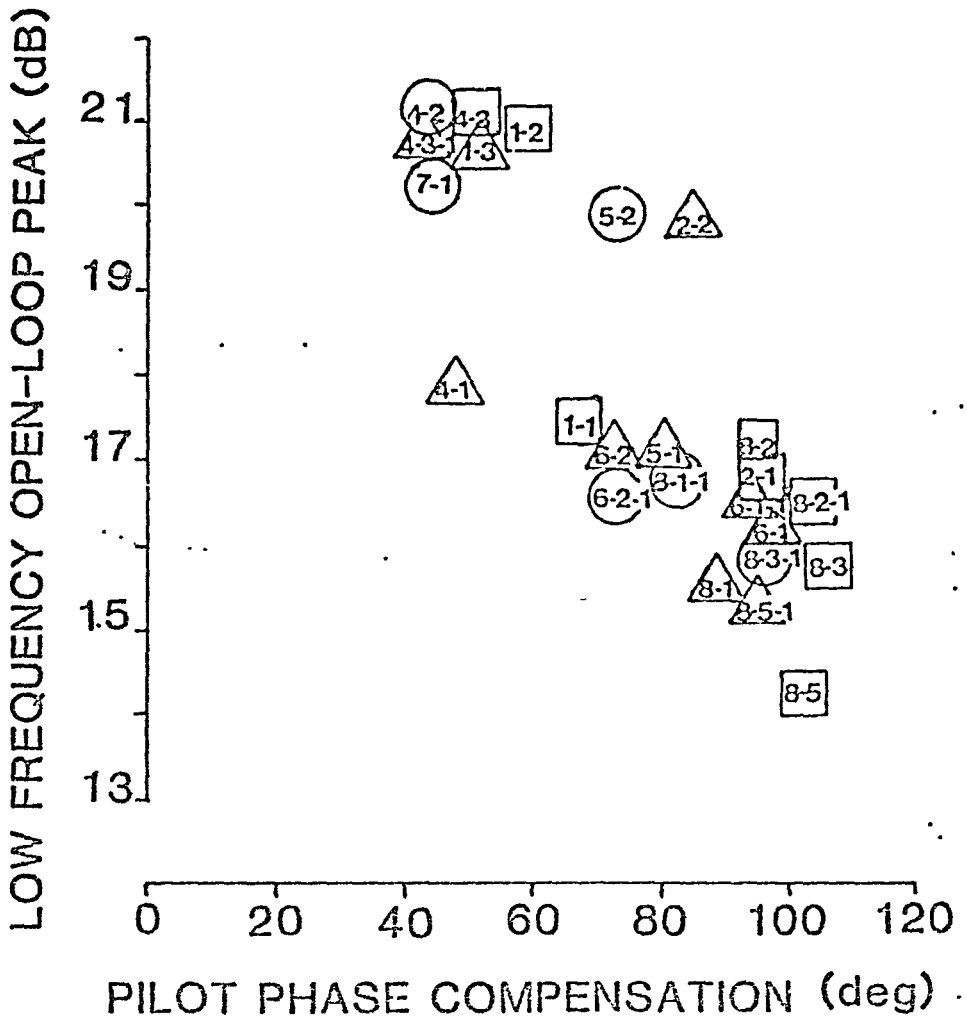

Figure 12

TIFS Results at c.g. Low-Frequency Open-Loop Peak versus Equivalent Pilot Phase Compensation

TABLE 2

TIFS Transfer Functions (responses at c.r.)

BASE CONFIGURATION

$$\frac{\dot{\theta}}{F_s} = \frac{K_\theta (s+k_1)(s+\frac{1}{T_{\theta_2}})}{[\zeta,\omega]_{sp}\,(s+\lambda_2')}, \quad 1/T_{\theta_2} \approx \lambda_2'$$

$$\frac{n_z}{F_s} = \frac{-K_\gamma (s+k_1)(s-z_1)(s+z_4)(s-z_2)}{[\zeta,\omega]_{sp}\,(s+\lambda_2')\,(s+x_1)}$$

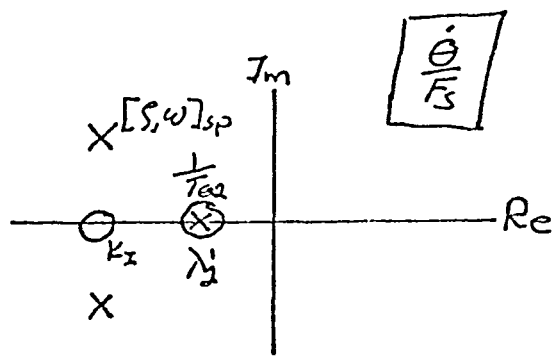

BASE + PREFILTER

$$\frac{\dot{\theta}}{F_s} = \frac{K_\theta (s+\frac{1}{T_{\theta_2}})}{[\zeta,\omega]_{sp}}$$

$$\frac{n_z}{F_s} = \frac{-K_\gamma (s-z_1)(s+z_4)(s-z_2)}{[\zeta,\omega]_{sp}\,(s+\lambda_1)}$$

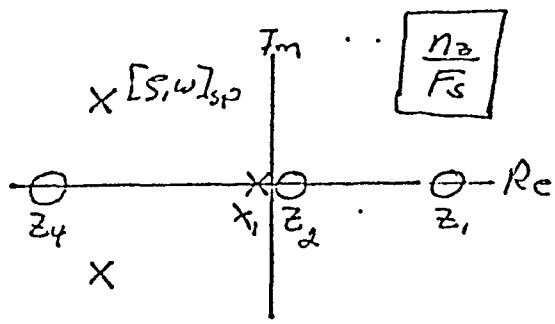

BASE + PREFILTER + W.O.

$$\frac{\dot{\theta}}{F_s} = \frac{K_\theta' s (s+\frac{1}{T_{\theta_2}})}{[\zeta,\omega]_{sp}\,(s+0.2)}$$

$$\frac{n_z}{F_s} = \frac{-K_\gamma' s (s-z_1)(s+z_4)(s-z_2)}{[\zeta,\omega]_{sp}\,(s+0.2)\,(s+\lambda_1)}$$

filter was added in some cases to provide monotonic (conventional) pitch stick forces in the landing flare. This was done by washing out the rate command characteristics at frequencies lower than ω=0.2 rad/sec thus making θ / F_s more like K at low frequencies.

At this point, a short discussion of some parameters used in this analysis will be undertaken to explain the importance of these variables, and hence why they were chosen. Those parameters that exhibit strong correlations with the experimental variables and pilot ratings will then be examined.

Flight-Path Bandwidth (rad/sec)- frequency at which the closed-loop, pilot/vehicle phase for the flight-path-tracking task (see Figure 1) equals -90 degrees. This is an indicator of the combined pilot/vehicle system's ability to track over the commanded frequency band.

Inner-Loop Bandwidth (rad/sec)- the flight-path-tracking task has been defined as the multi-loop task pictured in Figure 1. The Inner-Loop Bandwidth is defined as the frequency at which the phase of the closed-loop pitch-attitude inner-loop (see Figure 1) equals -180 degrees. This parameter will help provide some insight into the variations of this inner-loop with variations in the experimental variables.

Neal-Smith Inner-Loop Bandwidth (rad/sec)- When one chooses to approach the multi-loop, flared landing task analysis problem from a "conventional" point of view, a block diagram of the form shown in Figure 13 is usually assumed. This block diagram arrangement is different from that utilized in this study (see Figure 1).

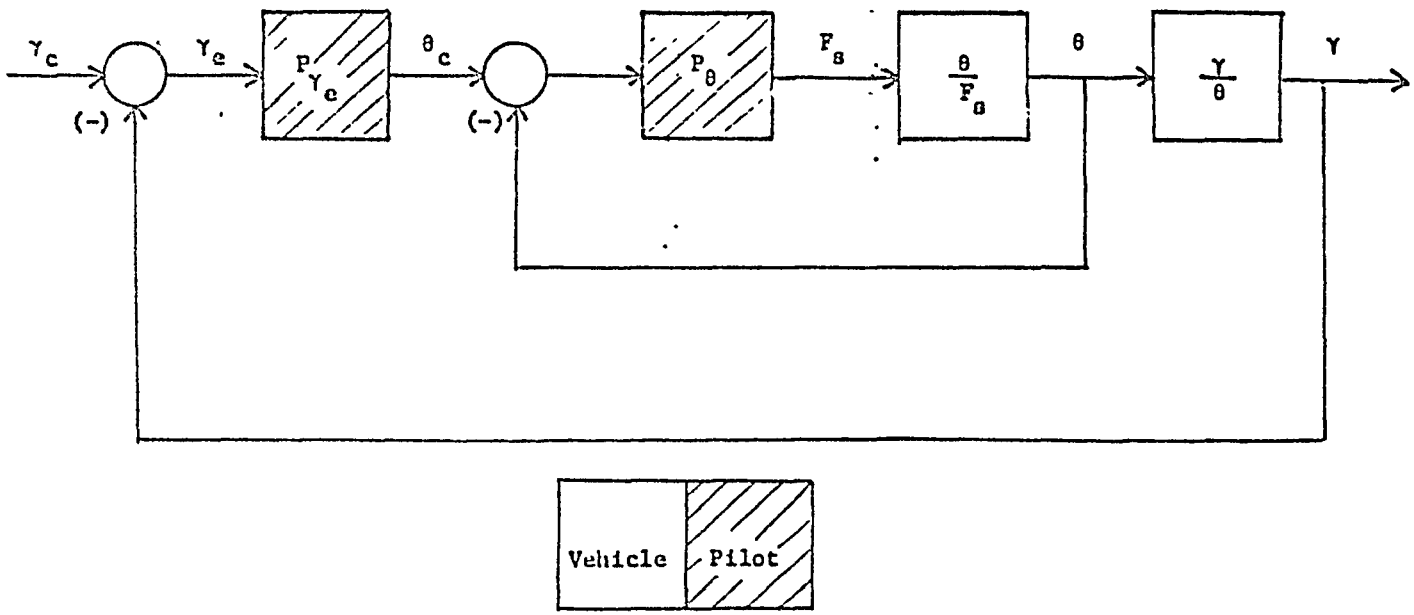

Figure 13

Neal-Smith Representation of the Flight-Path Tracking Task

Appendix A outlines the manipulations needed to transform the block diagram shown in Figure 1 to yield a result similar to Figure 13. This new block diagram arrangement can now be used to estimate the parameters used in the Neal-Smith approach. For example, the inner-loop bandwidth (closed-loop phase = -90 degrees) is important. The OC/FD analysis yields an estimate for the appropriate bandwidth. This bandwidth has been tabulated to provide insight into the appropriate choice of the inner-loop bandwidth.

Equivalent Pilot Phase Compensation (deg)- the maximum equivalent pilot phase equalization in the region of phase crossover. This is the same measure of pilot workload as used in References 3 and 4.

Low-Frequency Pilot Phase (deg)- the equivalent, single-loop pilot phase compensation at ω=0.1 rad/sec. Pitch-rate command systems result in considerably different low frequency vehicle characteristics than conventional aircraft. This parameter is an indicator of how the pilot must react to these differences.

RMS Tracking Error- the root-mean-square tracking error. An indicator of tracking performance.

Low-Frequency, Open-Loop Peak (dB)- As defined earlier (see Figure 7). Another indicator of tracking performance.

Resonance Peak (dB)- Defined as shown in Figure 14. An indicator of tracking performance and pilot/vehicle oscillatory tendencies. This was used in the original Neal-Smith analysis of the precision pitch-tracking task.

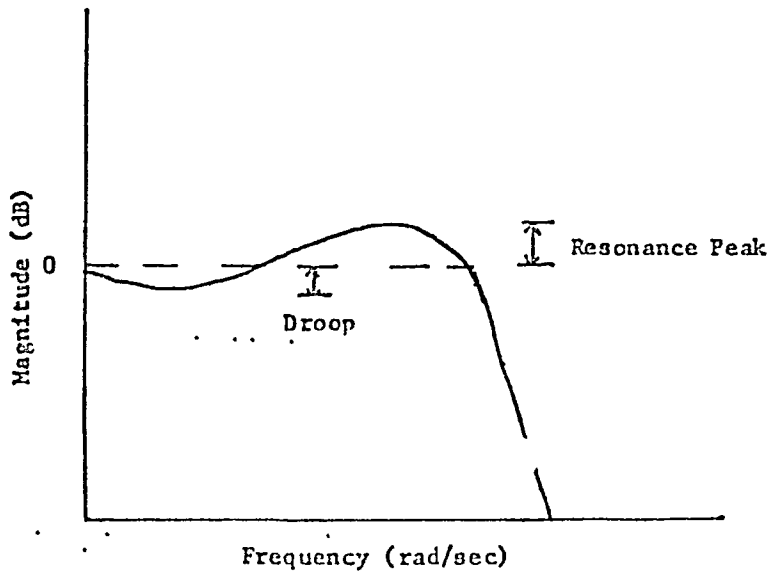

Figure 14
Definitions of Droop and Resonce Peak

Droop (dB)- Defined as shown in Figure 14. An indicator of low-frequency pilot/vehicle tracking performance.

Magnitude Crossover (rad/sec)- the frequency at which the open-loop pilot/vehicle gain equals 0 dB. This has similar implications to other bandwidth measures.

Phase Crossover (rad/sec)- the frequency at which the open-loop pilot/vehicle phase equals -180 degrees. Another bandwidth measure.

We will now examine the effect of each of the experimental variables on the system (pilot/vehicle) dynamics.

COCKPIT LOCATION RELATIVE TO CENTER OF ROTATION

One factor to consider is the pilot location relative to the center of rotation (c.r.) or to the c.g. The above analysis was not sensitive to this experimental variable. It can be easily argued that the pilot's "measurements" of the flight variables are obtained at the cockpit, where he is seated. If the pilot is far removed from the c.g. (or the c.r.), his acceleration cues (n_z) are significantly altered. Weingarten and Chalk in Ref. 6 present some flight test data that supports the importance of considering the cockpit location. They note a large variation in pilot ratings for configurations that were essentially the same except for pilot position relative to the c.r. A consistent improvement in pilot ratings was observed as the cockpit was moved forward. The hypothesis is that as the cockpit is moved forward, the pilot is provided with a more easily perceived pitch acceleration cue that supplies an early confirmation that the vehicle is responding to his command (i.e. lead).

Consider therefore, an analysis based on the assumption that the pilot operates on the flight-path, and perhaps more importantly the flight-path rate (proportional to n_z), that he senses at the cockpit. The important responses can therefore be obtained from the approximation

$$\dot{\gamma}_{c.p.} = V_o \, n_{z_{c.p.}} \qquad 2$$

where

$$n_{z_{c.p.}} = n_{z_{c.g.}} + \frac{l_p \ddot{\theta}}{g} \qquad 3$$

and l_p is defined as the distance from the c.g. to the cockpit.

At this point, attention should be turned towards the pilot's control objective. With the pilot remote from the c.g. and the c.r., the appropriate control objective is not immediately clear. The pilot could be trying to control either the flight-path of the c.g. or the c.r. Whatever the appropriate control objective is, it should be clear that the pilot's ability to control the flight-path at the cockpit is a necessary condition. If the pilot is not able to control this precisely, accurate flight-path control of any other point on the aircraft is not possible. This is illustrated nicely by the block diagram shown in Figure 15. This representation of the closed-loop dynamics shows control of the flight-path at the cockpit as an inner-loop, no matter what the ultimate control objective is.

With the use of Equations 2 and 3, the relevant responses are now those defined at the cockpit. What is significantly effected, as a result, is the location of

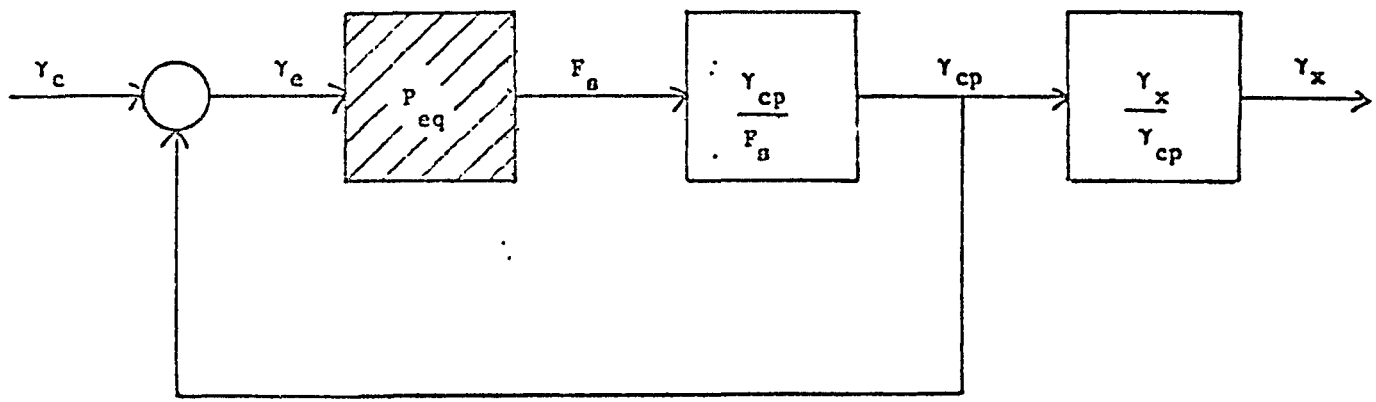

x - denotes ultimate control objective (c.g.,c.r.,...)

Figure 15

Ultimate Control Objective Block Diagram

the zeros of the n_z / F_s transfer function. This is illustrated in Figure 16. Figure 16(a) shows the zeros of the $n_{z_{c.g.}}$ / F_s transfer function. This constellation of zeros is typical of all the TIFS configurations. Figure 16(b) illustrates the results of transferring the dynamics to the cockpit for the non-shuttle configurations (cockpit 14 feet forward of c.r.). Two of the zeros remain approximately in the same location, but the other two moved to form a pair of minimum phase, but lightly damped zeros. The effect of these lightly damped zeros in the $n_{z_{c.p.}}$ / F_s transfer function can be seen from the corresponding Bode plots (Figure 17) for Conf. 1-1, for example. These zeros produce the "notch" seen in the magnitude plot near 2.6 rad/sec. The effect of these zeros is also seen in the resulting open-loop and closed-loop (θ / θ_c) pilot/vehicle Bode plots, as illustrated in Figure 18. Notches in the magnitudes are evident in both the open and closed-loop responses. One notes that the open-loop magnitude exhibits a slope near crossover close to the -20dB/decade slope required for good stability margins.

For the shuttle configurations (cockpit 10 feet behind c.r.), the dynamics at the cockpit are completely different. For these configurations the pilot's pitch acceleration cues are degraded with the apparent result of degraded pilot ratings. This trend was also noted in the flight tests of Weingarten and Chalk. For these configurations, considering the cockpit location instead of the c.g. has a lesser effect on the n_z / F_s numerator zeros. Compare Figure 19 with Figure 16, for example.

Table 3 presents the form of the $n_{z_{c.p.}}$ / F_s transfer

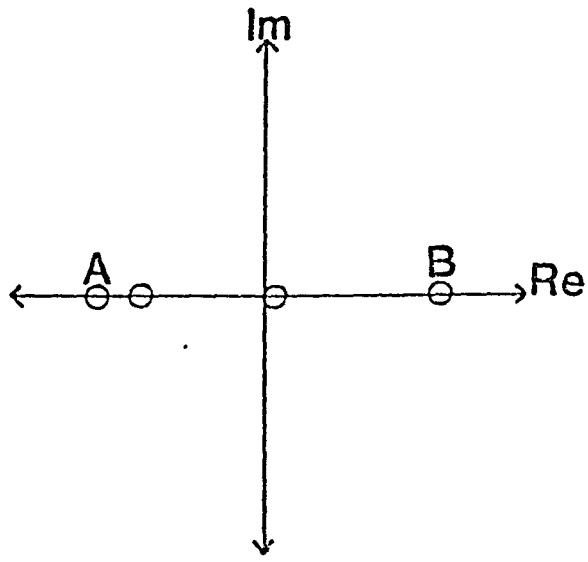

(a) at c.g.

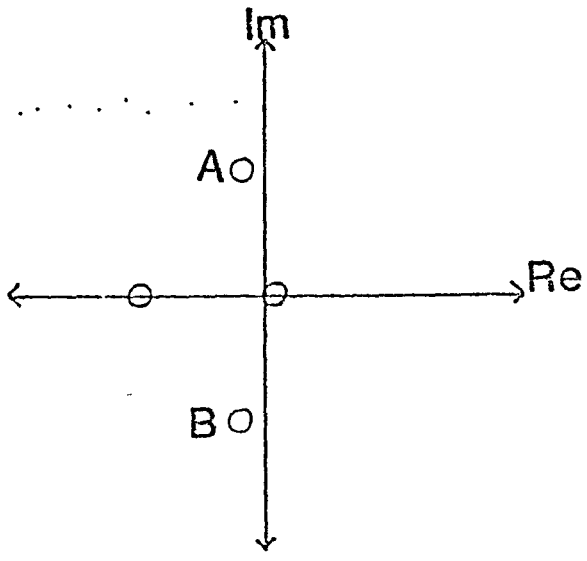

(b) at c.r.

Figure 16
Typical Zero Constellations of $\frac{n_z}{f_s}$ for Non-Shuttle Configurations

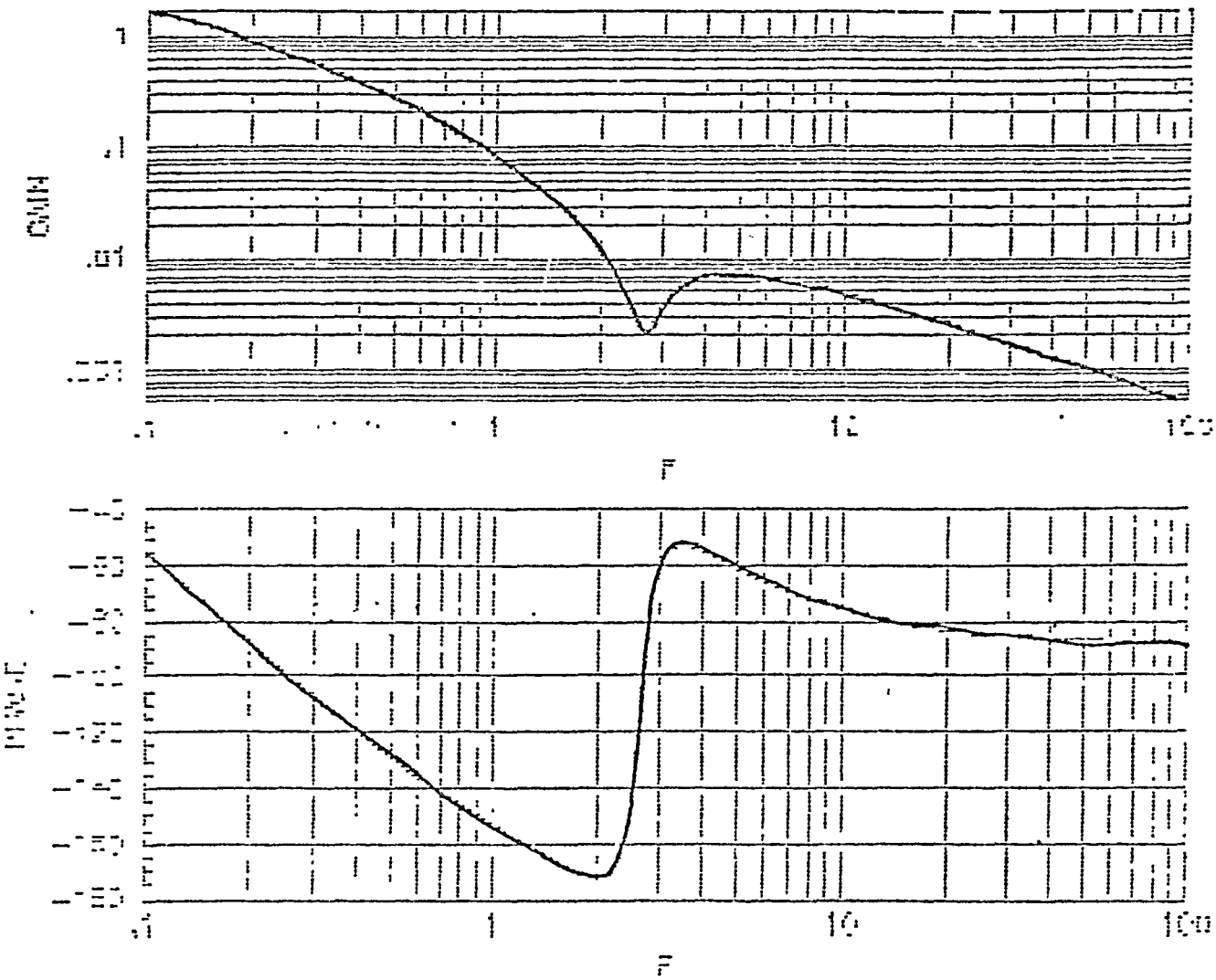

$\frac{Y_{cp}}{F_s}$ Transfer Function for Configuration 1-1

Figure 17

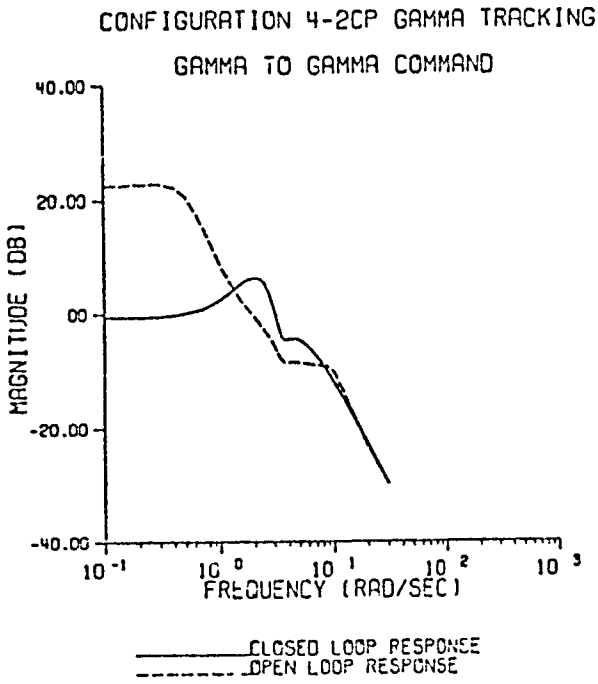

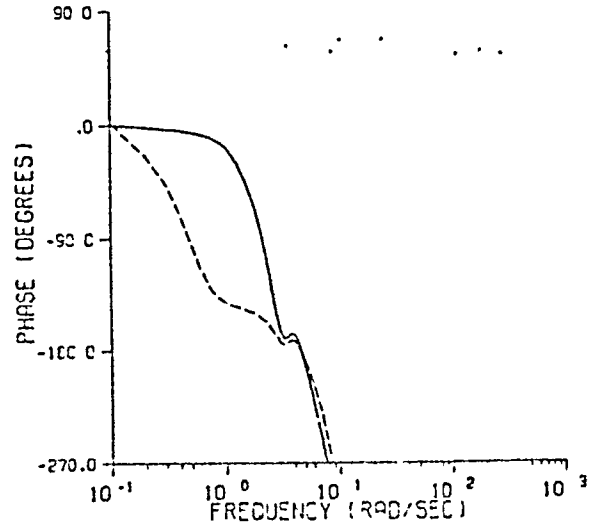

Figure 18

Effect of $\frac{n_{z_{cg}}}{\gamma_s}$ Zeros on Pilot/Vehicle Bode Plot

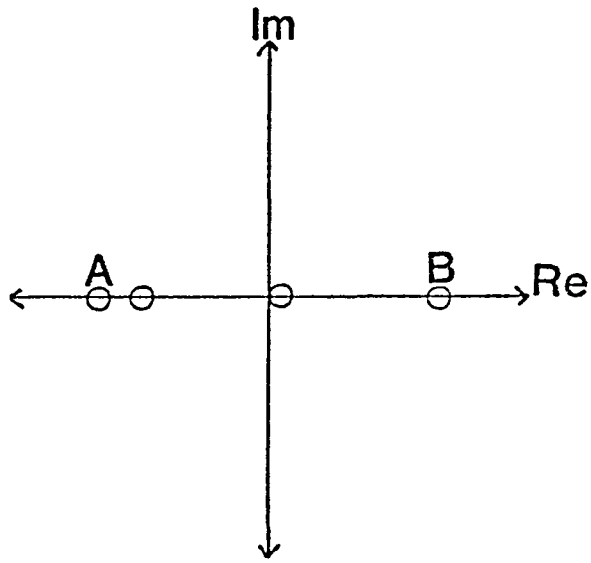

(a) at c.g.

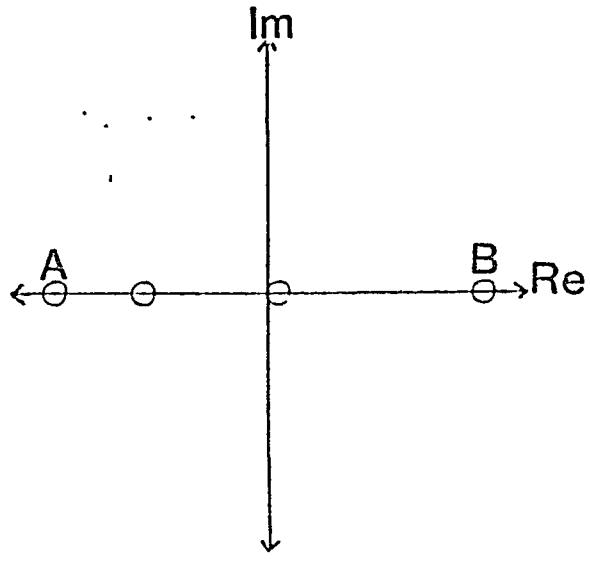

(b) at c.r.

Figure 19
Typical Zero Constellation of $\frac{n_z}{F_s}$ for Shuttle Configurations

TABLE 3

TIFS Transfer Functions (responses at c.p.)

BASL CO.:FIGURATION

$$\frac{n_z}{F_s} = \frac{K_\gamma [\zeta, \omega]_{cp} (s + z_3)(s - z_2)}{[\zeta, \omega]_{sp} (s + \lambda_\gamma')(s + \lambda_1)}$$

BASE + PREFILTER

$$\frac{n_z}{F_s} = \frac{K_\gamma [\zeta, \omega]_{cp} (s - z_2)}{[\zeta, \omega]_{sp} \cdot (s + \lambda_1)}$$

BASE + PREFILTER + W.O.

$$\frac{n_z}{F_s} = \frac{K_\gamma s [\zeta, \omega]_{cp} (s - z_2)}{[\zeta, \omega]_{sp} (s + 0.2)(s + \lambda_1)}$$

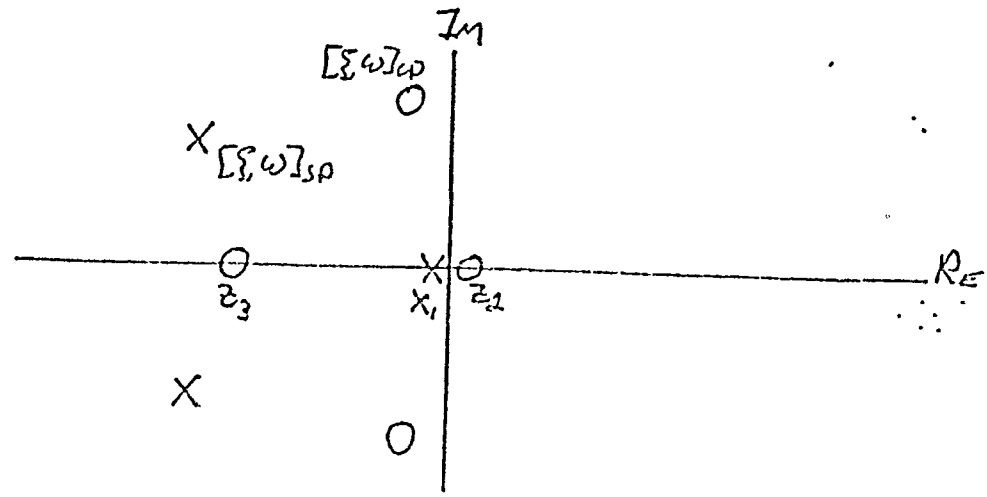

function. As mentioned earlier, only the location of two of the zeros change by evaluating the responses at the cockpit instead of the center of rotation. The new location of these zeros is dependent on the response at the c.g., the relative c.r. location, and the relative cockpit location. As a result of evaluating n_z and $\dot{\gamma}$ at the cockpit, the analysis reflects, or is sensitive to, the location of the center of rotation. This is clearly seen by comparing the open-loop pilot/vehicle Bode magnitude plots (n_z and $\dot{\gamma}$ at the cockpit) of the shuttle configurations (excluding 8-4) and the non-shuttle configurations (see Figure 20). The center of rotation for the shuttle configurations is 10 feet in front of the cockpit while for the non-shuttle configurations it is 14 feet behind the cockpit. The Bode magnitude plots clearly show that significantly different dynamics result.

The differences in the cockpit location relative to the c.r., is also evident in the step responses of the vertical acceleration at the cockpit ($n_{z_{cp}}$). For the configurations with the aft c.r., the responses at the cockpit include enhanced vertical acceleration cues. This is clearly shown in Figure 21. At the c.g., the initial response is in the opposite sense to that commanded. At the cockpit however, the initial transient response is in the direction of the commanded input. For the shuttle configurations, however, the pitch acceleration cues at the cockpit are only marginally better than the acceleration cues at the center of gravity, as shown in Figure 22. Thus these configurations have less desirable responses at the cockpit.

The lack of quality pitch acceleration cues for the shuttle configurations also results in reduced flight-path-tracking ability. It does appear however that the

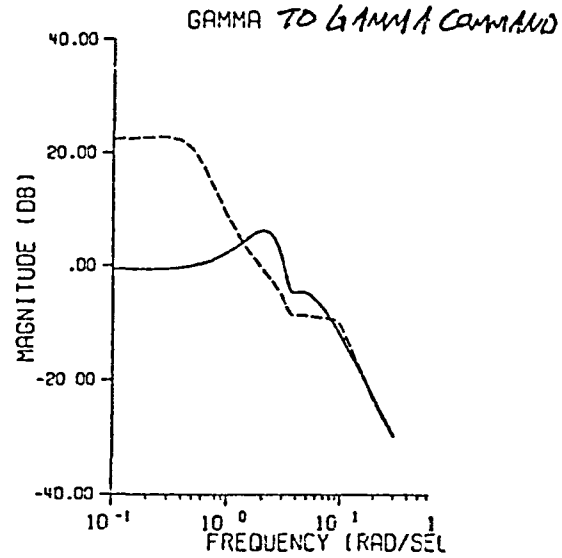

Non-Shuttle Configuration

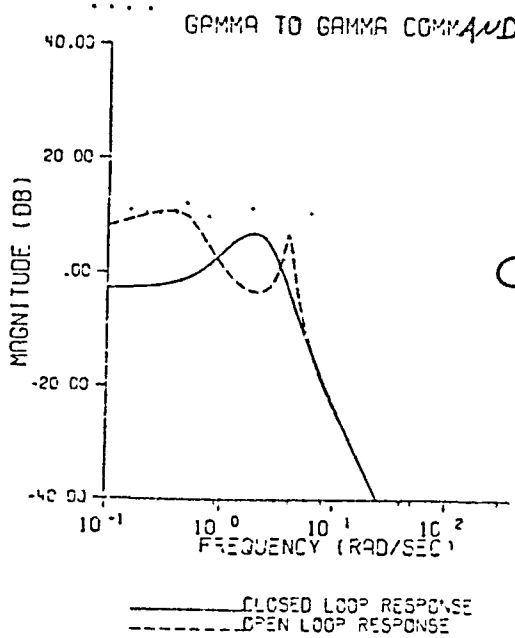

Shuttle Configuration

Figure 20
Pilot/Vehicle Bodes
Shuttle versus Non-Shuttle

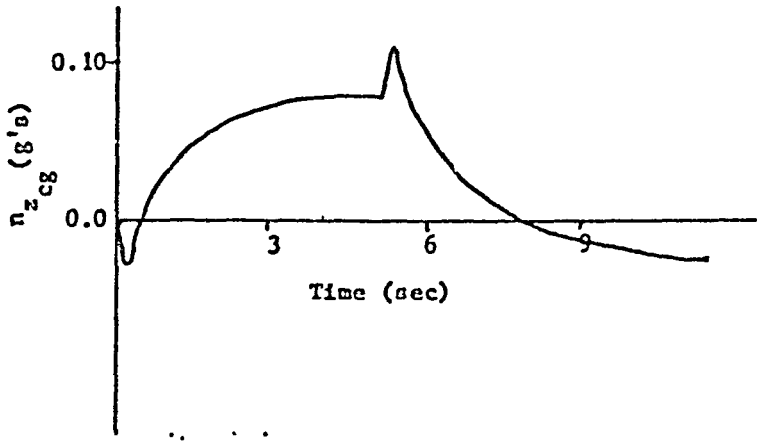

(a) at center of gravity

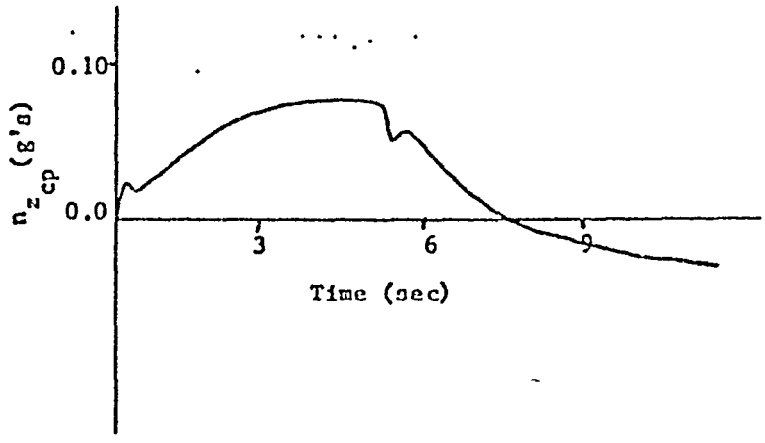

(b) at cockpit

Figure 21

Non-Shuttle n_z step responses (c.g. and c.p.)

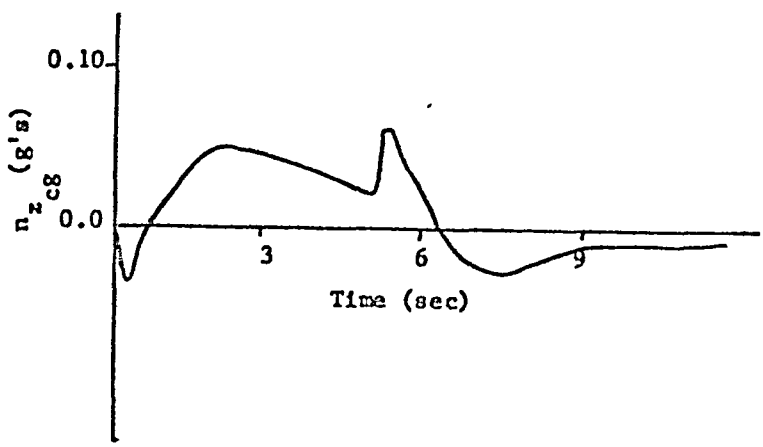

(a) at center of gravity

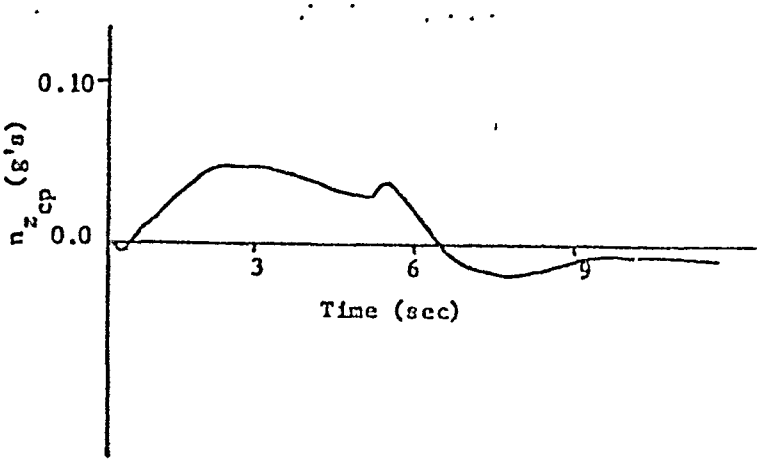

(b) at cockpit

Figure 22

Shuttle n_z Step Responses (c.g. and c.p.)

difficulties introduced in these configurations can be overcome through other design considerations since some of the shuttle configurations did receive Level 1 pilot ratings. That is not to say that the tracking ability can be significantly increased, just that other factors such as pilot workload and acceptable low frequency characteristics can compensate for this problem.

Tables 4-7 list some important variables obtained from the analysis of the response at the cockpit. (For completeness, Appendix B contains a complete listing of these variables for the analysis of flight-path response at the c.r.) These tables include results for two values of τ_n, the pilot's neuromuscular time constant. The value of 0.1 sec. was used in References 3 and 4, and was initially chosen for this study. This choice, however, resulted in extremely large distortions of the open-loop peak in the pilot/vehicle open-loop Bode magnitude plots for the shuttle configurations. A typical Bode plot is shown in Figure 23 Modeling the pilot as slightly less aggressive, or raising τ_n to 0.2 sec, eliminated these severe distortions of the open-loop Bode magnitude plots and did not significantly alter any of the other results The results discussed in the following sections are for τ_n= 0.2 sec. For completeness, however, results for both values of τ_n have been tabulated in Tables 4-7.

From these tables, Figure 24 can be constructed, for example. This is a plot of Low-Frequency Open-Loop Peak versus Equivalent Pilot Phase Compensation, similar to Figure 9. Unfortunately, this plot still does not explain these pilot ratings Therefore, at this point, further analysis into the effect of the experimental variables is called for.

Table 4

Flight-Path Analysis at c.p.: Closed-Loop Bandwidths (rad/sec)

Conf.	Pilot Ratings	τ_n=0.2		τ_n=0.1	
		Inner-Loop	Flight-Path	Inner Loop	Flight-Path
1-1	7,5	4.00	1.86	3.95	2.21
1-2	8,7,5.5	4.00	1.96	4.00	2.43
1-3	5,4,7	4.00	1.96	4.10	2.49
4-1	2.5,5	5.00	1.93	5.00	2.17
4-2	2,3	4.75	2.06	4.75	2.43
4-3	7	4.35	2.00	4.35	2.49
4-3-1	4	4.50	2.04	4.50	2.50
7-1	2.5,3	4.90	2.06	4.85	2.40
2-1	6,7	2.50	1.79	2.60	2.30
2-2	4.5,3	2.60	1.82	2.80	2.45
5-1	4.5,4.5	3.35	1.91	3.25	2.22
5-2	2,3	3.20	1.90	3.35	2.46
6-1	3,5,6	2.65	1.93	2.65	2.36
6-2	5,4,2	3.70	1.96	3.65	2.33
6-1-1	4	2.65	1.88	2.65	2 36
6-2-1	3	4.10	2.02	3.80	2.32
8-1	5.5,6	3.25	1.35	3 45	1.48
8-1-1	2	3.50	1.35	3.90	1.47
8-2	9,8,7	2.70	1.36	3.00	1.48
8-2-1	7	2.30	1.31	2.65	1.45
8-3	8,7	2 15	1.27	2.35	1.40
8-3-1	3	2.35	1.28	2.55	1.41
8-4	1	3.20	2.34	3.20	2 47
8-5	7	2.45	1.27	2.60	1.37
8-5-1	4	2 65	2 06	2.75	1.37

Table 5

Flight-Path Analysis at c.p.: Pilot Phase Considerations

(τ_n=0.2)

Conf.	Pilot Ratings	Max. Pilot Phase Comp. (deg)	Neal-Smith Inner-Loop Bandwidth	Low Freq. Pilot Phase (deg)
1-1	7,5	41.5	10.0	124
1-2	8,7,5.5	26.1	2.70	70
1-3	5,4,7	20.4	2.95	88
4-1	2.5,5	10.4	7.50	115
4-2	2,3	7.6	2.85	67
4-3	7	14.1	3.00	88
4-3-1	4	10.4	3.10	26
7-1	2.5,3	8.5	2.80	-42
2-1	6,7	67.1	11.0	125
2-2	4.5,3	53.2	2.35	69
5-1	4.5,4.5	42.6	2.05	118
5-2	2,3	40.4	2.55	67
6-1	3,5,6	58.4	10.0	125
6-2	5,4,2	18.9	2.25	115
6-1-1	4	51.2	2.15	60
6-2-1	3	16.4	2.35	52
8-1	5.5,6	60.7	2.55	93
8-1-1	2	55.8	2.55	53
8-2	9,8,7	73.0	2.35	95
8-2-1	7	80.0	2.30	66
8-3	8,7	81.5	2.25	96
8-3-1	3	77.6	2.40	57
8-4	1	-65.0	5.25	117
8-5	7	72.4	2.50	90
8-5-1	4	68.6	2.60	51

Table 5 (continued)

Flight-Path Analysis at c.g.: Pilot Phase Considerations

(τ_n=0.1)

Conf.	Pilot Ratings	Max. Pilot Phase Comp. (deg)	Neal-Smith Inner-Loop Bandwidth	Low Freq. Pilot Phase (deg)
1-1	7,5	50.7	10.5	127
1-2	8,7,5.5	36.6	2.80	76
1-3	5,4,7	35.0	3.10	99
4-1	2.5,5	18.8	7.70	116
4-2	2,3	16.5	2.90	72
4-3	7	28.1	3.20	98
4-3-1	4	17.5	3.25	35
7-1	2.5,3	17.5	2.80	-36
2-1	6,7	83.6	10.0	130
2-2	4.5,3	69.3	2.55	78
5-1	4.5,4.5	52.5	11.0	121
5-2	2,3	55.6	2.80	74
6-1	3,5,6	72.0	11.0	128
6-2	5,4,2	31.7	2.20	118
6-1-1	4	67.2	11.0	65
6-2-1	3	26.7	2.35	54
8-1	5.5,6	75.4	3.00	98
8-1-1	2	71.1	3.05	89
8-2	9,8,7	87.6	2.60	100
8-2-1	7	94.4	2.70	72
8-3	8,7	97.2	2.60	101
8-3-1	3	93.3	2.75	73
8-4	1	-58.4	6.10	118
8-5	7	87.7	2.85	94
8-5-1	4	84.5	3.00	57

Table 6

Flight-Path Analysis at c.p.: Tracking Considerations

(τ_n=0.2)

Conf.	Pilot Ratings	RMS Tracking Error	Low Freq. O.L. Peak (dB)	Resonance Peak (dB)
1-1	7,5	1.357	18.8	4.189
1-2	8,7,5.5	0.638	21.9	6.644
1-3	5,4,7	0.751	21.3	6.497
4-1	2.5,5	1.352	18.9	3.655
4-2	2,3	0.606	22.8	6.319
4-3	7	0.738	21.7	6.366
4-3-1	4	0.732	20.7	6.247
7-1	2.5,3	0.854	22.0	5.570
2-1	6,7	1.372	18.2	5.000
2-2	4.5,3	0.710	20.2	7.120
5-1	4.5,4.5	1.356	18.8	4.338
5-2	2,3	0.675	20.9	6.958
6-1	3,5,6	1.356	18.9	4.776
6-2	5,4,2	1.354	18.9	4.105
6-1-1	4	1.356	18.5	4.776
6-2-1	3	1.348	19.0	3.989
8-1	5.5,6	1.529	11.9	6.669
8-1-1	2	1.531	11.3	6.443
8-2	9,8,7	1.552	10.7	7.331
8-2-1	7	1.307	10.9	6.871
8-3	8,7	1.597	10.8	6.881
8-3-1	3	1.587	10.6	6.824
8-4	1	1.188	20.2	3.120
8-5	7	1.600	10.7	6.733
8-5-1	4	1.600	10.2	6.530

Table 6 (continued)

Flight-Path Analysis at c.p.: Tracking Considerations

(τ_n=0.1)

Conf.	Pilot Ratings	RMS Tracking Error	Low Freq. O.L. Peak (dB)	Resonance Peak (dB)
1-1	7,5	1.351	19.7	3.199
1-2	8,7,5.5	0.560	24.6	5.670
1-3	5,4,7	0.677	24.8	5.250
4-1	2.5,5	1.352	19.4	2.867
4-2	2,3	0.558	25.1	5.449
4-3	7	0.674	24.8	5.174
4-3-1	4	0.675	24.7	5.078
7-1	2.5,3	0.831	23.6	4.478
2-1	6,7	1.353	19.9	3.625
2-2	4.5,3	0.586	25.0	5.990
5-1	4.5,4.5	1.347	19.7	3.525
5-2	2,3	0.571	25.0	5.805
6-1	3,5,6	1.049	20.0	3.548
6-2	5,4,2	1.348	19.6	3.054
6-1-1	4	1.342	19.9	3.460
6-2-1	3	1.346	19.5	2.995
8-1	5.5,6	1.483	13.3	5.467
8-1-1	2	1.487	12.6	5.234
8-2	9,8,7	1.510	12.4	5.536
8-2-1	7	1.535	12.5	5.491
8-3	8,7	1.561	12 3	5.452
8-3-1	3	1.545	12.1	5.426
8-4	1	1.189	20.7	2.422
8-5	7	1.560	11.9	5.435
8-5-1	4	1.553	11.4	5.390

Table 7

Flight-Path Analysis at c.p.: Other Considerations

(τ_n=0.2)

Conf.	Pilot Ratings	Droop (dB)	Magnitude Crossover (rad/sec)	Phase Crossover (rad/sec)
1-1	7,5	-1.257	1.65	4.75
1-2	8,7,5.5	-0.699	1.85	4.20
1-3	5,4,7	-0.783	1.80	3.00
4-1	2.5,5	-1.240	1.70	4.90
4-2	2,3	-0.636	1.90	4.50
4-3	7	-0.755	1 85	3.10
4-3-1	4	-0.746	1.85	3.15
7-1	2.5,3	-0.790	1.90	4.70
2-1	6,7	-1.335	1.65	4.25
2-2	4.5,3	-0.836	1.65	2.60
5-1	4.5,4.5	-1.259	1.75	4.50
5-2	2,3	-0.772	1.75	2.75
6-1	3,5,6	-1.248	1.75	4.15
6-2	5,4,2	-1.248	1.80	4.45
6-1-1	4	-1.295	1.70	4.10
6-2-1	3	-1.230	1.80	4.50
8-1	5.5,6	-2.338	1.20	2.15
8-1-1	2	-2.649	1.20	2.20
8-2	9,8,7	-2.456	1.15	2.15
8-2-1	7	-2.585	1.15	2.05
8-3	8,7	-2.584	1.15	2.00
8-3-1	.3	-2.656	1.15	2.05
8-4	1	-1.033	2.00	4.40
8-5	7	-2.617	1.15	2.05
8-5-1	4	-2.926	1.15	2.05

Table 7 (continued)

Flight-Path Analysis at c.p.: Other Considerations

(τ_n=0.1)

Conf.	Pilot Ratings	Droop (dB)	Magnitude Crossover (rad/sec)	Phase Crossover (rad/sec)
1-1	7,5	-1.131	1.90	5.00
1-2	8,7,5.5	-0.490	2.20	4.90
1-3	5,4,7	-0.553	2.20	4.70
4-1	2.5,5	-1.172	1.90	5.00
4-2	2,3	-0.497	2.20	5.00
4-3	7	-0.552	2.20	4.75
4-3-1	4	-0.562	2.20	4.75
7-1	2.5,3	-0.673	2.15	5.00
2-1	6,7	-1.102	2 10	4.85
2-2	4.5,3	-0 503	2.25	4.75
5-1	4.5,4.5	-1.137	1.95	4.85
5-2	2,3	-0 503	2.25	4.75
6-1	3,5,6	-1.097	2.10	4.75
6-2	5,4,2	-1.137	2.05	4.90
6-1-1	4	-1.112	2.10	4.80
6-2-1	3	-1.153	2.00	4.90
8-1	5.5,6	-2.036	1.30	2.60
8-1-1	2	-2.305	1.30	2.60
8-2	9,8,7	-2.116	1.25	2.60
8-2-1	7	-2.196	1.30	2.50
8-3	8,7	-2.214	1 20	2.40
8-3-1	3	-2.284	1.20	2.40
8-4	1	-0.985	2 00	5.00
8-5	7	-2.317	1 20	2.35
8-5-1	4	-2.561	1.20	2.35

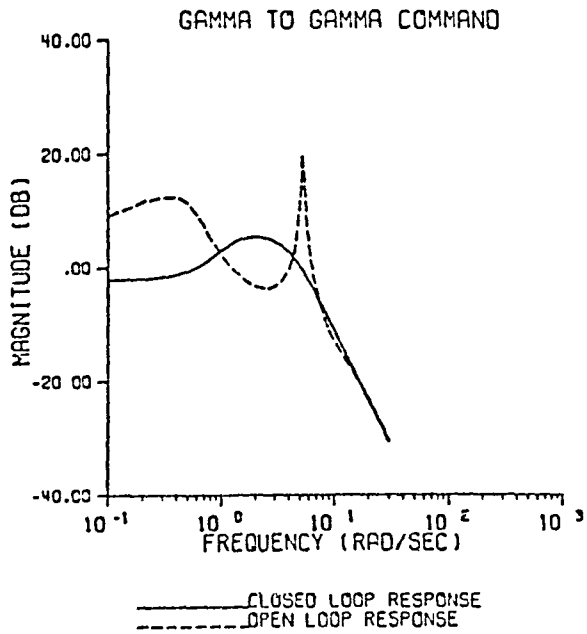

Figure 23
Typical Shuttle Pilot/Vehicle Bode
for $\tau_n = 0.1$ rad/sec.

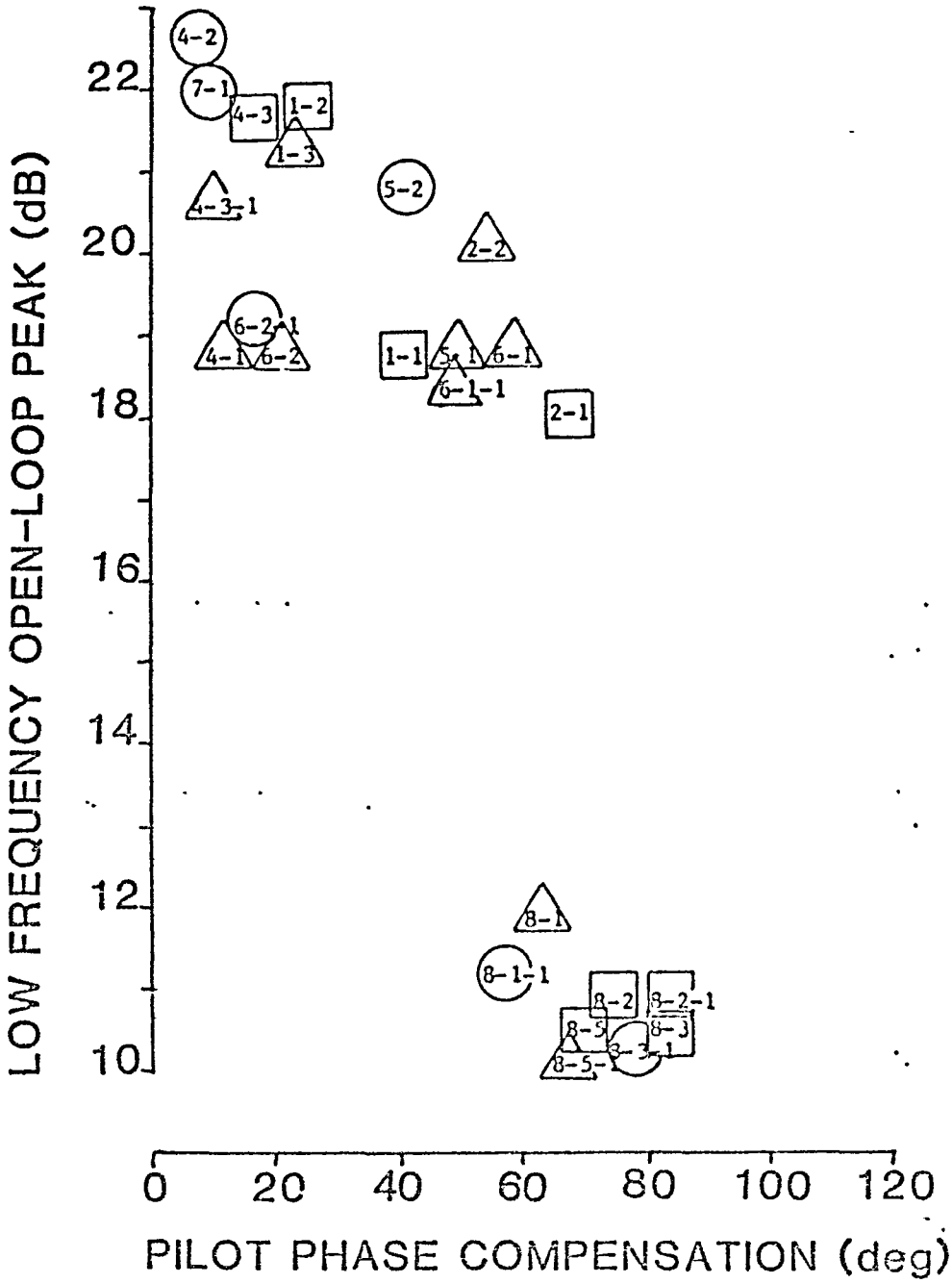

Figure 24

TIFS Results at c.p.j Low-Frequency Open-Loop Peak versus Equivalent Pilot Phase Compensation

PREFILTER

The dynamics introduced by the pitch-rate command system (K_I , λ'_2) result in an additional lag in the pitch attitude dynamics. That is, K_I, a zero, is larger than λ'_2, a pole, (see Table 2). The introduction of the lead/lag prefilter cancels this lag and results in more "conventional" aircraft dynamics in the region of crossover. As Figure 25 shows, this in turn results in an increase in pitch attitude phase in the region of crossover. This should reduce the required Equivalent Pilot Phase Compensation (in the γ / γ_c loop) as Figure 26 indicates.

The introduction of the prefilter also restores the conventional attitude dependence on 1 / T_{θ_2} that was lost in the implementation of the rate command control system. This also re-introduces the pitch overshoot associated with conventional flight vehicles (See Figure 27). At first glance, the rate command system (no prefilter) would appear to be preferable, exhibiting an excellent pitch-rate response to a step input (i.e. good rise time with minimal overshoot). In fact, the control system was designed with this in mind. The important variables in the flared landing task however are flight-path-angle, γ, vertical acceleration, n_z (proportional to γ), and altitude, h. As Figure 27 indicates, the pure rate command system has a sluggish response to these flight variables. On the other hand, with the additional of the prefilter (restoring pitch overshoot), the system displays a much quicker response. This should result in improved system performance which will manifest itself in an increased Flight-Path Bandwidth. Figure 28 displays that this is indeed true.

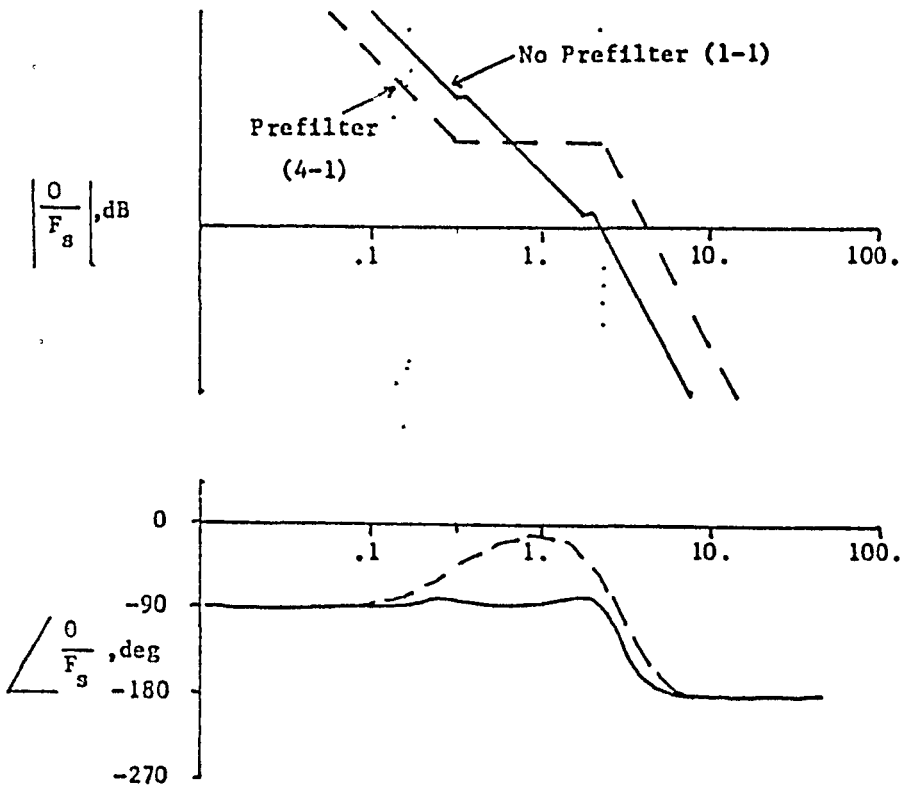

Figure 25

Effect of Prefilter on $\frac{\theta}{F_s}$

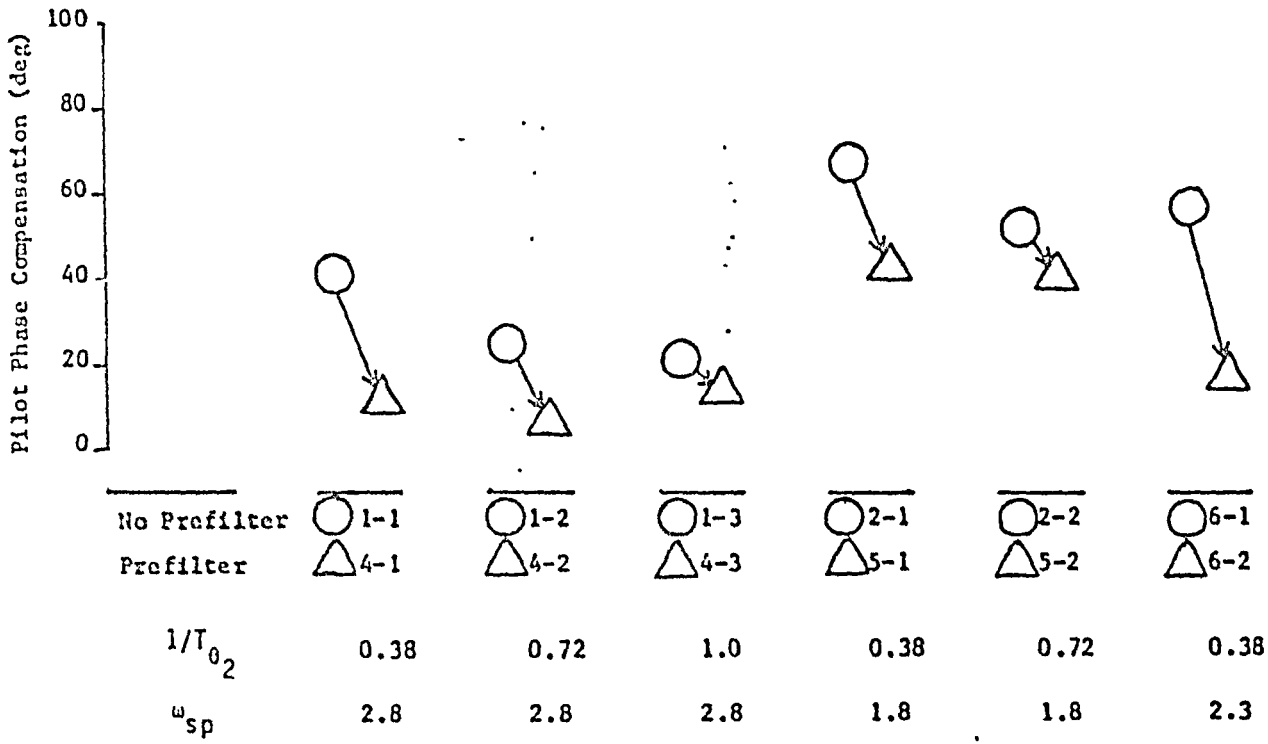

Figure 26

Effect of Prefilter on Equivalent Pilot Phase Compensation

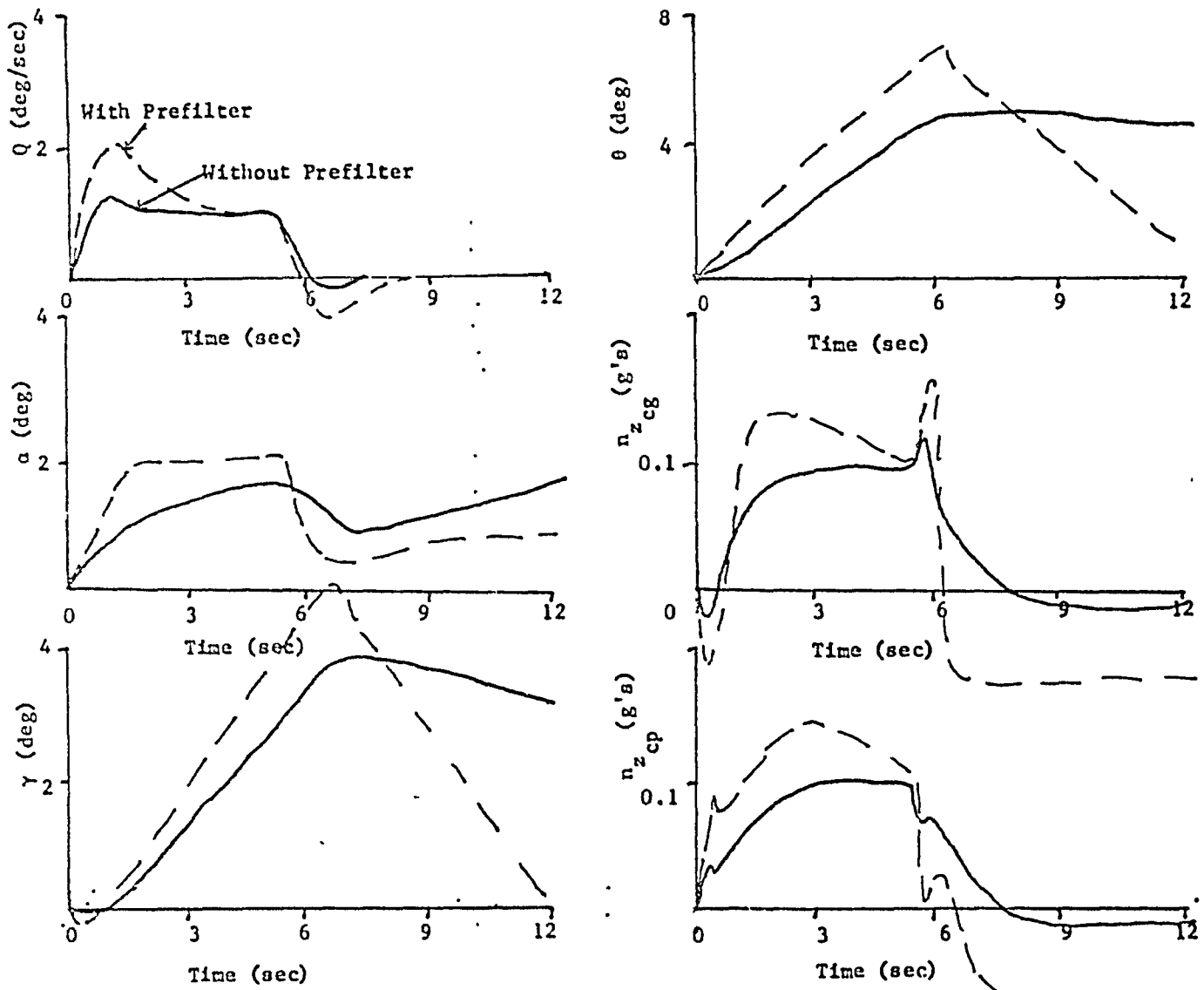

Figure 27

Effect of Prefilter on Flight Variable Step Responses.

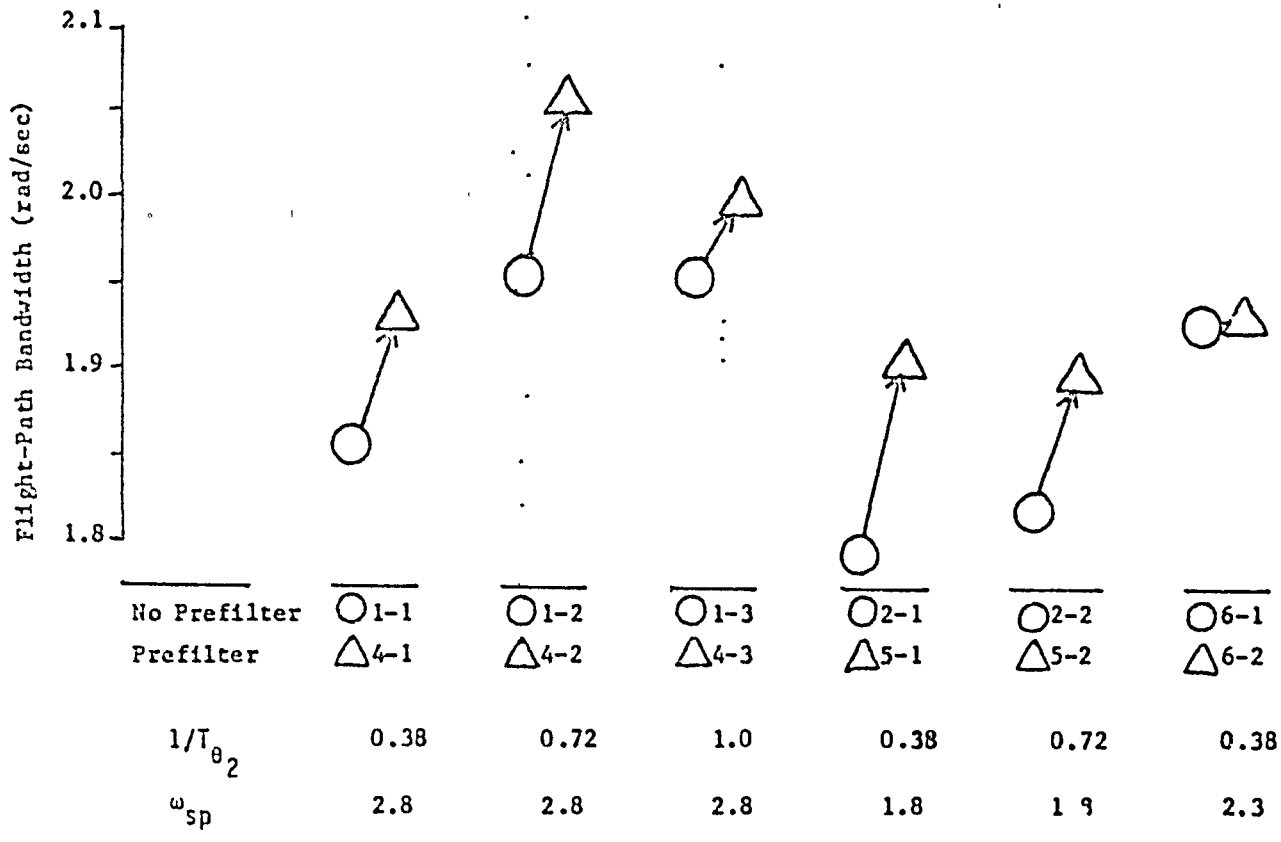

Figure 28

Effect of Prefilter on Flight-Path Bandwidth

Figure 27 also indicates a quickened θ response with the addition of the prefilter. This should result in an increase in the bandwidth of the inner pitch-attitude loop (see Figure 1). This is shown clearly in Figure 29. This again indicates the advantages of maintaining the conventional pitch-attitude overshoot.

Since the prefilter increases the system bandwidth as well as reducing the pilot workload (phase lead), one would expect the overall pilot ratings to improve. Figure 30 indicates that this is indeed true. The exception to this is Configuration 4-3. It received about the same rating as Conf. 1-3. A simple explanation for this exists. In this case, the prefilter did not significantly alter the vehicle dynamics because of the high value of $1 / T_{\theta_2}$. This is clearly shown in Figure 31.

Finally, as Figure 32 indicates, the addition of the prefilter significantly reduces the vehicle's PIO tendencies as measured on the PIO Tendency Rating Scale. The reduced Equivalent Pilot Phase Compensation is partially responsible for this since pilot phase lead distorts the open-loop, pilot/vehicle Bode magnitude plot in the region of crossover. The less lead the pilot is required to introduce, the less distortion there is in the magnitude plot and therefore stability robustness is improved.

WASHOUT FILTER

The washout filter was added to provide monotonic pitch stick forces in the landing flare. This results in a pitch response similar to a conventional aircraft by changing from a pitch-rate command to a pitch-position command system at low frequencies. This is illustrated in

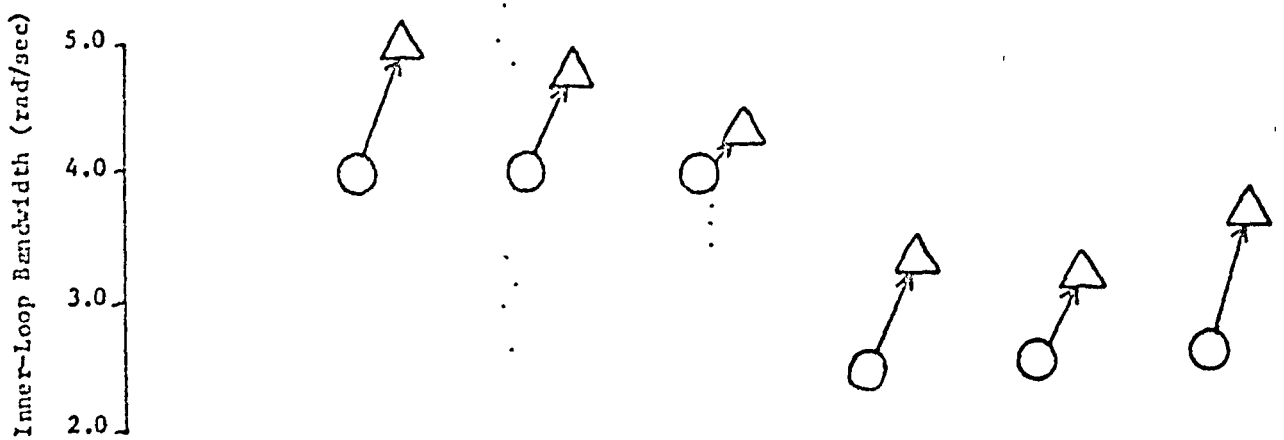

No Prefilter	○ 1-1	○ 1-2	○ 1-3	○ 2-1	○ 2-2	○ 6-1
Prefilter	△ 4-1	△ 4-2	△ 4-3	△ 5-1	△ 5-2	△ 6-2
$1/T_{\theta_2}$	0.38	0.72	1.0	0.38	0.72	0.38
ω_{sp}	2.8	2.8	2.8	1.8	1.8	2.3

Figure 29

Effect of Prefilter on Inner-Loop Bandwidth

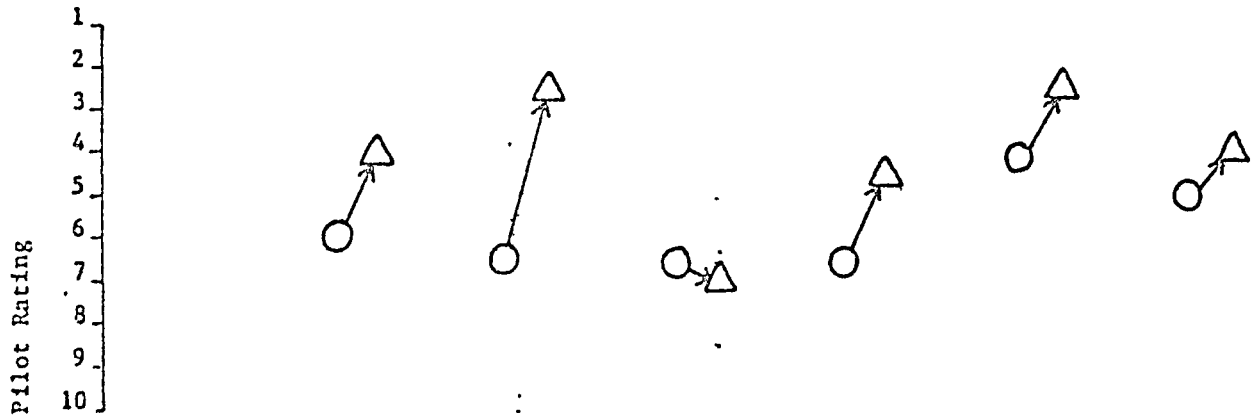

No Prefilter	○1-1	○1-2	○1-3	○2-1	○2-2	○6-1
Prefilter	△4-1	△4-2	△4-3	△5-1	△5-2	△6-2
$1/T_{a_2}$	0.38	0.72	1.0	0.38	0.72	0.38
ω_{sp}	2.8	2.8	2.8	1.8	1.8	2.3

Figure 30

Effect of Prefilter on Pilot Rating

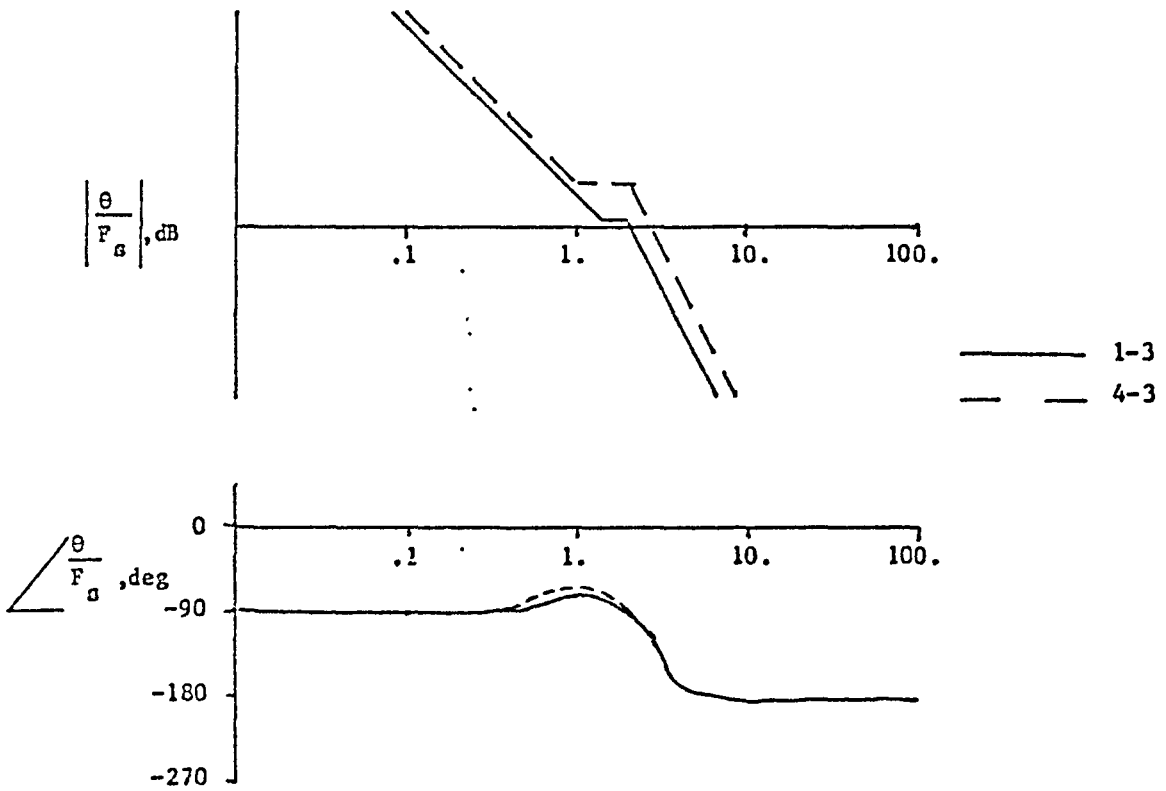

Figure 31

Effect of Prefilter on Conf. 1-3

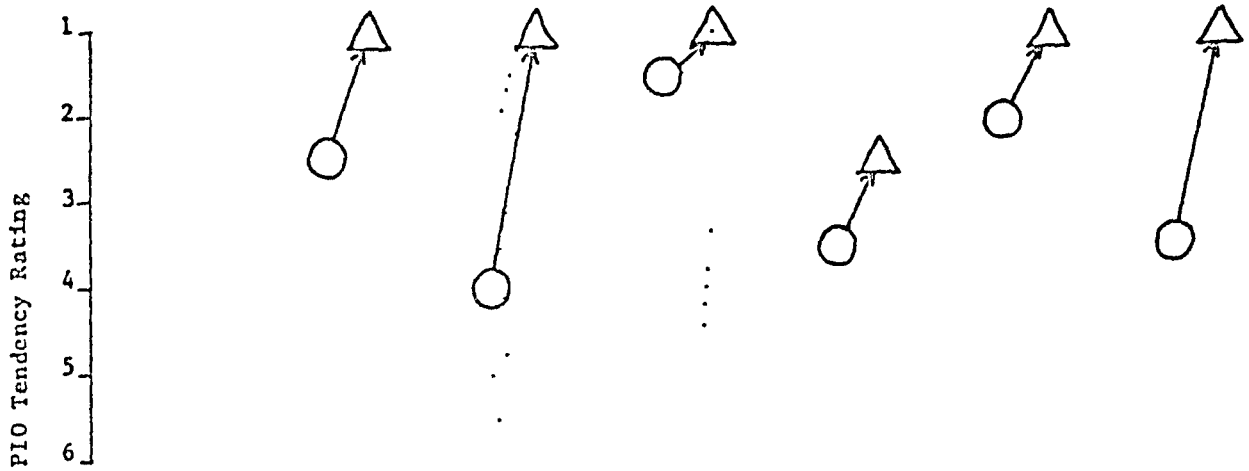

No Prefilter	○1-1	○1-2	○1-3	○2-1	○2-2	○6-1
Prefilter	△4-1	△4-2	△4-3	△5-1	△5-2	△6-2
$1/T_{\theta_2}$	0.38	0.72	1.0	0.36	0.72	0.38
ω_{sp}	2.8	2.8	2.8	1.8	1.8	2.3

Figure 32

Effect of Prefilter on PIO Tendencies

Figure 33. At first glance the rate command pitch response would appear desirable since it exhibits the characteristic K/s behavior which is required for good tracking. However, pitch-tracking is not the ultimate objective in the landing task. The important variables are flight-path-angle (or sink rate), $\dot{h}$, and altitude, h. The K/s behavior in the θ / F_s transfer function translates into K/s^2 behavior at low frequencies in the h/F_s transfer function. This is known to be much harder to control than a K/s plant (or even a pure gain) and results in pilots adopting a pulse control strategy. Pilots find this objectionable. This pulse control technique also results in a floating tendency in the aircraft and requires the pilot to push the stick forward near the ground. Pilots familiar with conventional aircraft dynamics find this very objectionable.

On the other hand, with the washout filter (pseudo-conventional dynamics), the h/F_s transfer function exhibits K/s behavior at low frequencies (much easier to control). With this type of plant, the pilots are able to use continuous control inputs instead of a pulse control strategy. Also, since at low frequencies the pitch dynamics are position command, the pilot is not forced to push the stick near the runway.

Figure 34 shows the significant differences in the low frequency flight-path phase between the pitch-rate configurations and a conventional aircraft (7-1). The absence of the conventional phugoid mode in the pitch-rate command configurations results in significantly different phase characteristics at low frequencies. This accounts for the fact that Conf. 7-1 has a Low Frequency Pilot Phase of -45 degrees whereas the TIFS configurations have values of this parameter between 30 and 130 degrees. The

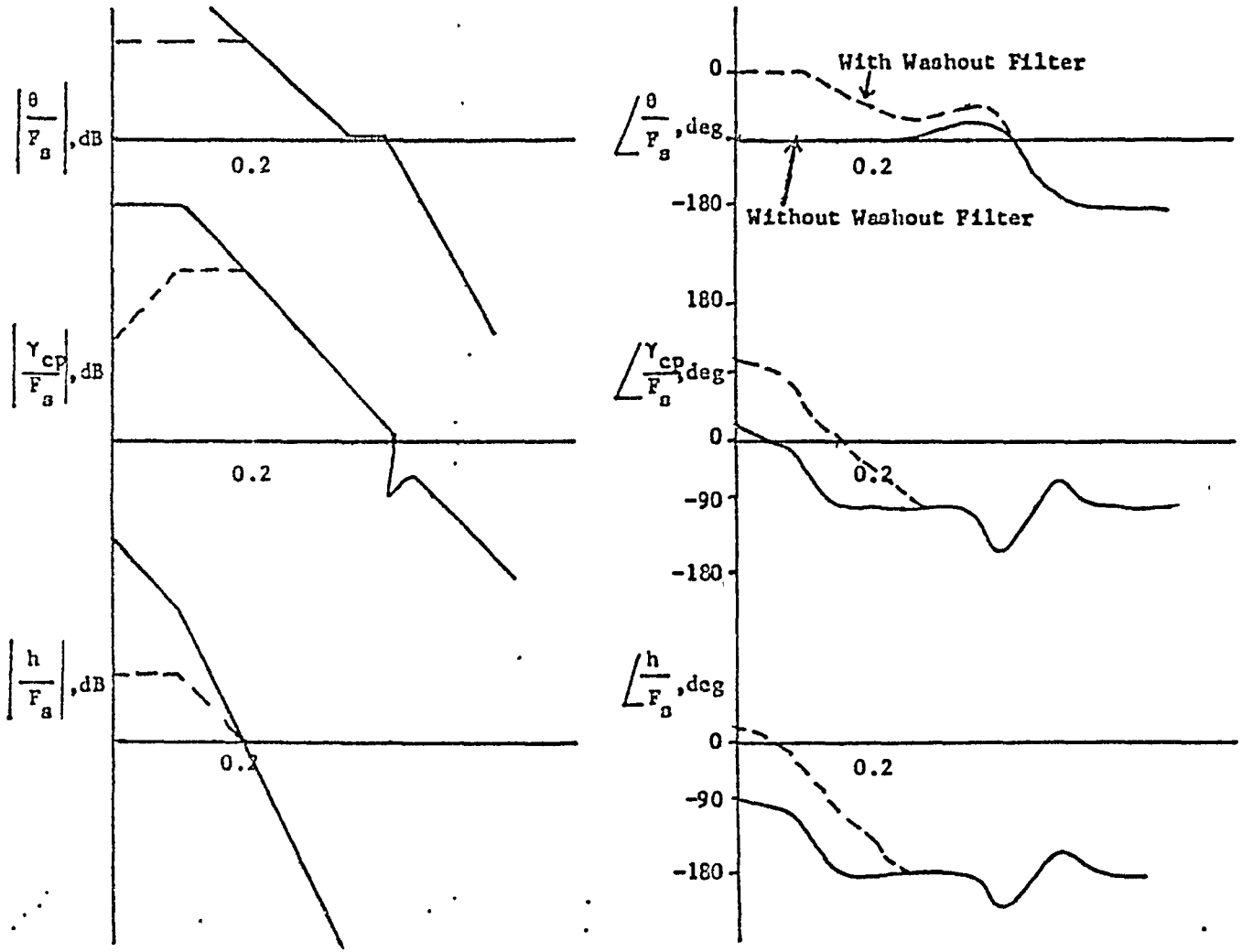

Figure 33

Effect of ~~Prefilter~~ Washout Filter on $\frac{\theta}{F_s}$, $\frac{\gamma_{cp}}{F_s}$, and $\frac{h}{F_s}$

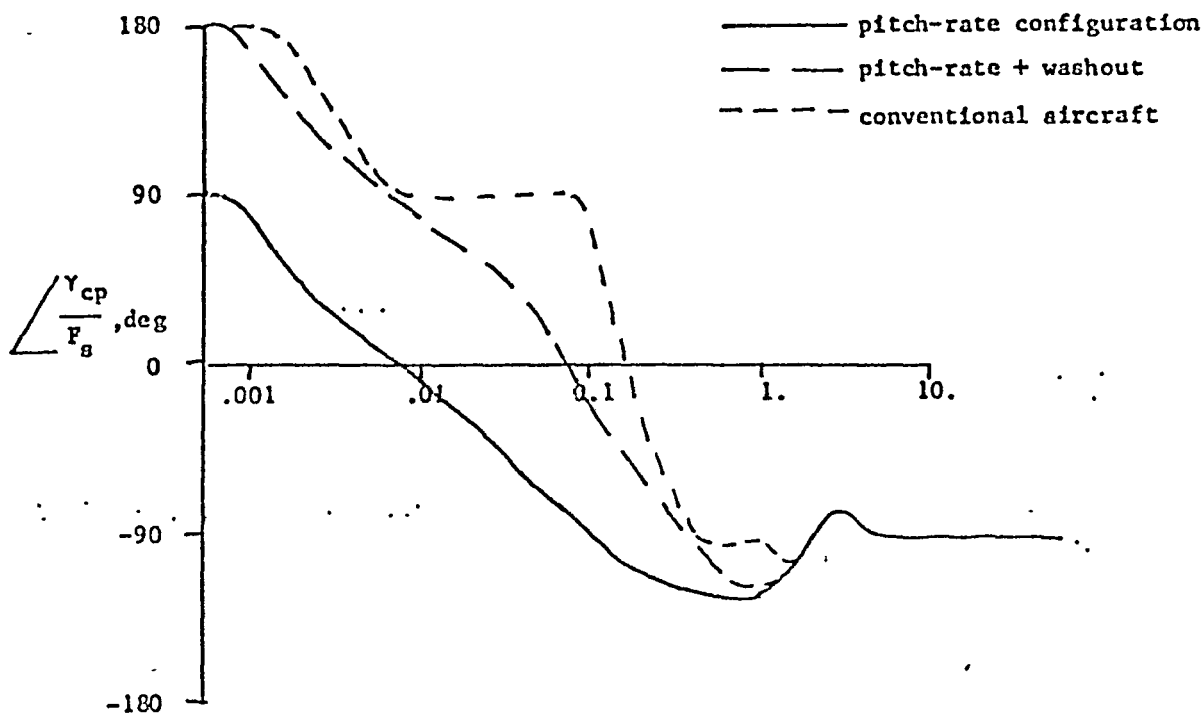

Figure 34

Effect of Washout Filter on Low-Frequency Vehicle Phase

washout filter significantly reduces this difference, as Figure 34 shows.

The washout filter also reduces the pilot/vehicle PIO tendencies in the cases where this is a problem as shown in Figure 35. This can be attributed to many factors. First, as mentioned earlier, the addition of the washout filter results in low frequency dynamics which are easier to control. These "easier" dynamics require less pilot work (phase), thus the pilot is less likely to inadvertently initiate an undesired oscillation. Secondly, the continuous control inputs resulting from the addition of the washout filter are less likely to initiate a PIO than the abrupt stick forces associated with a pulse control strategy. Finally, the washout filter restores the conventional, low-frequency aircraft dynamics that pilots are familiar with. The more familiar a pilot is with an aircraft, the less likely it is that he will inadvertently initiate a PIO. Admittedly, with training and experience, this last factor can be eliminated, but, for these flight tests, this possibility cannot be eliminated.

From the above arguments, it is clear that low frequency vehicle characteristics are an important consideration in determining flying qualities in the landing task. Our analysis therefore should be sensitive to these factors. Another look at Figure 33 indicates that the low frequency pitch attitude phase is increased by 90 degrees at low frequencies with the addition of the washout filter. In addition, this figure indicates that the same is true of the $\dot{\gamma} / F_s$ transfer function. This increase in vehicle phase at low frequencies should result in a corresponding decrease in the phase the pilot must introduce at these low frequencies. Figure 36 shows that

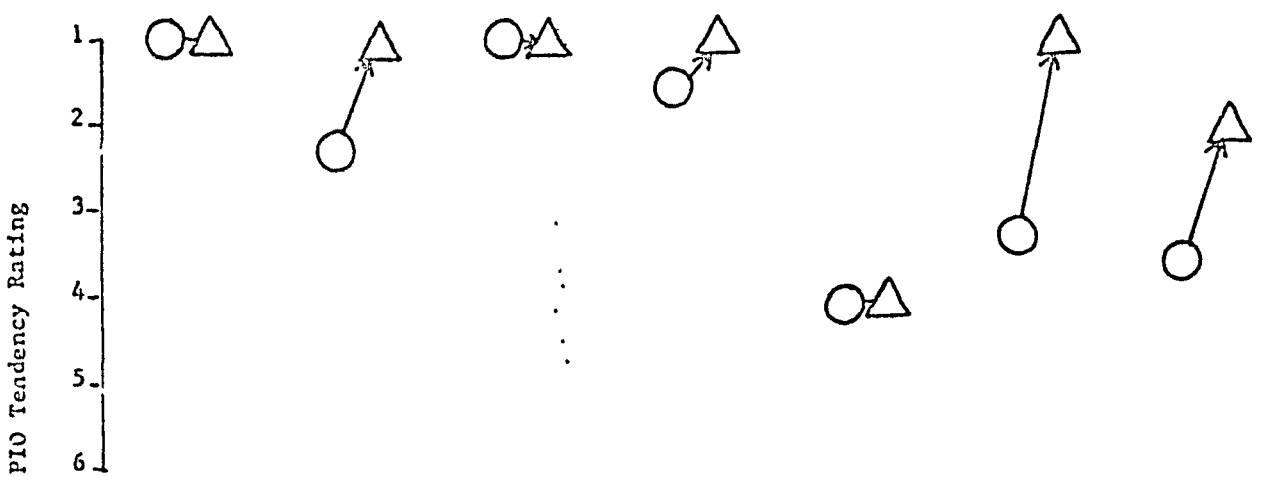

	○ 4-3 △ 4-3-1	○ 6-1 △ 6-1-1	○ 6-2 △ 6-2-1	○ 8-1 △ 8-1-1	○ 8-2 △ 8-2-1	○ 8-3 △ 8-3-1	○ 8-5 △ 8-5-1
$1/T_{\theta_2}$	1.0	0.38	0.38	0.40	0.40	0.40	0.40
ω_{sp}	2.8	2.3	2.3	1.45	1.09	1.45	1.45

Figure 35

Effect of Washout Filter on PIO Tendencies

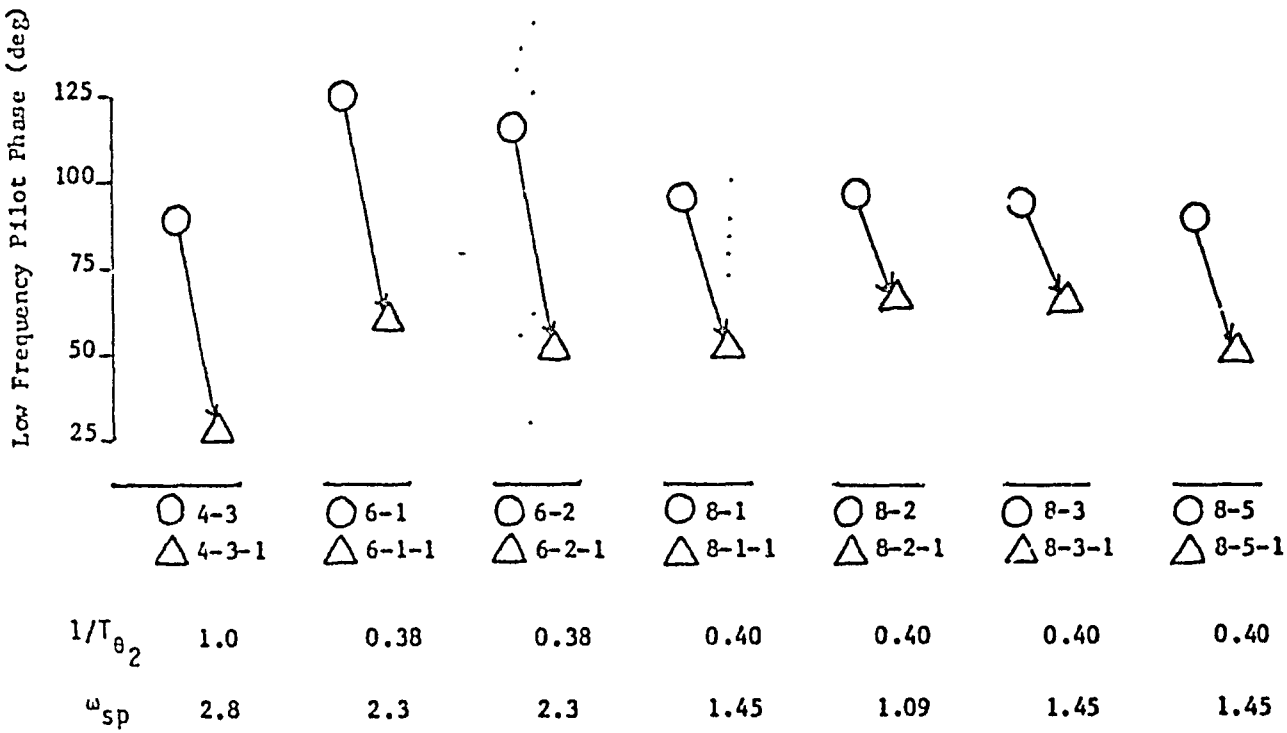

$1/T_{\theta_2}$	1.0	0.38	0.38	0.40	0.40	0.40	0.40
ω_{sp}	2.8	2.3	2.3	1.45	1.09	1.45	1.45

Figure 36

Effect of Washout Filter on Low-Frequency Pilot Phase

this is indeed the case. This figure indicates the effect that adding the washout filter has on the equivalent, single-loop pilot phase compensation as measured at ω=0.1 rad/sec. In all cases it decreased considerably.

When the plant exhibits a K/s pitch attitude behavior at low frequencies, it was shown above that the pilot introduces more lead at these frequencies to compensate. This means that the pilot is behaving like a differentiator at these frequencies. Figure 37 shows this is the case for Conf (4-3), while the addition of the washout filter results in pilot dynamics exhibiting less lead at these low frequencies (Conf 4-3-1). This is also shown nicely in Figure 37.

If all of the above arguments have been correct, the addition of the washout filter to the TIFS pitch rate configurations should result in improved pilot ratings. This is indeed the case as Figure 38 clearly shows.

VARIATION OF $1 / T_{\theta_2}$; Without Prefilter

A characteristic of high gain pitch-rate command systems is that the attitude dynamics are independent of $1 / T_{\theta_2}$. The pole introduced by the control system, λ'_2, cancels $1 / T_{\theta_2}$ in the θ / F_s transfer function and leaves the transfer function shown in Table 2. As Figure 39 indicates, the pitch attitude inner-loop bandwidth is invariant with changes in $1 / T_{\theta_2}$ in these cases.

The flight-path dynamics, however, are not independent of $1 / T_{\theta_2}$. As Table 3 shows, λ'_2 appears in the denominator of the γ / F_s transfer function ($\lambda'_2 \approx 1 / T_{\theta_2}$). As λ'_2 ($1 / T_{\theta_2}$) is increased, the

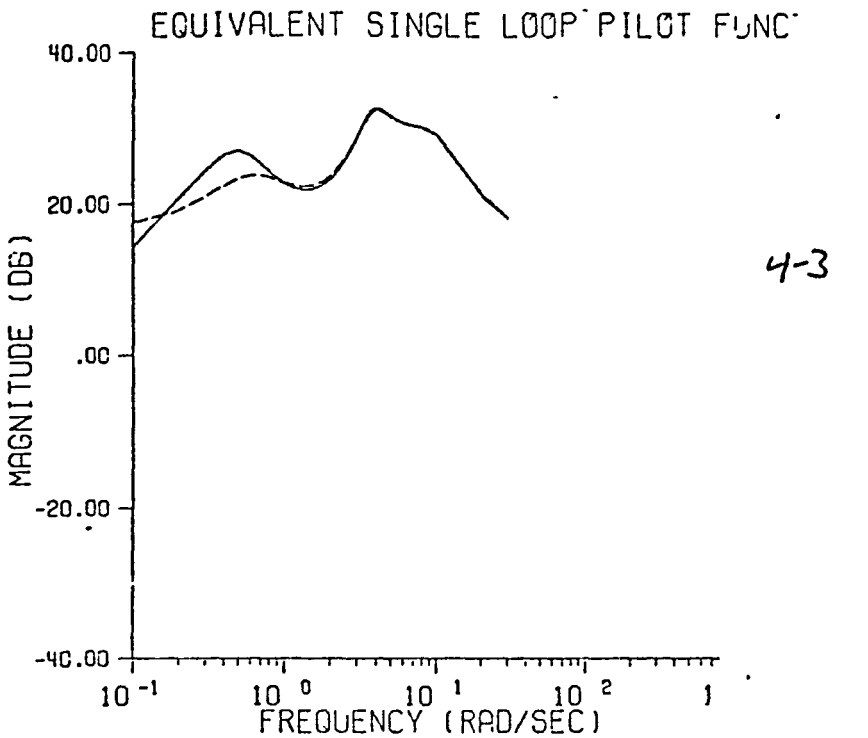

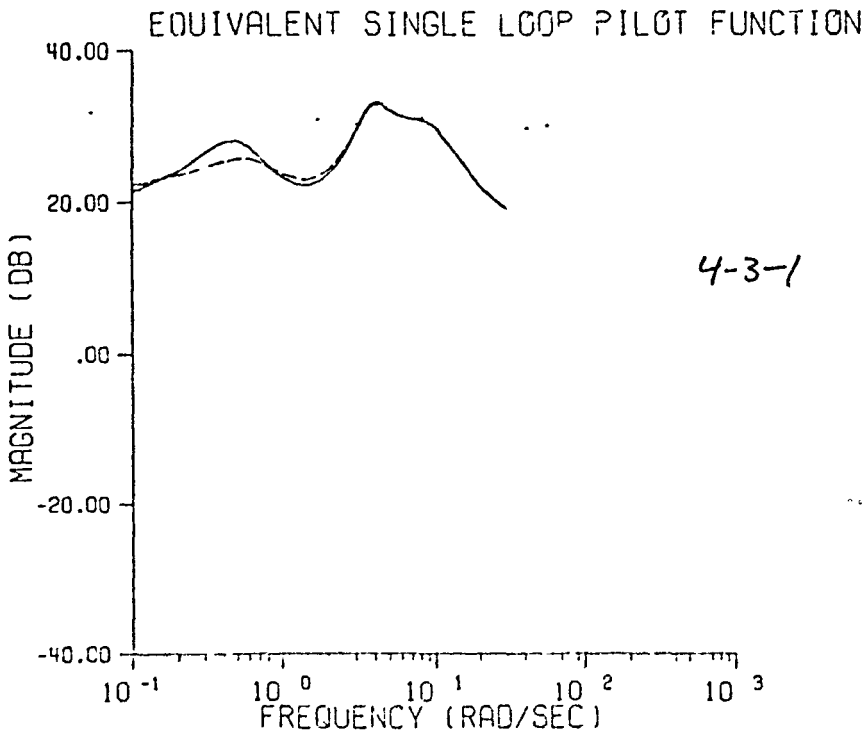

Figure 37
Effect of Washout Filter on Equivalent

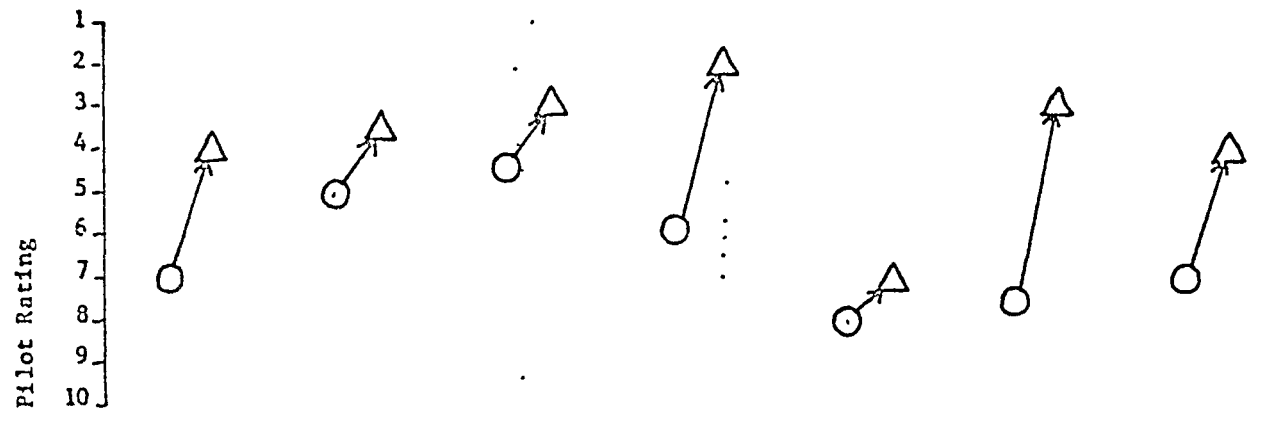

	○4-3 △4-3-1	○6-1 △6-1-1	○6-2 △6-2-1	○8-1 △8-1-1	○8-2 △8-2-1	○8-3 △8-3-1	○8-5 △8-5-1
$1/T_{\theta_2}$	1.0	0.38	0.38	0.40	0.40	0.40	0.40
ω_{sp}	2.8	2.3	2.3	1.45	1.09	1.45	1.45

Figure 38

Effect of Washout Filter on Pilot Ratings

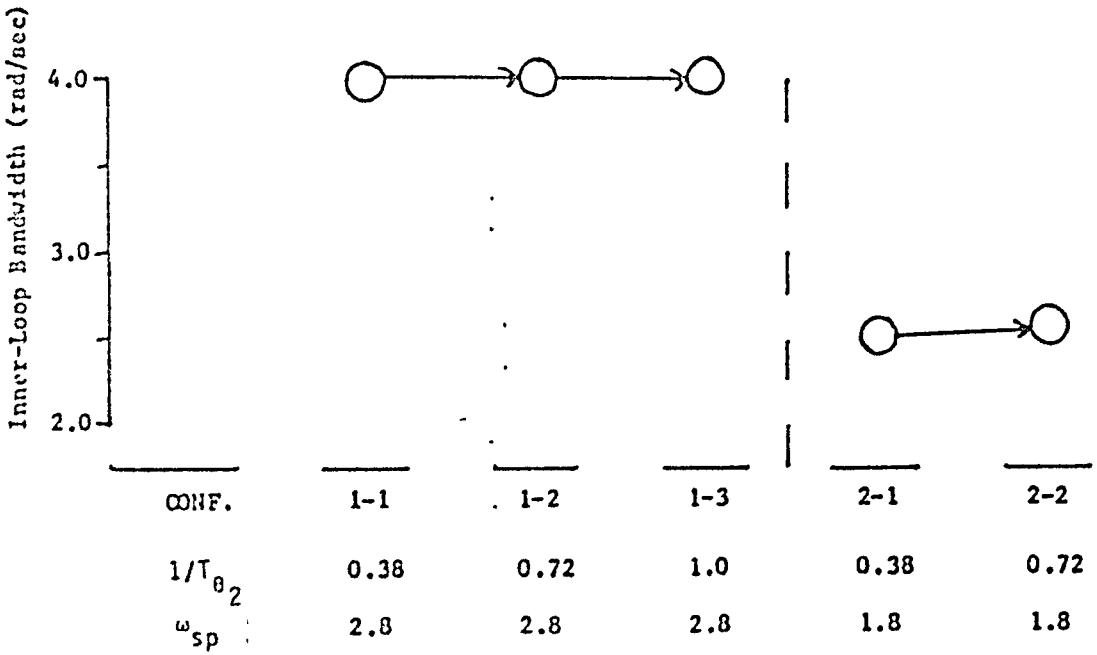

CONF.	1-1	1-2	1-3	2-1	2-2
$1/T_{\theta_2}$	0.38	0.72	1.0	0.38	0.72
ω_{sp}	2.8	2.8	2.8	1.8	1.8

Figure 39

Effect of $\frac{1}{T_{\theta_2}}$ No Prefilter on Inner-Loop Bandwidth

flight-path response bandwidth increases (see Figure 40). Our flight-path analysis showed the same trends (Figure 41). As $1 / T_{\theta_2}$ was increased, the Flight-Path Bandwidth increases as predicted. In addition, as $1 / T_{\theta_2}$ is increased, the Equivalent Pilot Phase Compensation decreases (Figure 42). This is a result of the increased vehicle phase in the region of crossover as $1 / T_{\theta_2}$ is increased as seen in Figure 40.

In the discussion of the washout filter, it was noted that the Low Frequency Pilot Phase appears to be reflected in the pilot ratings. $1 / T_{\theta_2}$ also appears to have an effect on this parameter, as shown in Figure 43. The reason for this is indicated in Figure 40. The pilot introduces lead (or lag) to bring the closed-loop system (pilot/vehicle) phase to zero degrees at low frequencies. ($\omega \approx 0.1$ rad/sec.), a characteristic of a good closed-loop tracking system. As $1 / T_{\theta_2}$ increases, the vehicle phase decreases resulting in more required pilot lead. Care is required in attributing this effect directly to $1 / T_{\theta_2}$ though. The phase of the flight-path dynamics at ω=0.1 rad/sec. is more an effect of the low frequency vehicle dynamics (z_2 and x_1; see Table 3) than it is of $1 / T_{\theta_2}$. For the TIFS configurations, these dynamics change with $1 / T_{\theta_2}$.

The amount of phase lead required at these low frequencies is also a function of the relationship between γ and θ. This relationship is approximated by

$$\frac{\gamma}{\theta} \approx \frac{1 / T_{\theta_2}}{s + 1 / T_{\theta_2}} .$$

As $1 / T_{\theta_2}$ is decreased, this lag is increased.

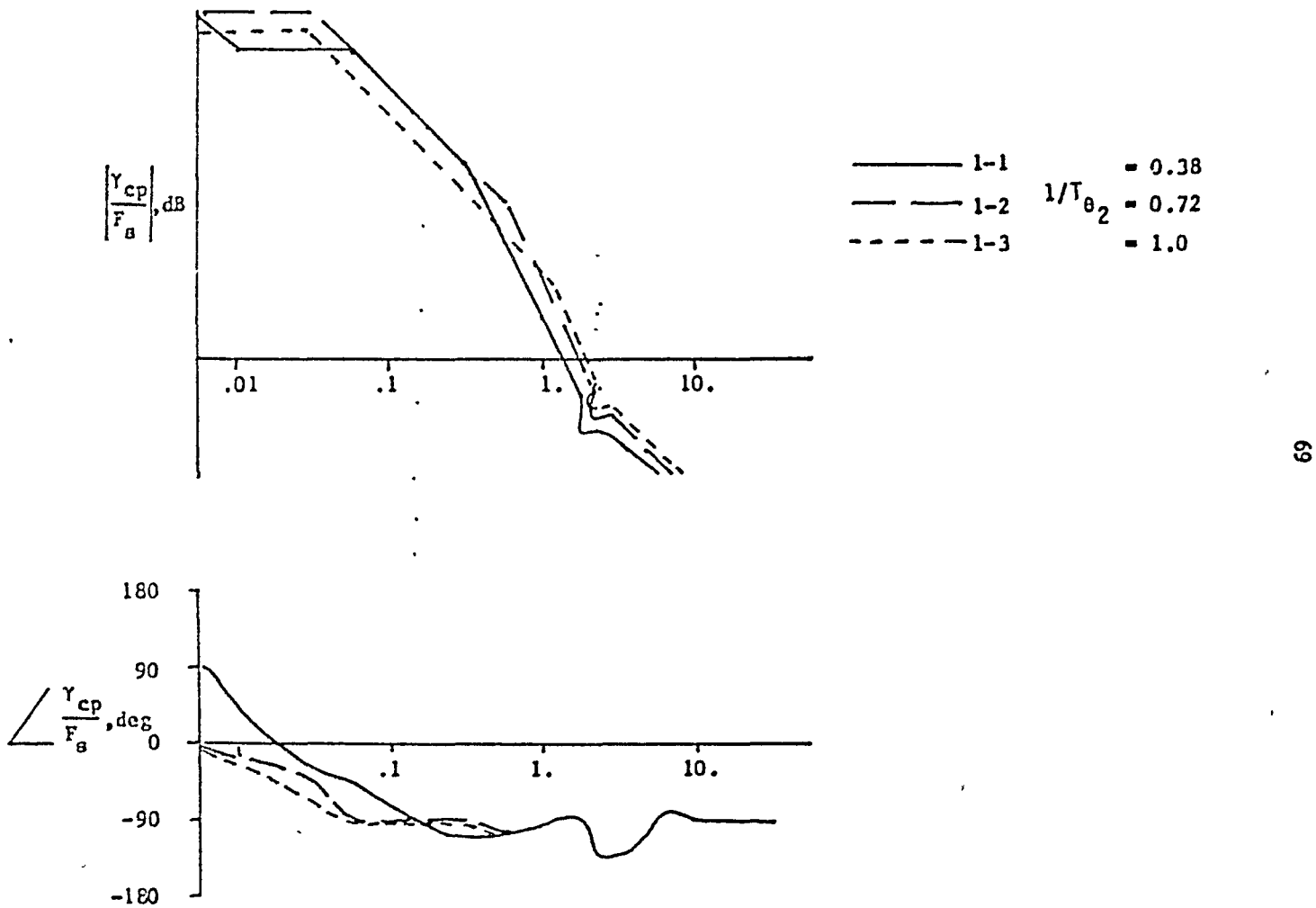

Figure 40.
Effect of $1/T_{\theta_2}$ / No Prefilter on Flight-Path Response Bandwidth

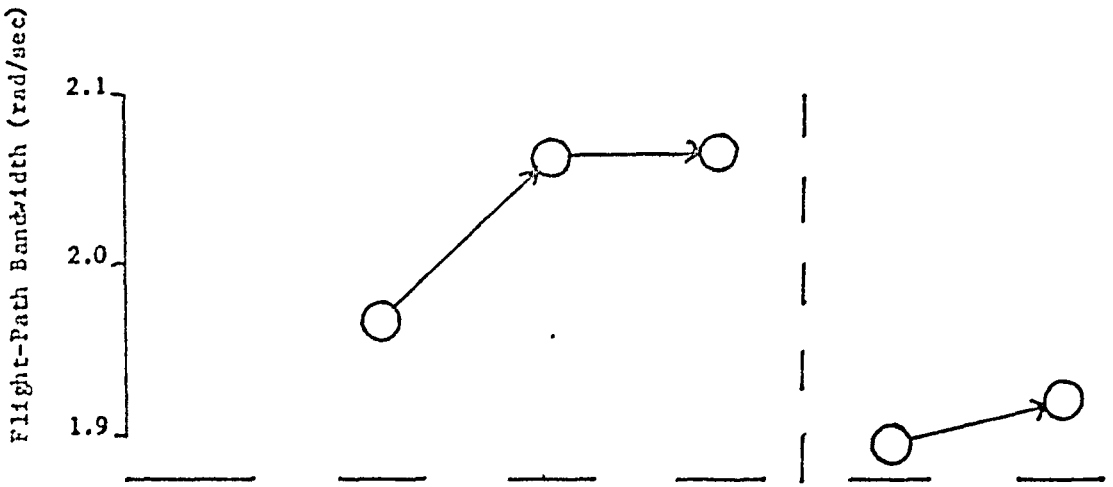

CONF.	1-1	1-2	1-3	2-1	2-2
$1/T_{\theta_2}$	0.38	0.72	1.0	0.38	0.72
ω_{sp}	2.8	2.8	2.8	1.8	1.8

Figure 41

Effect of $\frac{1}{T_{\theta_2}}$ /No Prefilter on Flight-Path Bandwidth

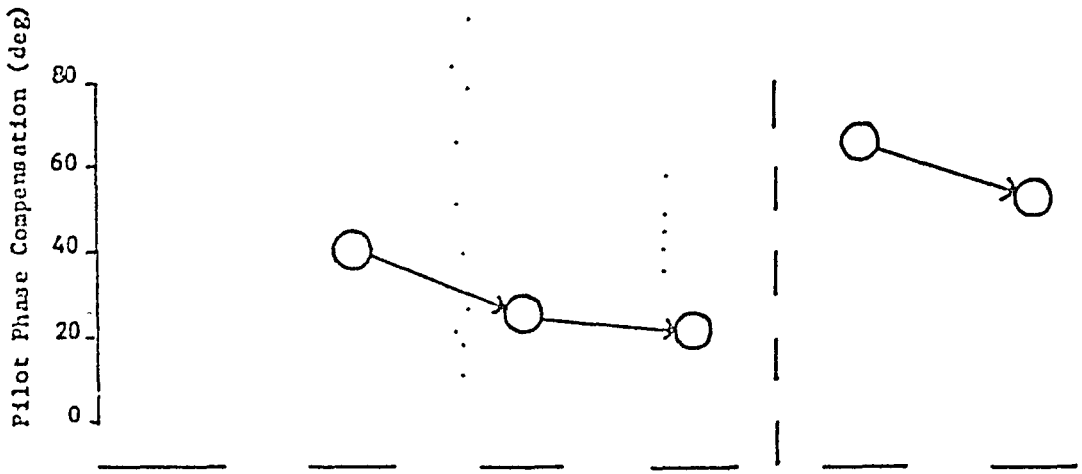

CONF.	1-1	1-2	1-3	2-1	2-2
$1/T_{\theta_2}$	0.38	0.72	1.0	0.38	0.72
ω_{sp}	2.8	2.8	2.8	1.8	1.8

Figure 42
Effect of $Y_{T_{\theta_2}}$ /No Prefilter on Equivalent Pilot Phase Compensation

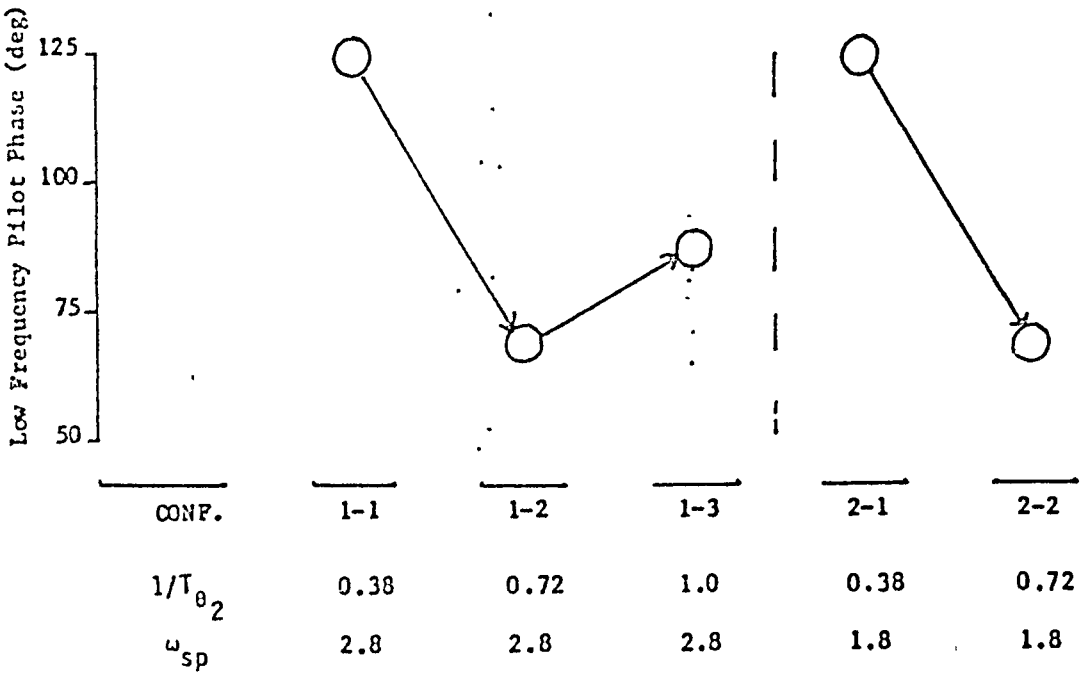

Figure 43

Effect of $\frac{1}{T_{\theta_2}}$ / No Prefilter on Low-Frequency Pilot Phase

Therefore, for low values of $1 / T_{\theta_2}$ (such as 0.38), there is a significant lag between the pitch response and the flight-path response. Since the pilot uses pitch attitude to control the flight-path-angle, the larger this lag becomes, the more difficult control of the flight-path becomes. As this lag increases, the pilot must increase his phase equalization (i.e. introduce additional lead into the system) to compensate. This should be reflected in the Low Frequency Pilot Phase. As $1 / T_{\theta_2}$ increases, the Low Frequency Pilot Phase should decrease corresponding to the decreasing lag between γ and θ. This is opposite to the before-mentioned effect of $1 / T_{\theta_2}$. The overall effect is that the Low Frequency Pilot Phase is lowest for intermediate values of $1 / T_{\theta_2}$, a compromise between the two effects. This is seen in Figure 43.

$1 / T_{\theta_2}$ also effects the amount of phase lead the pilot must introduce for the inner, pitch-attitude loop (P_θ in Figure 1). This is clearly shown in Figure 44. For $1 / T_{\theta_2}$ =0.38, the pilot must introduce a large amount of pitch phase lead to precisely control the flight-path This phase lead is significantly reduced for $1 / T_{\theta_2}$ =0.72 This corresponds to the decreased lag between the pitch and flight-path responses. This variation in P_θ in turn effects the Neal-Smith Inner-Loop Bandwidth. The large pilot lead introduced for low values of $1 / T_{\theta_2}$ significantly increases this bandwidth parameter (see Table 5).

Finally, the effect of $1 / T_{\theta_2}$ on pilot/vehicle tracking performance should be noted As Figures 45 and 46 indicate, the tracking performance, as measured by RMS

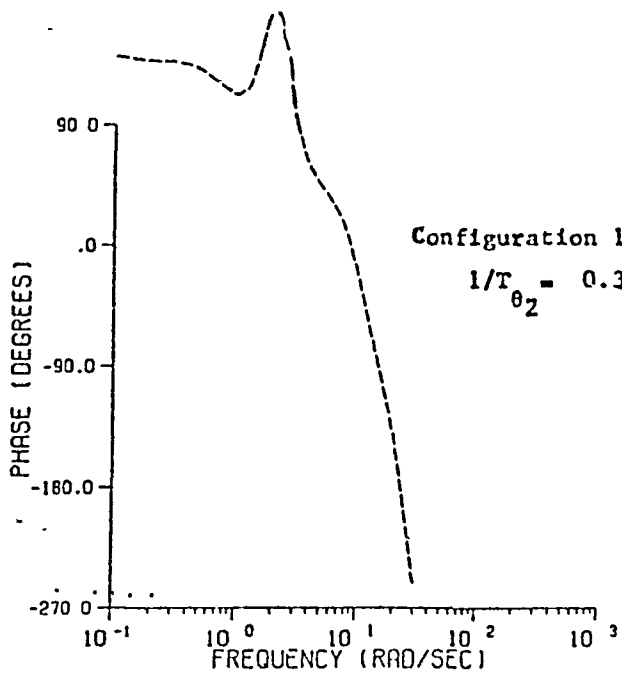

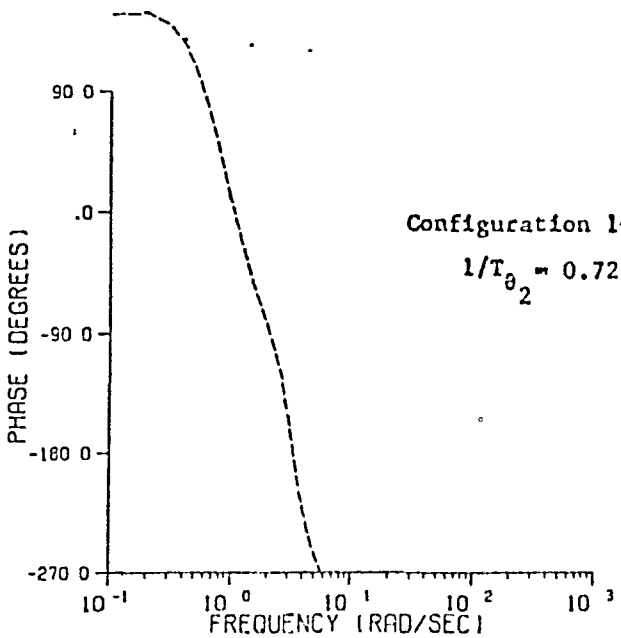

Figure 44
Effect of $Y_{T_{\theta_2}}/N_\delta$ Prefilter on P_α

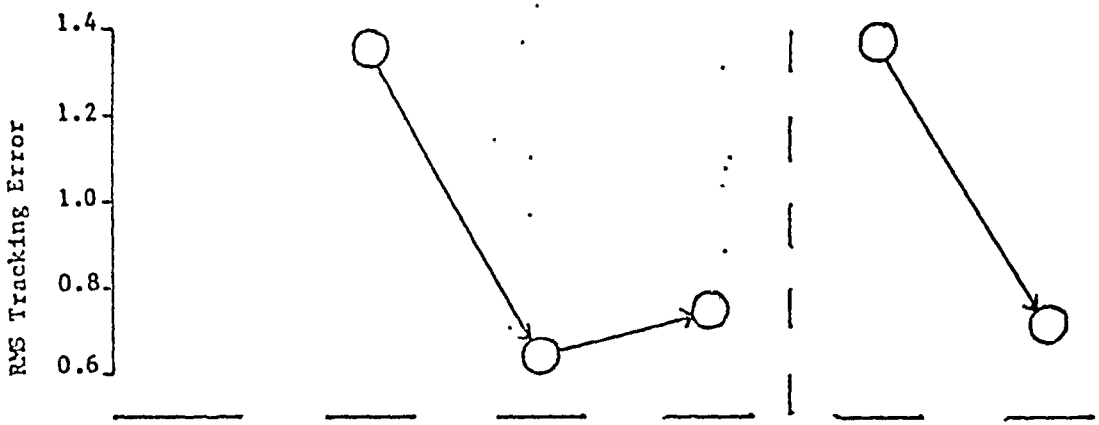

CONF.	1-1	1-2	1-3	2-1	2-2
$1/T_{\theta_2}$	0.38	0.72	1.0	0.38	0.72
ω_{sp}	2.8	2.8	2.8	1.8	1.8

Figure 45
Effect of $\frac{1}{T_{\theta_2}}$ / No Prefilter on RMS Tracking Error

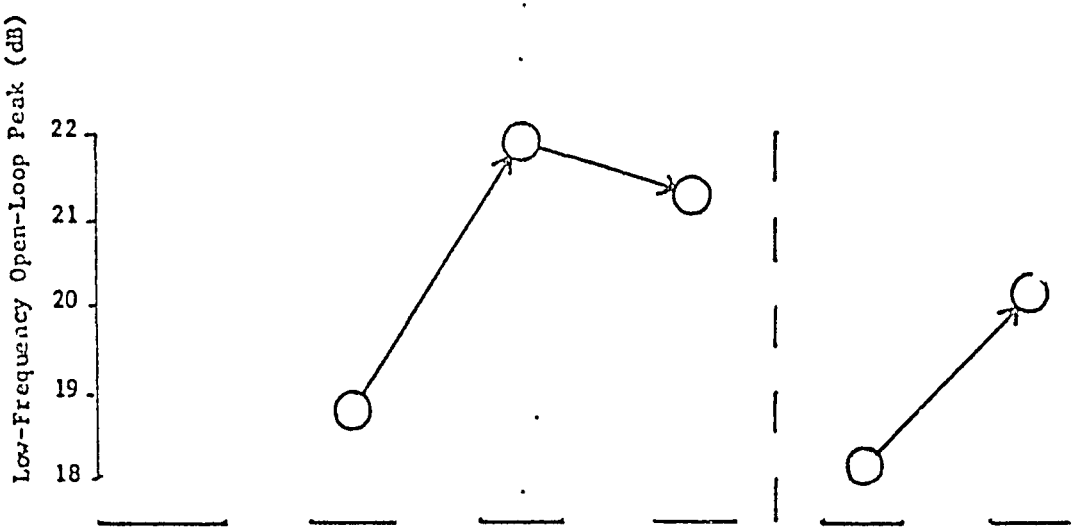

CONF.	1-1	1-2	1-3	2-1	2-2
$1/T_{\theta_2}$	0.38	0.72	1.0	0.38	0.72
ω_{sp}	2.8	2.8	2.8	1.8	1.8

Figure 46

Effect of $\frac{1}{T_{\theta_2}}/\frac{1}{T_b}$ Prefilter on Low Frequency Open-Loop Peak

error and the Low-Frequency Open-Loop Peak respectively, changes considerably with variations in $1 / T_{\theta_2}$. For example, the RMS error is significantly larger for low values of $1 / T_{\theta_2}$ than for higher values. It is hypothesized that this results from the large lag between the flight-path and pitch responses that exists for low values of $1 / T_{\theta_2}$. This large lag creates difficulty in controlling the flight-path through variations in pitch-attitude. It is interesting to note that for every one of these low $1 / T_{\theta_2}$ configurations, which are predicted to have degraded flight-path tracking ability, the pilots noted a lack of h or flight-path control.

VARIATION OF $1 / T_{\theta_2}$; With Prefilter

The prefilter restores the attitude dependence on $1 / T_{\theta_2}$ associated with conventional aircraft dynamics (see Table 2). The inner-loop attitude dynamics should therefore be sensitive to variations of this variable. As Figure 47 indicates, the Inner-Loop Bandwidth decreases with increasing $1 / T_{\theta_2}$. As shown in Table 3, the only influence of $1 / T_{\theta_2}$ on the flight-path dynamics is on the γ / F_s transfer function gain. Higher values of $1 / T_{\theta_2}$ result in higher DC gains which result in higher flight-path response bandwidths (see Figure 48). Figure 49 indicates that this is also the case for Flight-Path Bandwidth. Since $1 / T_{\theta_2}$ only influences the gains, the phase (at least at high frequencies) is relatively unaffected by $1 / T_{\theta_2}$. Thus the Equivalent Pilot Phase Compensation should change very little with variations in $1 / T_{\theta_2}$, though the inner-loop dynamics do have an

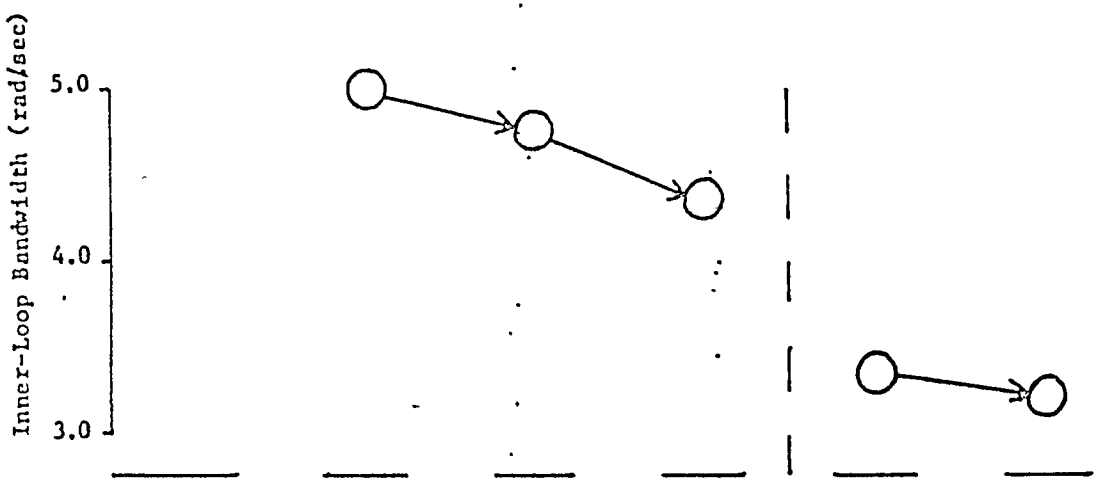

CONF.	4-1	4-2	4-3	5-1	5-2
$1/T_{\theta_2}$	0.38	0.72	1.0	0.38	0.72
ω_{sp}	2.8	2.8	2.8	1.8	1.8

Figure 47

Effect of $1/T_{\theta_2}$ Prefilter on Inner-Loop Bandwidth

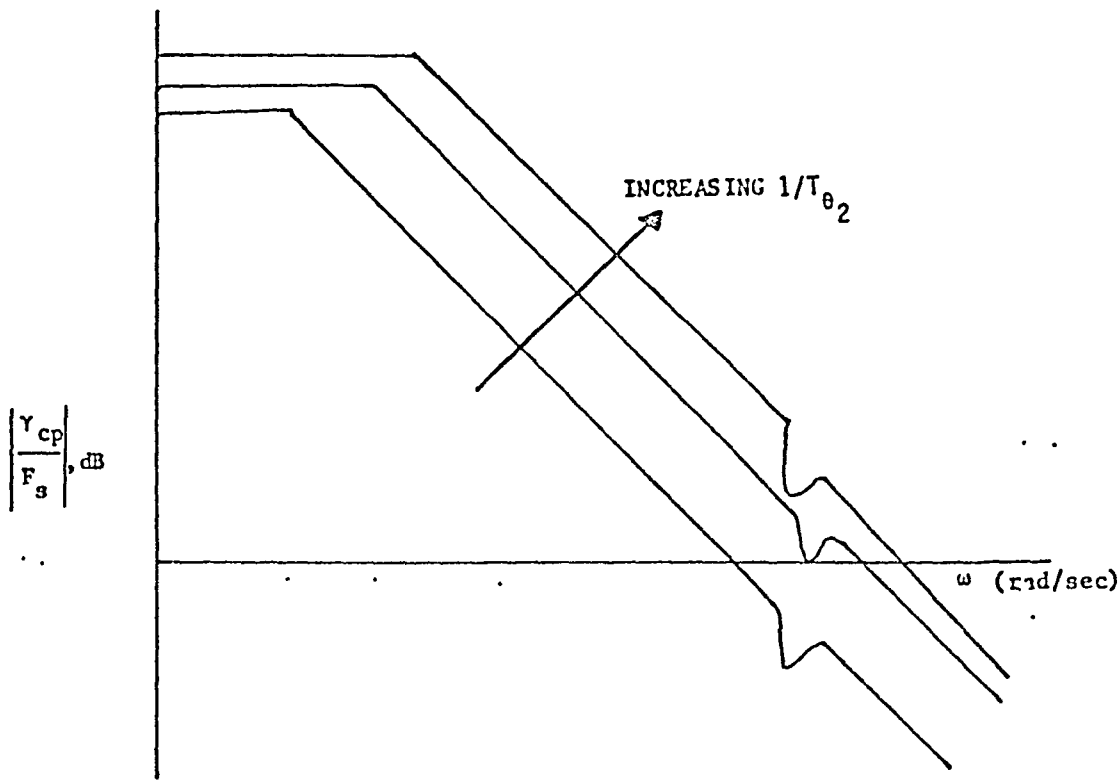

Figure 48
Effect of $\frac{1}{T_{\theta_2}}$ Prefilter on Flight-Path Response Bandwidth

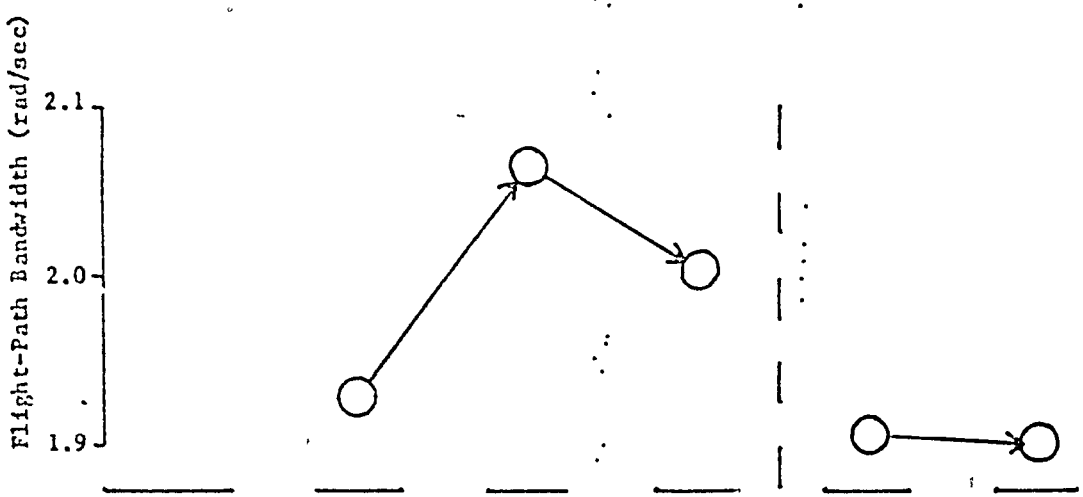

CONF.	4-1	4-2	4-3	5-1	5-2
$1/T_{\theta_2}$	0.38	0.72	1.0	0.38	0.72
ω_{sp}	2.8	2.8	2.8	1.8	1.8

Figure 49

Effect of $\frac{1}{T_{\theta_2}}$ Prefilter on Flight-Path Bandwidth

indirect influence on this. Figure 50 indicates that this is true.

The effect of $1 / T_{\theta_2}$ on the Low Frequency Pilot Phase is exactly the same as for the case without the prefilter. The low frequency dynamics (z_2 and x_1) and the γ/θ relationship are unaffected by the addition of the prefilter. Comparison of Figures 51 and 42 show that the trends are exactly the same as discussed earlier. In addition, the effect of $1 / T_{\theta_2}$ on the tracking performance is identical to the no prefilter case as seen in Figures 52 and 53.

Finally, the effect that $1 / T_{\theta_2}$ has on pilot opinion ratings should be noted. Both the Low Frequency Pilot Phase and the measures of tracking performance indicate that the best pilot ratings should be obtained for the intermediate values of $1 / T_{\theta_2}$. These parameters also indicate that the worst pilot ratings should correspond to the low values of $1 / T_{\theta_2}$. . Figure 54 indicates that the pilot ratings, in general, follow these same trends. Therefore, Low Frequency Pilot Phase and the measures of tracking performance seem to correlate well with pilot ratings.

SHORT PERIOD FREQUENCY

The effect of the short period frequency, ω_{sp}, on the pitch attitude and flight-path frequency responses is shown in Figure 55. This figure clearly shows that decreasing ω_{sp} results in a decrease in bandwidth for both the pitch-attitude and the flight-path responses. Figure 56 and 57 indicate that this decrease in open-loop bandwidths results in a decrease in the corresponding

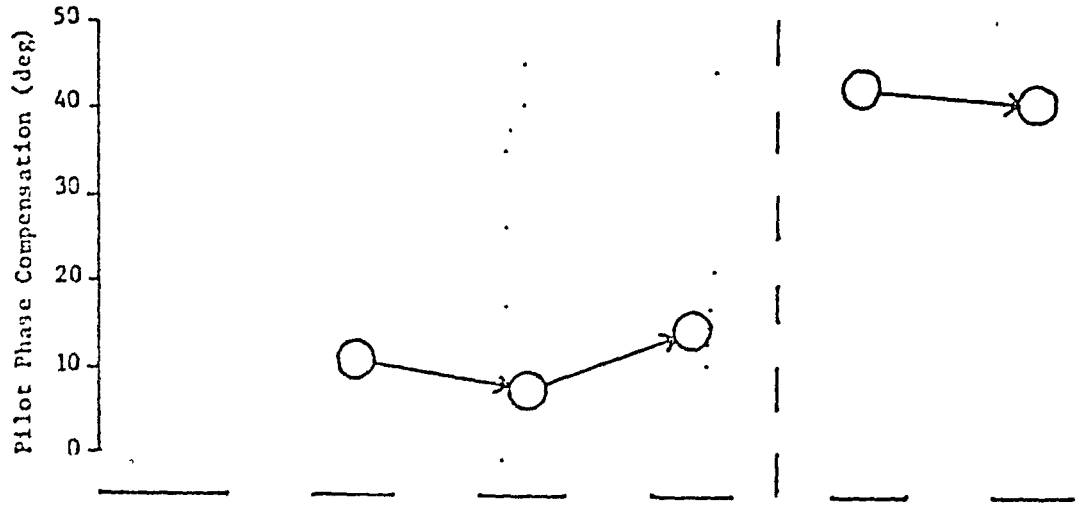

CONF.	4-1	4-2	4-3	5-1	5-2
$1/T_{\theta_2}$	0.38	0.72	1.0	0.38	0.72
ω_{sp}	2.8	2.8	2.8	1.8	1.8

Figure 50

Effect of $\frac{1}{T_{\theta_2}}$ Prefilter on Equivalent Pilot Phase Compensation

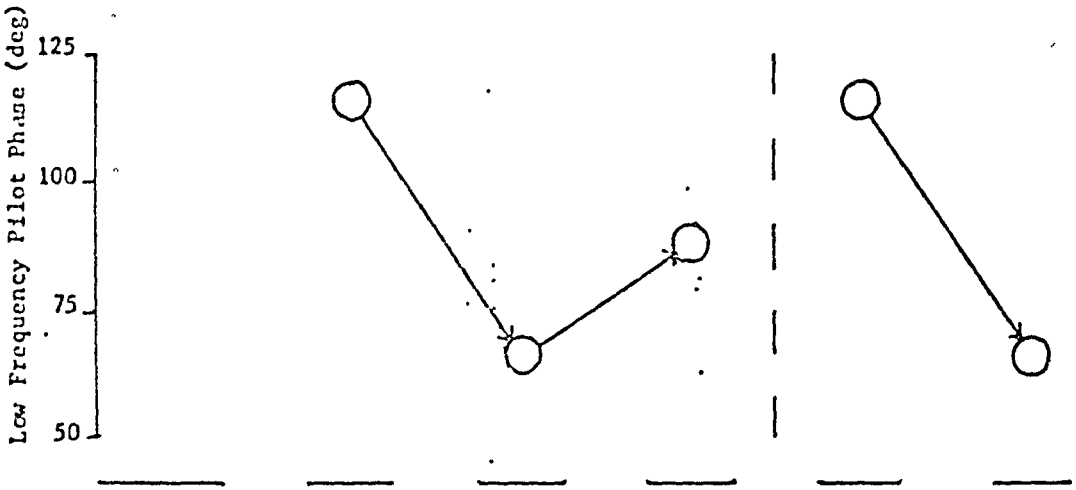

CONF.	4-1	4-2	4-3	5-1	5-2
$1/T_{\theta_2}$	0.38	0.72	1.0	0.38	0.72
ω_{sp}	2.8	2.8	2.8	1.8	1.8

Figure 51

Effect of $\frac{1}{T_{\theta_2}}$ Prefilter on Low Frequency Pilot Phase

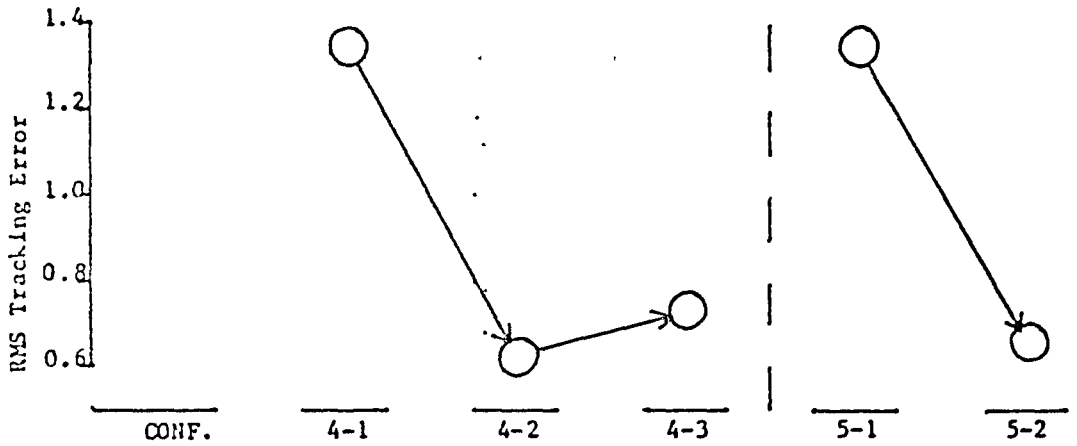

CONF.	4-1	4-2	4-3	5-1	5-2
$1/T_{\theta_2}$	0.38	0.72	1.0	0.38	0.72
ω_{sp}	2.8	2.8	2.8	1.8	1.8

Figure 52

Effect of $\frac{1}{T_{\theta_2}}$ Prefilter on RMS Tracking Error

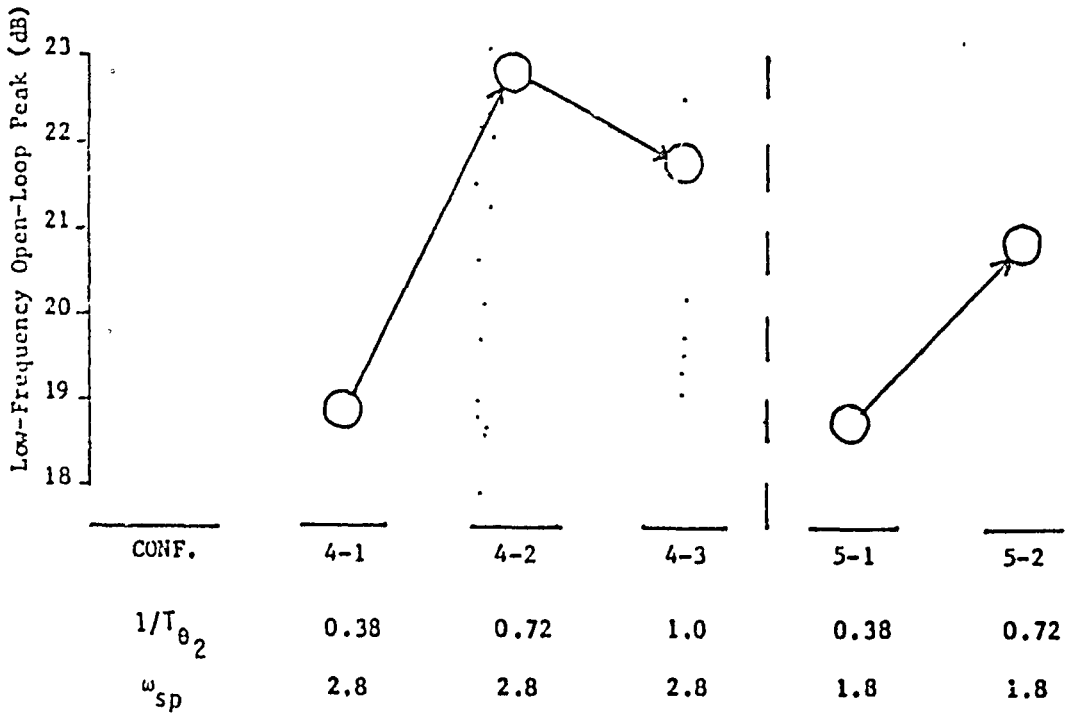

Figure 5B

Effect of $\frac{1}{T_{\theta_2}}$ Prefilter on Low-Frequency Open-Loop Peak

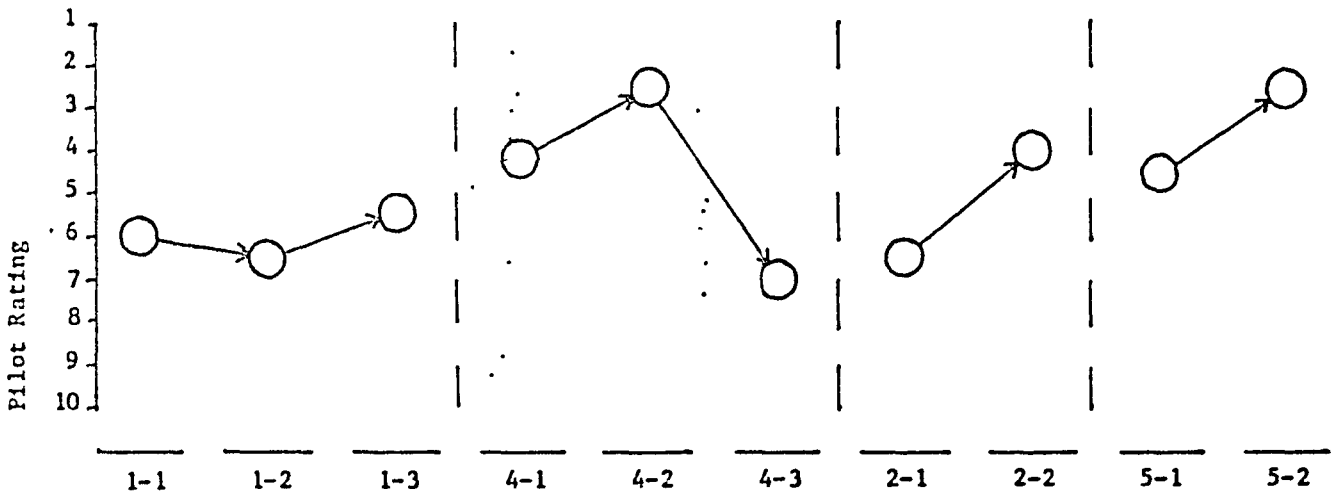

Figure 54

Effect of Y_{TS} on Pilot Ratings

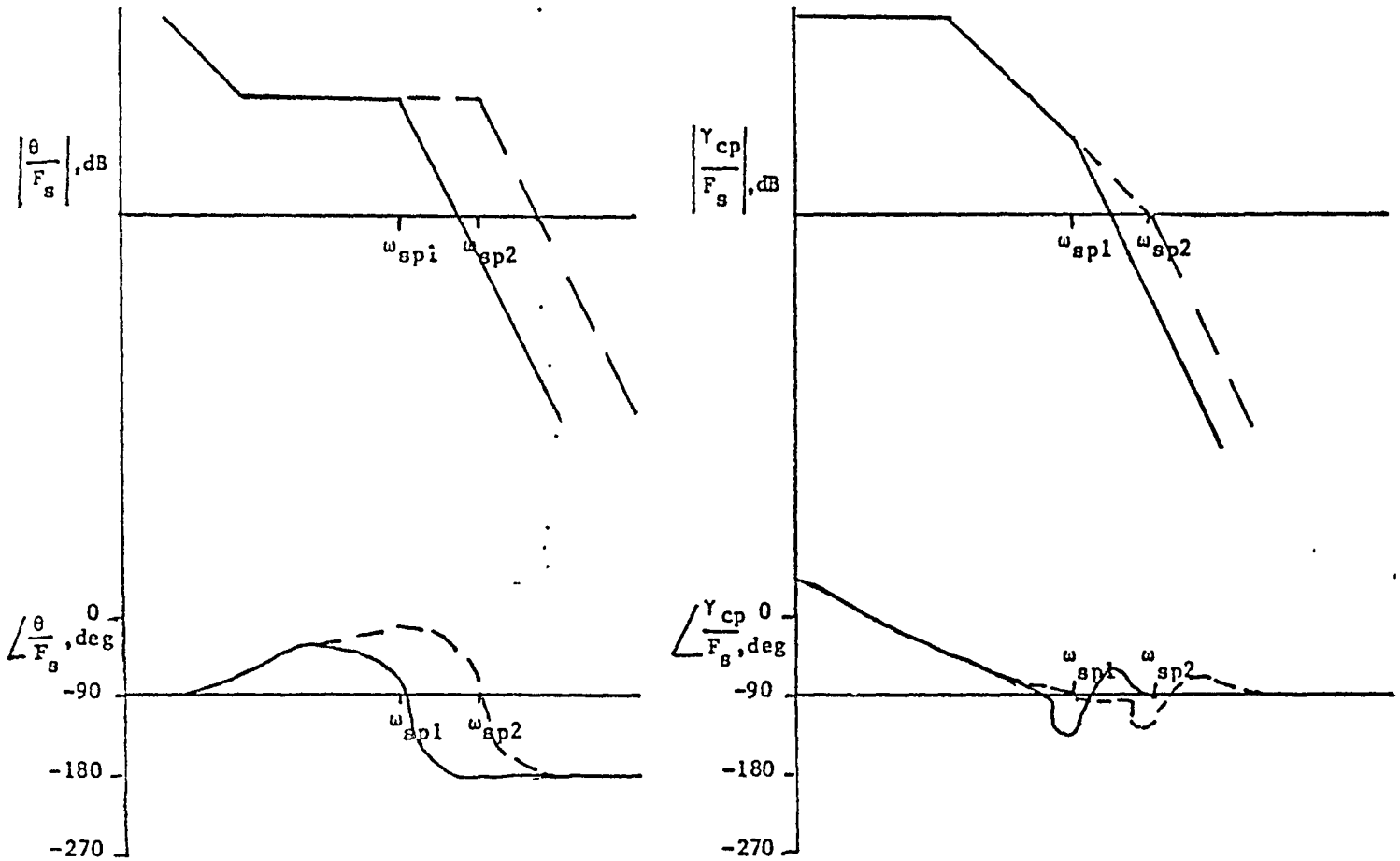

Figure 55
Effect of ω_{sp} on θ and γ
Response Bandwidths

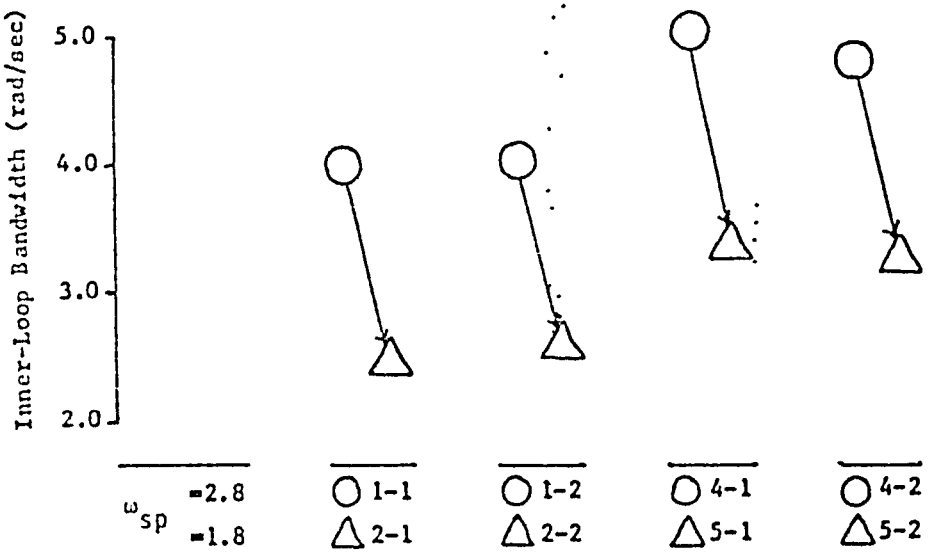

Figure 56
Effect of ω_{sp} on Inner-Loop Bandwidth

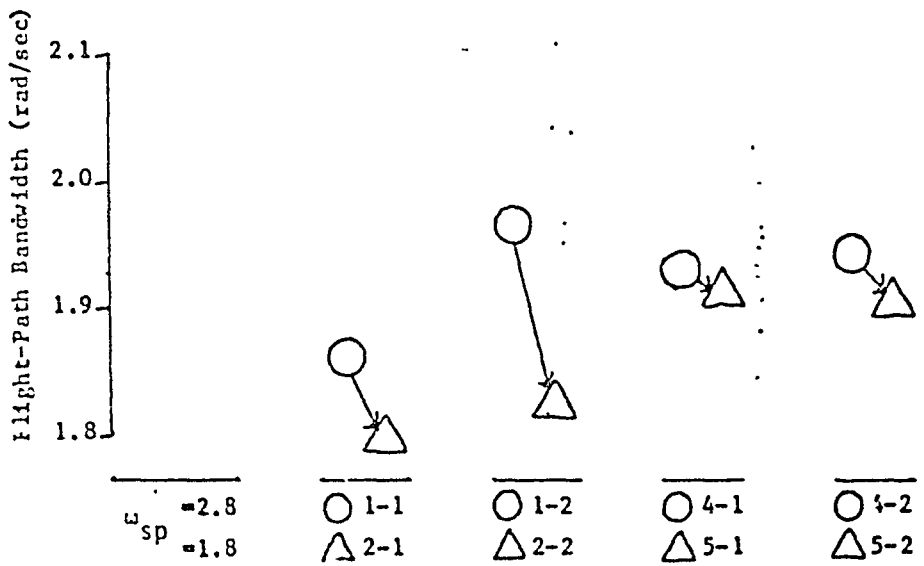

Figure 57

Effect of ω_{sp} on Flight-Path Bandwidth

bandwidths. In addition, due to this decrease in both inner and outer loop bandwidths, the pilot must introduce additional phase lead to achieve the maximum achievable bandwidth. This effect is exhibited in Figure 58. There is not, however, a one-to-one correlation between ω_{sp} and pilot ratings for these configurations (see Figure 59).

SUMMARY

The analysis performed in the previous section was necessary because our previously developed analysis tools for the flared approach and landing task were not sufficient to explain the experimental pilot ratings for these TIFS Pitch-Rate configurations. This in-depth analysis looked at the effect the variation of each experimental variable had on the pilot/vehicle closed-loop dynamics. This in turn was related to pilot opinion ratings where applicable. A brief summary of these results will now be presented

Many of the parameters defined earlier were shown to be reflected, to some degree, in pilot ratings. Equivalent Pilot Phase Compensation has been advanced in other studies as an indicator of pilot workload, and has been used in this study in a similar capacity Likewise, bandwidth has been previously advanced as a measure of achievable system performance, a key example is the Flight-Path Bandwidth. Tracking performance, as characterized by either RMS Error or the Low-Frequency, Open-Loop Peak (gain), has also been shown to correspond, in most cases, to pilot ratings.

The prefilter restored the overshoot associated with conventional aircraft pitch dynamics This quickens the flight-path and altitude responses and accentuates the initial pitch acceleration cues. The result is increased

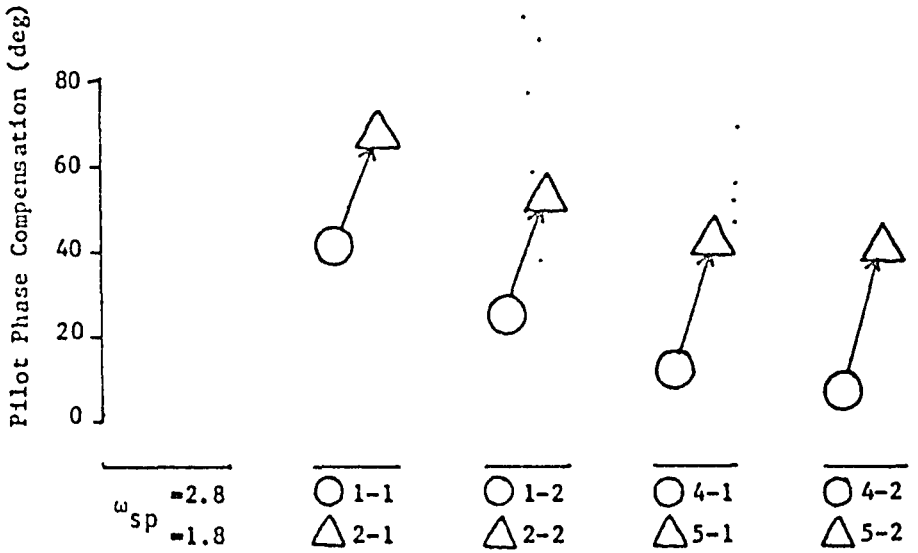

Figure 58

Effect of ω_{sp} on Equivalent Pilot Phase Compensation

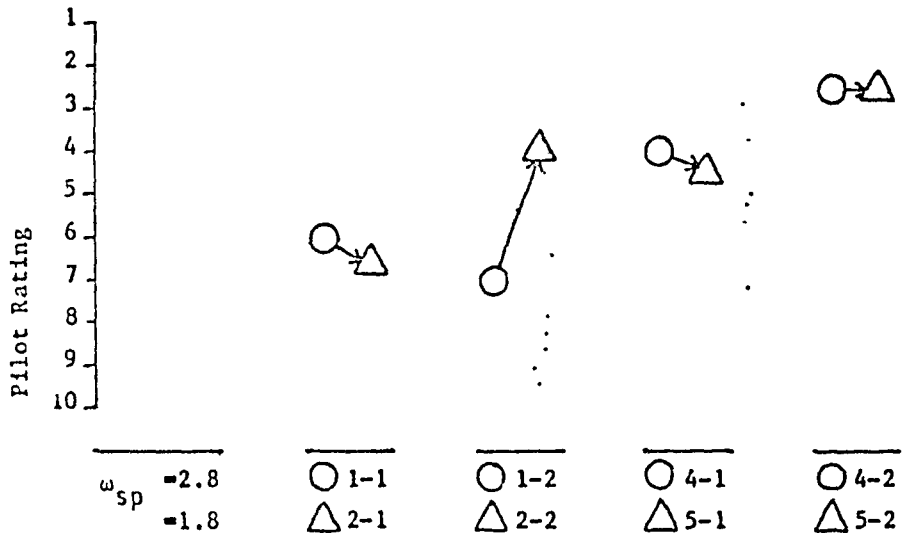

Figure 59
Effect of ω_{sp} on Pilot Ratings

system performance, as indicated by an increase in the Flight-Path Bandwidth. Pilot workload and pilot/vehicle PIO tendencies were also reduced. All of these factors contribute to the improved pilot ratings obtained upon implementation of the prefilter.

Pitch-rate command systems exhibit significantly different low frequency dynamics than conventional aircraft. The pilot must adopt a pulse control strategy instead of the conventional continuous stick movements associated with conventional aircraft. The result is a tendency to float during the landing flare and a requirement to sometimes push the stick forward near the ground. The washout filter eliminates these tendencies by changing the pitch dynamics from rate-command to position-command at low frequencies ($\omega \leq 0.2$ rad/sec). The washout filter also reduces vehicle sensitivity to pilot induced oscillations. As a consequence of all of the above, the introduction of the washout filter improved pilot ratings In addition, the Low Frequency Pilot Phase was introduced as a model-based quantity sensitive to these low frequency phenomena.

$1 / T_{\theta_2}$ also effected pilot opinion ratings It was shown that for low values of $1 / T_{\theta_2}$, the large lag between the flight-path and pitch responses significantly effected the pilot/vehicle tracking performance. Overall, the tracking performance was best for the middle values of $1 / T_{\theta_2}$. In addition, the Low-Frequency Pilot Phase was highest (worst) for the low values of $1 / T_{\theta_2}$ and lowest (best) for the middle values of $1 / T_{\theta_2}$. The pilot ratings, in general, followed this same trend.

Finally, the changes corresponding to variation in short period frequency, ω_{sp}, were discussed Increased ω_{sp} results in increased Flight-Path Bandwidth and decreased Equivalent Pilot Phase Compensation. These changes, however, did not have a one-to-one correlation with pilot opinion ratings. It should be noted however that only a small amount of data is available on this variable since only two values of ω_{sp} were available for analysis. With more data points, it might be possible to correlate this parameter to pilot ratings.

The in-depth analysis is intended to yield insight into the factors influencing pilot ratings. All of the pilot ratings, however, cannot be explained at the present time with a single handling quality criteria Work is continuing along these lines. Part of the problem is a result of the large number of variations in the experimental variables in a relatively few flights Any additions to the data base obtained with follow-up tests would therefore be helpful.

LIST OF REFERENCES

1 Berthe,C.J.,Chalk, C.R.,and Sarrafian,S., Pitch Rate Flight Control Systems in the Flared Landing Task and Design Criteria Development, Calspan Report No. 7205-6, June 1984.

2. Neal, T.P. and Smith, R.E., An In-Flight Investigation to Develop Control System Design Criteria for Fighter Airplanes. AFFDL-TR-70-74, Vol. I, December (1970).

3 Anderson, M.R., and Schmidt, D.K., "Closed-Loop, Pilot/Vehicle Analysis of the Approach and Landing Task", AIAA Paper 85-1851 CP, Guidance and Control Conference, Snowmass CO., Aug. 1985.

4 Anderson, M.R., Closed-Loop, Pilot/Vehicle Analysis of Approach and Landing, M.S. Thesis, Purdue University, December 1984.

5 Schmidt, D.K., The Integrated Manual and Automatic Control of Complex Flight Vehicles, Semi-Annual Status Report, July 1984 -March 1985, April 12, 1985.

6 Weingarten, Norman C., and Chalk, Charles R., "In-Flight Investigation of Large Airplane Flying Qualities for Approach and Landing", Journal of Guidance, Control, and Dynamics, Vol. 7, Jan.-Feb. 1984, pp. 92-98.

Cp 2

Appendix A
Flight Path Tracking Block Diagrams

The pilot observations γ_{error}, $\dot{\gamma}$, and θ in the OCM pilot model for the flight-path-tracking task reflect a block diagram form shown in Figure (A.1). It is desired to convert this into the block diagram form shown in Figure A.2. This manipulation can be accomplished using simple block diagram arithmetic.

First, find the closed loop transfer function of the inner attitude loop. This loop is shown inside the dotted box of Figure (A.1). The resulting closed loop function is

$$\frac{\theta}{F_\gamma}\Big|_{C.L.} = \frac{(\theta/F_s)}{1-P_\theta(\theta/F_s)} \qquad (A.1)$$

Now define

$$G_\theta = \frac{1}{1-P_\theta(\theta/F_s)} \qquad (A.2)$$

so that Eq. (A.1) becomes

$$\frac{\theta}{F_\gamma}\Big|_{C.L.} = G_\theta\,(\theta/F_s) \qquad (A.3)$$

Now define,

$$\theta_c = -\frac{1}{P_\theta} F_\gamma \qquad (A.4)$$

where θ_c is a pseudo-pitch command. Eqn. (A.3) can now be written as

$$\frac{\theta}{F_c}\Big|_{C.L.} \left(\frac{F_\gamma}{\theta_c}\right) = \frac{\theta}{\theta_c}\Big|_{C.L.} \qquad (A.5)$$

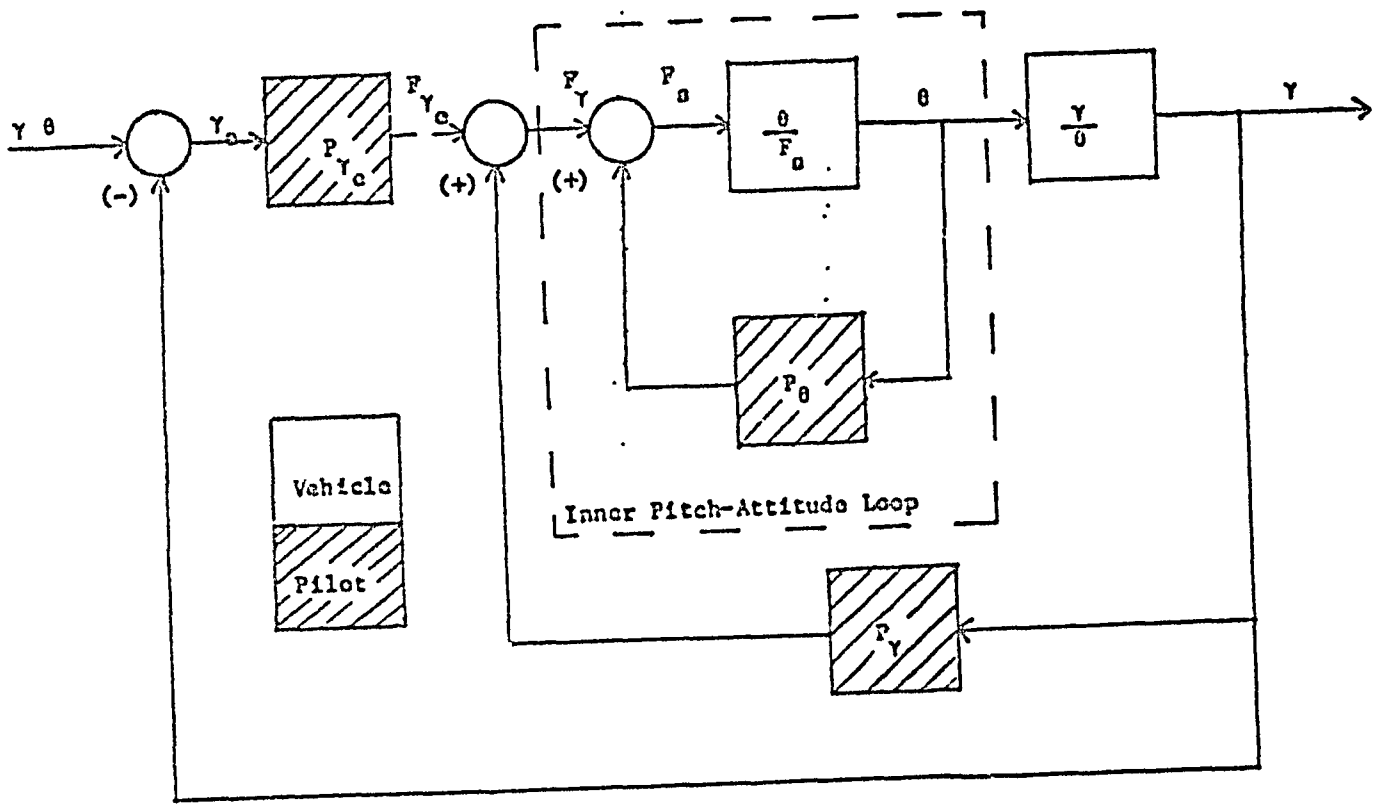

Figure A.1

The Multi-Loop Flight-Path Tracking Task

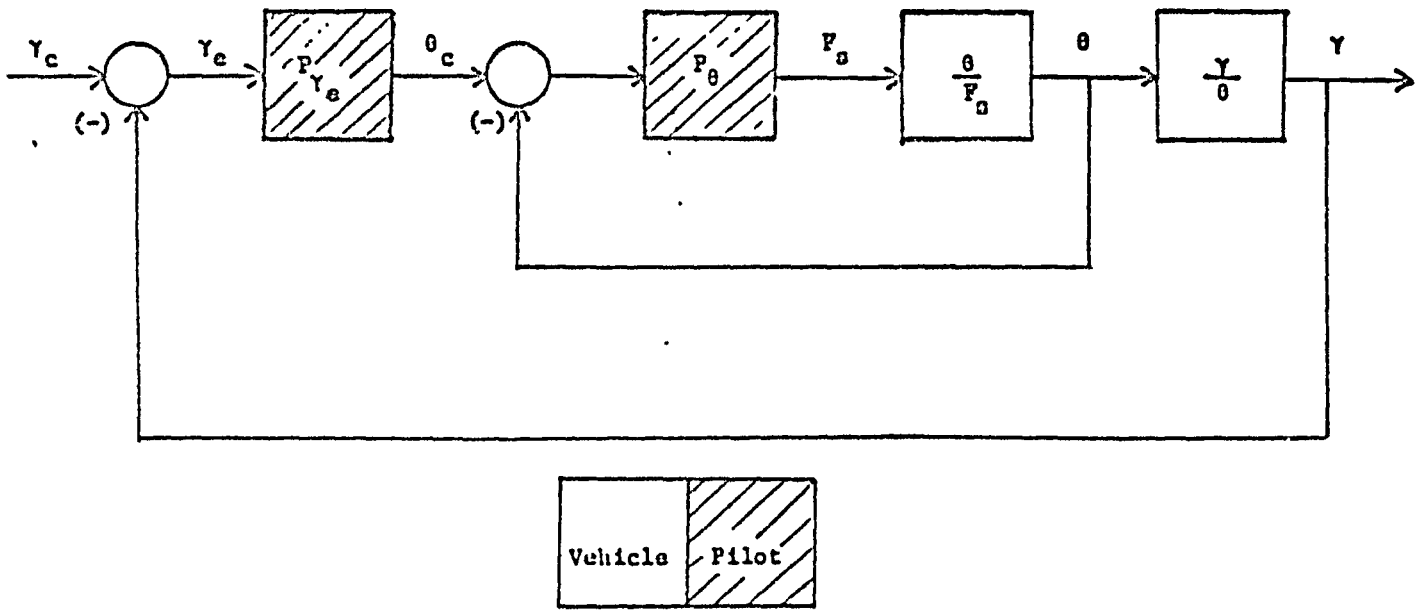

Figure 2.1

Neal-Smith Representation of the Flight-Path Tracking Task.

so that

$$\left.\frac{\theta}{\theta_c}\right|_{C.L.} = (-P_\theta)\, G_\theta\, (\theta/F_s) \quad . \tag{A.6}$$

This manipulation changes the block diagram of Figure (A.1) to the block diagram shown in Figure (A.3). The boxed section of Figure (A.3) can then be written as

$$\frac{\gamma}{F_{\gamma_c}} = \frac{\left(-\frac{1}{P_\theta}\right)}{1 + \left(\frac{P_\gamma}{P_\theta}\right)\left(\frac{\theta}{\theta_c}\right)\left(\frac{\gamma}{\theta}\right)} \left(\frac{\theta}{\theta_c}\right)\left(\frac{\gamma}{\theta}\right) \tag{A.7}$$

which can be simplified to

$$\frac{\gamma}{F_{\gamma_c}} = \left(-\frac{1}{P_\theta}\right) G_\gamma \left(\frac{\theta}{\theta_c}\right)\left(\frac{\gamma}{\theta_c}\right) \tag{A.8}$$

where

$$G_\gamma = \frac{1}{1 - P_\gamma\, G_\theta \left(\frac{\gamma}{F_s}\right)} \tag{A.9}$$

Finally, define inner and outer loop pilot compensators as

$$P_I(s) = -P_\theta(s) \tag{A.10}$$

$$P_O(s) = \frac{-P_{\gamma_c}}{P_\theta}\, G_\gamma(s) \tag{A.11}$$

so that the flight-path-tracking block diagram can now be represented by the block diagram in Figure (A.4).

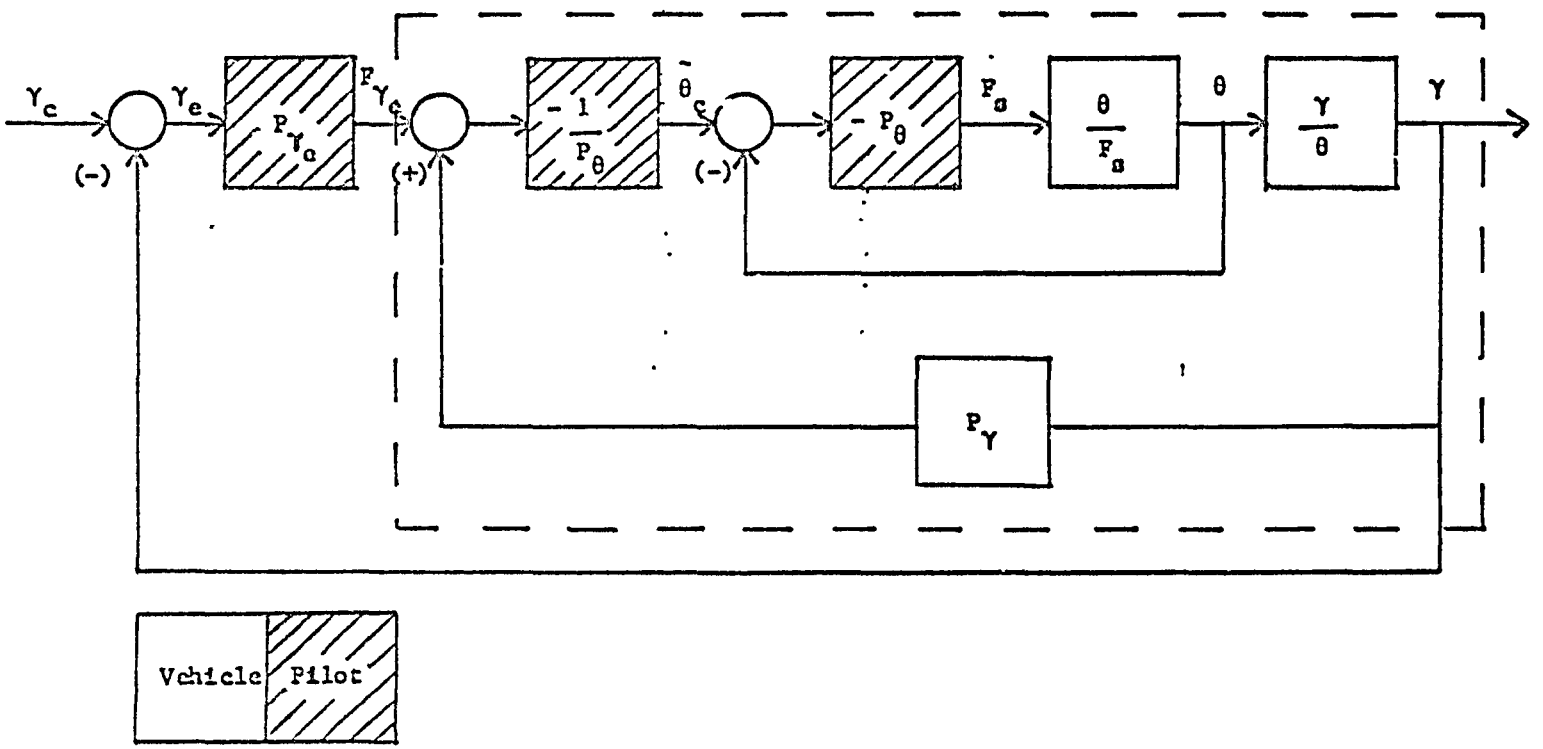

Figure A B.3

Modified Flight-Path Tracking Diagram with Inner Attitude Command

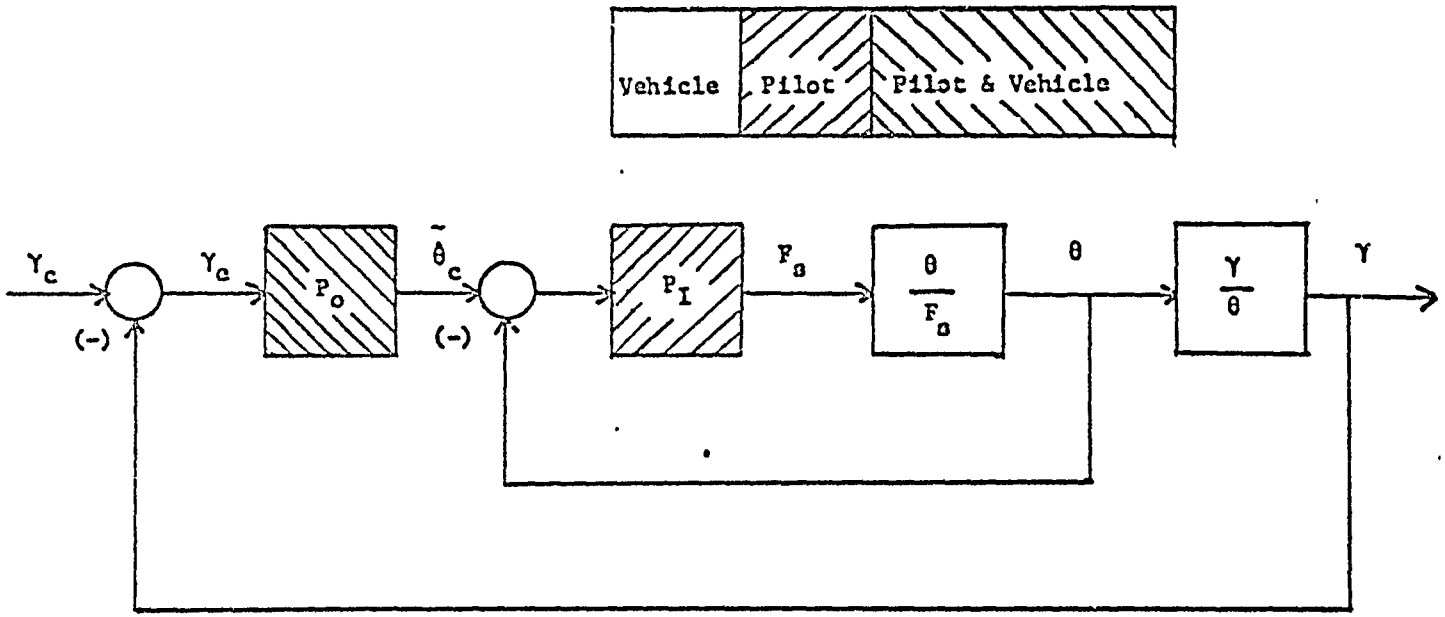

Figure 4

Flight Path Tracking Block Diagram

with Inner-Loop Attitude Feedback

The OCM pilot model is used to obtain the frequency responses for each block shown in Figure (A.1). The frequency responses can be manipulated in the same manner as the transfer function blocks in the preceding derivations.

Appendix B

Table B.1
Attitude Analysis

Conf.	Pilot Ratings	Magnitude Crossover (rad/sec)	Phase Crossover (rad/sec)	Open-Loop Peak (dB)
1-1	7,5	2.20	4.45	4.63
1-2	8,7,5.5	2.25	4.45	4.62
1-3	5,4,7	2.20	4.45	4.62
4-1	2.5,5	2.35	4.50	4.25
4-2	2,3	2.30	4.50	4.57
4-3	7	2.30	4.45	4.69
4-3-1	4	2 30	4.50	4.71
7-1	2.5,3	2.35	4.50	4.66
2-1	6,7	2.20	4.20	3.75
2-2	4.5,3	2.20	4.20	3.75
5-1	4.5,4.5	2.35	4.25	4.27
5-2	2,3	2.30	4.25	4.16
6-1	3,5,6	2.30	4.10	3.64
6-2	5,4,2	2.60	4.25	4.22
6-1-1	4	2.35	4.10	3.77
6-2-1	3	2.60	4.20	4.05
8-1	5.5,6	2.35	4.35	3.36
8-1-1	2	2.40	4.35	3.50
8-2	9,8,7	2.25	4.20	3.84
8-2-1	7	2.15	4.15	3.71
8-3	8,7	2.10	3.90	5.29
8-3-1	3	2.15	3.90	5.39
8-4	1	2.35	4 40	3.43
8-5	7	2.10	3.75	7.30
8-5-1	4	2 15	3.75	7.56

Table B.2
Attitude Analysis (continued)

Conf.	Pilot Ratings	Droop (dB)	Resonance Peak (dB)	RMS Tracking Error
1-1	7,5	-.674	4.38	0.977
1-2	8,7,5.5	-.642	4.41	0.975
1-3	5,4,7	-.640	4.42	0.975
4-1	2.5,5	-1.079	4.89	0.998
4-2	2,3	-.881	4.64	0.978
4-3	7	-.708	4.44	0.971
4-3-1	4	-.988	4.54	0.969
7-1	2.5,3	-1.046	4.50	0.972
2-1	6,7	-.635	4.89	1.028
2-2	4.5,3	-.690	4.94	1.028
5-1	4.5,4.5	-1.069	5.16	1.004
5-2	2,3	-.874	4.97	1.005
6-1	3,5,6	-.760	5.45	1.049
6-2	5,4,2	-1.260	6.26	1.042
6-1-1	4	-1.084	5.65	1.042
6-2-1	3	-1.445	6.60	1.058
8-1	5.5,6	-1.004	4.97	0.982
8-1-1	2	-1.302	5.19	0.984
8-2	9,8,7	-.902	4.96	1.021
8-2-1	7	-1.372	5.00	1.034
8-3	8,7	-.893	5.12	1.115
8-3-1	3	-1.360	5.32	1.107
8-4	1	-.965	4.87	0.976
8-5	7	-1.345	5.43	1.183
8-5-1	4	-1.700	5.73	1.183

Table B.3
Flight-Path Analysis at c.r.: Pilot Phase Considerations
(τ_n=0.1)

Conf.	Pilot Ratings	Max. Pilot Phase Comp (deg)	Freq. at Which this Occurs	Low Freq. Pilot Phase (deg)
1-1	7,5	67.4	3.50	122
1-2	8,7,5.5	57.6	3.50	69
1-3	5,4,7	52.5	3.75	88
4-1	2.5,5	50.2	4.00	117
4-2	2,3	44.9	4.00	65
4-3	7	47.4	3.75	87
4-3-1	4	45.1	4.00	24
7-1	2.5,3	43 5	3.75	-47
2-1	6,7	98 9	3.00	121
2-2	4.5,3	89.6	3.00	70
5-1	4.5,4.5	78.9	3.25	115
5-2	2,3	74.8	3.25	66
6-1	3,5,6	100.8	3.25	119
6-2	5,4,2	73 8	3.75	111
6-1-1	4	98.2	3.25	56
6-2-1	3	70.7	3.75	47
8-1	5.5,6	90.5	3.00	107
8-1-1	2	84.8	3.00	88
8-2	9,8,7	97.2	2.75	115
8-2-1	7	105.6	2.50	90
8-3	8,7	109.1	2.75	114
8-3-1	3	105.4	2.75	91
8-4	1	72.3	2.25	77
8-5	7	101 1	3.00	104
8-5-1	4	97 4	3.25	84

Table B.4

Flight-Path Analysis at c.r.: Tracking Considerations

(τ_n=0.1)

Conf.	Pilot Ratings	RMS Tracking Error	Low Freq. O.L. Peak (dB)	Resonance Peak (dB)
1-1	7,5	1.413	17.6	4.621
1-2	8,7,5.5	0.724	20.8	5.972
1-3	5,4,7	0.796	21.0	5.556
4-1	2.5,5	[illegible]	17.7	4.293
4-2	2,3	0.702	21.1	5.725
4-3	7	0.786	21.1	5.488
4-3-1	4	0.784	21.1	5.381
7-1	2.5,3	[illegible]	20.4	4.900
2-1	6,7	1.465	16.8	4.691
2-2	4.5,3	0.817	20.0	5.783
5-1	4.5,4.5	1.417	17.2	4.510
5-2	2,3	0.772	20 0	5.772
6-1	3,5,6	1.454	16.7	4.449
6-2	5,4,2	1.412	17.2	4.070
6-1-1	4	1 435	16.8	4.530
6-2-1	3	1.409	16.7	4.048
8-1	5.5,6	2.252	15.9	4.574
8-1-1	2	1.327	17 4	4.859
8-2	9,8,7	1.369	17.0	4.930
8-2-1	7	1.407	16.7	5.028
8-3	8,7	1.446	16.1	4.845
8-3-1	3	1.411	16.2	4.914
8-4	1	1.490		
8-5	7	2.462	14.6	4.681
8-5-1	4	1 394	15 8	4.881

Table B.5

Flight-Path Analysis at c.r.: Other Considerations

(τ_n=0.1)

Conf.	Pilot Ratings	Droop (dB)	Magnitude Crossover (rad/sec)	Phase Crossover (rad/sec)
1-1	7,5	-1.414	1.70	3.30
1-2	8,7,5.5	-0.785	1.80	3.35
1-3	5,4,7	-0.811	1.85	3.50
4-1	2.5,5	-1.076	1.70	3.35
4-2	2,3	-0.760	1.80	3.50
4-3	7	-0.798	1.85	3.55
4-3-1	4	-0.808	1.85	3.60
7-1	2.5,3	-0.918	1.80	3.60
2-1	6,7	-1.511	1.60	3.10
2-2	4.5,3	-0.856	1.75	3.30
5-1	4.5,4.5	-1.454	1.65	3.25
5-2	2,3	-0.854	1.75	3.35
6-1	3,5,6	-1.524	1.60	3.10
6-2	5,4,2	-1.461	1.65	3.30
6-1-1	4	-1.517	1.60	3.10
6-2-1	3	-1.480	1.65	3.30
8-1	5.5,6	-1.695	1.20	2.15
8-1-1	2	-1.393	1.20	2.20
8-2	9,8,7	-1.424	1.15	2.15
8-2-1	7	-1.480	1.15	2.05
8-3	8,7	-1.557	1.15	2.00
8-3-1	3	-1.549	1.15	2.05
8-4	1		2.00	4.40
8-5	7	-1 909	1.15	2.05
8-5-1	4	-1 616	1.15	2.05

Table B.6
Flight-Path Analysis at c.r.: Tracking Considerations
(τ_n=0.1)

Conf.	Pilot Ratings	High Freq. O.L. Peak (dB)	Bandwidth (-90 deg) (rad/sec)
1-1	7,5	7.90	1.939
1-2	8,7,5.5	5.70	1.981
1-3	5,4,7	5.80	2.045
4-1	2.5,5	8.30	1.989
4-2	2,3	6.90	2.034
4-3	7	6.00	2.059
4-3-1	4	6.00	2.070
7-1	2.5,3	6.40	2.034
2-1	6,7	7.10	1.865
2-2	4.5,3	4.60	1.993
5-1	4.5,4.5	7.60	1.925
5-2	2,3	6.50	1.975
6-1	3,5,6	7.90	1.827
6-2	5,4,2	8.30	1.913
6-1-1	4	8.00	1.849
6-2-1	3	8.30	1.912
8-1	5.5,6	8.10	1.885
8-1-1	2	7.40	1.914
8-2	9,8,7	8.20	1.863
8-2-1	7	7.70	1.851
8-3	8,7	9.90	1.753
8-3-1	3	10.30	1.769
8-4	1		
8-5	7	13.3	1.909
8-5-1	4	14.2	1.721

END

DATE

FILMED

NOV 19 1985

End of Document